Theses and Dissertations   Theses, Dissertations, and Senior Projects

January 2013

Towards More Efficient Enhanced Sampling Methods To Study Phase Transitions

Kenneth Ndumbe Ngale

Follow this and additional works at: https://commons.und.edu/theses

Towards More Efficient Enhanced Sampling Methods To Study
Phase Transitions

by

Kenneth Ndumbe Ngale

Bachelor of Science, University of Buea, Cameroon, 1999
Master of Science, University of Yaounde I, Cameroon, 2002
Master of Science, Technical University of Denmark, 2007

A Dissertation

Submitted to the Graduate Faculty

of the

University of North Dakota

in partial fulfillment of the requirements
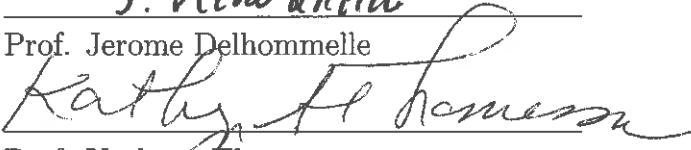

for the degree of
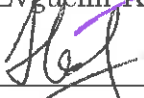
Doctor of Philosophy

Grand Forks, North Dakota
August
2013

This dissertation, submitted by Kenneth Ndumbe Ngale in partial fulfillment of the requirements for the Degree of Doctor of Philosophy from the University of North Dakota, has been read by the Faculty Advisory Committee under whom the work has been done, and is hereby approved.

_____
Prof. Jerome Delhommelle
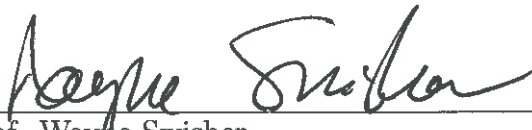
_____
Prof. Kathryn Thomasson

_____
Prof. Evguenii Kozliak

_____
Prof. Alexei Novikov

_____
Prof. Graeme Dewar

This dissertation is being submitted by the appointed advisory committee as having met all of the requirements of the Graduate School at the University of North Dakota and is hereby approved.

_____
Prof. Wayne Swisher
Dean of the Graduate School

_____
August 2013

ii

Title   Towards More Efficient Enhanced Sampling Methods To Study Phase Transitions

Department   Chemistry

Degree   Doctor of Philosophy

In presenting this dissertation in partial fulfillment of the requirements for a graduate degree from the University of North Dakota, I agree that the library of this University shall make it freely available for inspection. I further agree that permission for extensive copying for scholarly purposes may be granted by the professor who supervised my dissertation work or, in his absence, by the Chairperson of the department or the dean of the Graduate School. It is understood that any copying or publication or other use of this dissertation or part thereof for financial gain shall not be allowed without my written permission. It is also understood that due recognition shall be given to me and to the University of North Dakota in any scholarly use which may be made of any material in my Dissertation.

Kenneth Ndumbe Ngale _____

Date _____ **May 30, 2013** _____

iii

TABLE OF CONTENTS

LIST OF FIGURES

LIST OF TABLES

ACKNOWLEDGEMENTS

missing something.

I would also like thank all members of our research group; Dr. Tsvetan Aleksandrov, John Persson, Serges Nguelo, Jason and Erica Hicks, for giving insightful comments and suggestions during discussions sessions and group meetings.

My special and unreserved thanks go to all the lecturers and Faculty of the Chemistry Department at UND, especially Pr. Mark Hoffmann, Pr. Lothar Stahl and Mr. Michael Whitney and to the non-teaching staff in the Department, for the knowledge transmitted to me, their assistance with administrative procedures necessary for completing my doctoral program and their words of encouragement.

My profound gratitude also goes to the Faculty of the Chemistry Department at the University of Buea, Cameroon, particularly, Pr. Simon Efange, Pr. Samuel F. FANSO, Dr. Joseph Yong and Dr. M. T. AKAM for their contributions toward my academic growth.

I am particular indebted to all the graduate students in the chemistry department at UND. I owe them a very important debt especially those who made meticulous and helpful comments during seminar practice talks contributed enormous in improving my presentation and public speaking skill which were key to my success.

Last but not the least, I would like to thank my families; my parents Mrs Sophie Ngowo Ilongo and Mr. John Ewange Ngale first for giving birth to me and supporting me spiritually throughout my life. My in-laws, my brothers and sisters, and my numerous friends and relatives who have always given me that moral revitalization cannot be left out. The list may be long, but I cherish each input towards my career development as a scholar, teacher and above all as a scientist.

DEDICATION

This work is dedicated to God Almighty

And to My Lovely wife Sophie Enjema Mbua Tande and Our Son Shane
Lajule Ndumbe Ngale and to all our children and grand children.

ABSTRACT

The most familiar phase transitions observed in nature are associated with a change in the state of matter (solid, liquid, and gas). In some rare cases this may involve the plasma phase. Such transitions are often referred to as first order phase transitions and often occur commonly such as during the melting of snow or freezing of lakes and rivers during winter. This project focuses on the most ubiquitous phase changes such as, liquid-solid and vapor-liquid as well as the less prevalent vapor-solid transitions. These types of phase transitions are also known as classical phase transitions. They usually involve symmetry breaking and can be identified by a singularity in the free energy or one of its derivatives. More modern classification of phase transitions rely on the order parameters as exemplified by the Landau's theory. An order parameter is a quantity that takes a value of zero in the disordered phase and assumes finite values in the ordered phase. In the case of liquid-vapor transition, the order parameter is the density.

The study of phase transitions is often complicated by the amount of time required by these phase changes and the presence of a high free energy barrier. Consequently, changes occurring close to coexistence are hard or even impossible to follow via conventional experimental techniques. Molecular simulation is therefore the method of choice to study these processes. Molecular simulations are numerical experiments carried out on model systems and have a number of advantages over traditional experiments. Simulations do not have any limitation as to the type of molecules or conditions under which they can be applied.

Current simulation methods used to accomplish this task, such as the grand canonical and Gibbs ensemble Monte Carlo methods, employ the concept of particles insertion and deletion moves or require the knowledge of at least one point

at coexistence. These type of moves are extremely inefficient when dense fluids are involved and limit the accuracy of these methods. To circumvent these difficulties, non-Boltzmann sampling methods such as the umbrella sampling and Wang-Landau sampling techniques, have been employed to study these phase transitions.

Vapor-solid and liquid-solid phase transitions were studied using a combination of hybrid Monte Carlo (HMC) and the umbrella sampling on a system of C_{60} molecules. The crystallization process occurs in two steps, nucleation and growth. The nucleation step is an activated process that involves a high free energy barrier. The free energy barrier is overcome through a series of HMC steps. The growth step on the other hand is studied by means of unconstrained molecular dynamics (MD). This study illustrates that the body centered cubic structure plays no role in the crystallization of C_{60}. This is because only the face centered cubic and the hexagonal closed parked crystal structures were observed in both the nucleation and growth steps. In addition, the growth process is observed to follow a complex mechanism known as cross nucleation. The process of cross nucleation has also been observed in model fluids such as Lennard-Jones fluid and in the experimental study of D-mannitol.

Hybrid Monte Carlo and configurational bias Monte Carlo (CBMC) were combined with the Wang-Landau (WL) sample method to study the vapor-liquid equilibria of Polycyclic aromatic hydrocarbons (PAHs) with four fused benzene rings and α-olefins (C_2 - C_6), respectively. These studies are conducted in the isothermal-isobaric (NPT) ensemble to avoid the particle insertion and deletion moves that resulted in low acceptance rates in previous simulations. These studies led to the prediction of the critical temperatures, pressures and densities of both systems.

CHAPTER I

INTRODUCTION

1.1 Motivation

Phase transitions are important in a variety of applications in science and engineering especially in the areas of separation, manufacturing, and processing.[1–3] In environmental science for example, first and second order phase transitions play a vital role in the mobility of atmospheric particles.[4] Fast moving gas phase organic aerosol particles are known to have detrimental health effects.[5] Common illustrations of the importance of phase transitions can be seen in medicinal application like drug design and drug delivery. Capsules for example, are used to store drugs that are required to produce a desired effect at a specific location in the body. Different mechanisms can be used to trigger the release of an encapsulated content. These could be light activated release, slight changes in Ph or the presence of certain chemicals may trigger the release of drugs in biological tissues. In most cases the solubility of the outer coating as well as the active ingredient is vital for the uptake of the drug. This implies both the coating and active ingredient have to first undergo a phase change (solid-liquid transition) before they can be absorbed by the body.[6,7] In addition, phase transitions play an important role in drug design because polymorphism (the phenomenon of one compound having two of more crystal structures) occurs as a result of inappropriate control of crystallization (liquid-solid transition).[8] This can be wasteful when the inactive crystalline form is produced. It is worst if the transformation from one form to the other cannot be discovered early enough as the other form may have a different bioavailability and may be dangerous to patients. For example, the unintentional formation of 10% amorphous solid in aspirin leads to moisture uptake and hydrolysis of the drug.[9]

Induced hardening in tablets may lead to a decrease in uptake by the body due to slow solubility rate (solid-liquid transition).[10] Also, unanticipated crystallization/solidification of syrup-like drugs may lead to difficulties in storage (solid-liquid transition).[8,11]

Critical properties play a pivotal role in predicting thermodynamic and transport properties of hydrocarbons in the petroleum industry.[12] These properties are difficult to determine experimentally, given the wide variety of petroleum fluids (Figure 1b).[13] Failure to adequately understand the temperatures and pressures at which these different phases solidify may result in clogging of pipelines that could be very costly to maintain. Similarly, knowledge of the properties of these different phases is critical in the separation and purification process.[12]
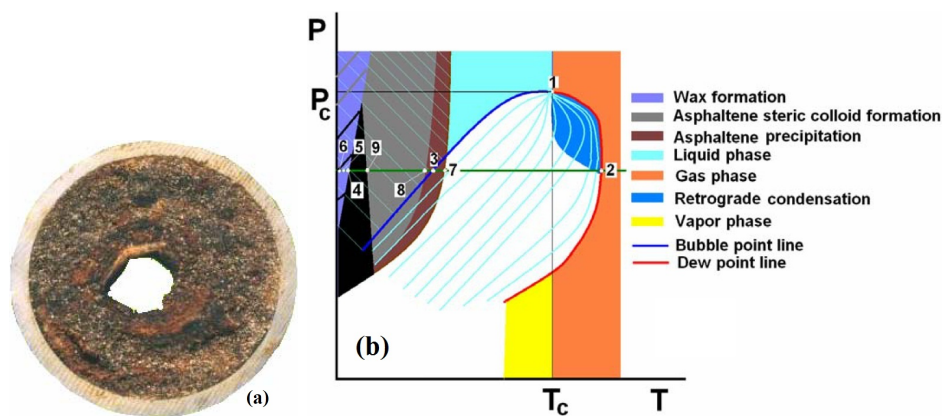
Figure 1. (a) Clogged transportation pipeline due to solidification of petroleum fluids; (b) Complex phase diagram for a mixture of hydrocarbon fluids.[12]

The processing and use of various crude oil fractions releases toxic particles and gases into the environment (Figure 2). These processes involve simple and complex mixtures of hydrocarbon as depicted in the phase diagram (Figure 1) as well as variations in temperature (Figure 2). Consequently, they represent most of the common phase transitions (liquid-vapor, liquid-solid, solid-vapor,etc) studied in this project.[12]
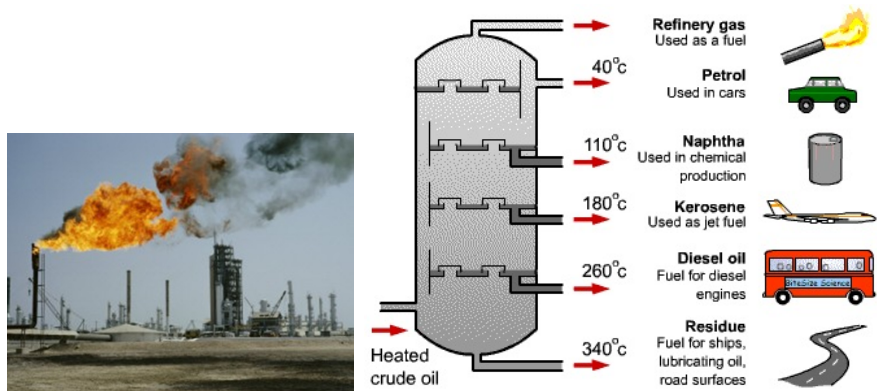
Figure 2. Separation and use of the different crude oil fraction.

1.2   Importance of Molecular Simulations to the Understanding of Phase Transition

Molecular simulations offer a means to understand macroscopic properties or behavior through the study of microscopic (interatomic) interactions.[14] Simulations can be viewed as experiments performed on model systems. Such computer experiments shed light and aid the understanding as well as interpretation of real world experimental results.[15] Molecular simulations have marked advantages over traditional experiments in that they can be used to study very expensive, dangerous and/or complex molecular systems and eliminate human errors. By using molecular simulations, regions and properties that are generally inaccessible by experiments can be studied. Molecular simulations can be used to confirm and reproduce experimental results. Even in such situations, molecular simulations reveal microscopic details that are not visible and cannot be explained by experiments.[14] Although large amounts of experimental data on phase properties of a variety of fluids exist in the literature and have been used to produce phase diagrams as well as to characterize these fluids, experiments fail with increase in molecular complexity and instability. Furthermore, most phase transitions occur at extreme conditions that may not be attainable through experiments but as mentioned earlier, knowledge of thermodynamic properties at these extreme conditions is essential for scientific and engineering applications.[16] A typical example is the discovery of the process for destruction of aqueous waste with supercritical water

3

oxidation.[15] This process is based on the reaction of organic contaminates with oxygen at temperatures and pressures above the critical point of water. This design process has been halted because of the need for trials that are difficult to perform experimentally. Studies are currently being pursued to determine suitable modeling techniques that can handle aqueous/organic mixtures at high temperatures and pressures.

As a consequence of these difficulties and discrepancies in experimental results, molecular simulations are gaining ground in the study of phase transitions.[17] Presumably, this can be attributed to the advantages simulations have over experiments, like the time and the ease of repeating simulations or reproducing simulation results.[14] Numerical studies also permit access to all states of the modeled system, thus revealing details that are otherwise inaccessible to experiments. In this line, numerous molecular simulation methods have been developed. A few of them related to the study of fluid coexistence are detailed in the next section.

1.2.1 Force Field

The success of computational chemistry (molecular simulations) strongly depends on the quality of the potential energy function.[2,18] Since the real intermolecular potential for a given molecule is hard to assess, simulations are based on potential models.[19] An adequate force field that can effectively describe intermolecular and intramolecular interactions and thus accurately predict the molecular shape as well as thermodynamic properties is therefore crucial for any model system.[20] There are as many potential energy models as there are simulation techniques.[21–24] Most potential energy models can be classified under two main headings: all-atom and coarse grain model.[18,25] These models are used interchangeably depending on the system under consideration,[26] simulation method, software package,[27] and quality of details expected from the simulation.[18] In very complex systems, a combined force field can be used as a potential energy function

to study the system.[25]

1.2.2   Parameterization

The potential energy function generally employed for the parameterization of most atomistic force field takes the form of Equation (1.1).

$$E_{total} = E_{internal} + E_{external} \tag{1.1}$$

where

$$
\begin{aligned}
E_{internal} =& \sum_{bonds} K_b(b - b_{eq})^2 + \sum_{angles} K_\theta(\theta - \theta_{eq})^2 \\
&+ \sum_{dihedrals} K_\phi[1 + cos(n\phi - \gamma)] + \sum_{impropers} K_\varphi(\varphi - \varphi_{eq})^2
\end{aligned}
\tag{1.2}
$$

and

$$E_{external} = \sum_{nonbond} \left(\epsilon_{ij} \left[\left(\frac{R_{min,ij}}{r_{ij}} \right)^{12} - 2 \left(\frac{R_{min,ij}}{r_{ij}} \right)^{6} \right] + \left(\frac{q_i q_j}{4\pi\epsilon_0 r_{ij}} \right) \right) \tag{1.3}$$

Parameters K_b, K_θ, K_ϕ, and K_φ represent the bond length, bond angle, dihedral angle, and improper dihedral angle force constants, respectively; b, θ, ϕ, φ, and γ are the bond length, bond angle, dihedral angle, improper torsion angle, and the phase angle respectively. The Lennard-Jones 12-6 potential and Coulombic terms represent the external or nonbonded interactions. The Lennard-Jones potential is also used for the van der Waals interactions. ϵ_{ij} is the Lennard-Jones well depth, R_{min} is the distance at the Lennard-Jones minimum, q_i is the partial atomic charge, ϵ_0 is the dielectric constant and r_{ij} is the distance between atoms i and j.

Parameterization involves assigning specific values for the parameters in Equations 1.2 and 1.3 for different atoms and different bonding types. The

parameter set and atomic charges are implemented mostly as described in the literature for the given force field.[27] The force constant terms are usually adjusted by fitting vibrational data for model systems associated with bond length, bond angle, dihedral angle and improper torsion. Gas phase infrared and Raman data are used as the primary sources for such data.

In order to supplement experimental data, *ab initio* density functional theory (DFT) calculations are performed where necessary. This entails assigning vibrational frequencies in the absence of experimental values. The parametrized force field is tested by utilizing it to reproduce known results, especially results obtained from experiments. Such tests help to ensure that the force field treats the system with sufficient accuracy.

1.3   Advances in Molecular Simulations Studies of Fluid Coexistence

Despite the importance and numerous applications of phase transitions, phase properties of most systems have not been studied due to the high free energy barrier associated with phase transitions.[28,29] In addition, locating the phase boundary has been hampered by the difficulties of simulating both coexisting phases with a single simulation.[17] To overcome this difficulty, methods that can efficiently sample the configurational space of the system under consideration are needed. The trend changed with the advent of the Gibbs ensemble Monte Carlo (GEMC) scheme by Panagiotopoulos and co-workers.[15] Over the past two decades, different simulation methods have been developed to determine the vapor-liquid coexistence of various systems. Some of these schemes rely on the insertion/deletion of particles originally proposed in the Panagiotopoulos method, or require knowledge of the chemical potential of the phases involved. Besides, current simulation methods also rely on experimental data for the determination of some parameters for most systems that have been adequately modeled. Additionally, the availability of numerous simulation techniques makes it challenging to select an appropriate methodology for

the system to be studied.

There are basically two main simulation methods, namely Molecular Dynamics (MD) and Monte Carlo (MC). Most of the techniques applied for the study of phase transition are based on MC. This is because MD that rely on Newton's equations of motion is inefficient for longtime relaxation phenomenon compared to MC that depends on random but clever particle movements.[2] This is because the integration process using the equations of motion usually overestimates the transition point due to a discontinuity in the energy during first order phase transitions.[14] Most molecular simulation applications involve representation of fluid properties for a single isolated phase. The extension of simulation techniques to multiple phases proves a versatile tool for the investigation of the phase coexistence of both pure fluids and fluid mixtures. Two methods have been routinely used for the study of phase coexistence, namely: Grand Canonical Ensemble Monte Carlo (GCEMC) and Gibbs Ensemble Monte Carlo (GEMC).

1.3.1   Grand Canonical Ensemble Monte Carlo

The Grand canonical (μVT) ensemble Monte Carlo (GCEMC) simulations keep the chemical potential μ, temperature T, and volume V constant. This method has been used to study the vapor-liquid coexistence properties of the Lennard-Jones fluid. The total configurational energy E and number of particles N are varied through the insertion and deletion of particles. Both processes occur with equal probability and each trial is accepted following a Metropolis rule designed to respect the conditions for detail balance necessary for thermodynamic equilibrium. For an energy change of insertion ΔE_I, the insertion process is accepted with a probability given by;

$$P_{acc}(N \longrightarrow N+1) = min\left[1, \frac{zV}{(N+1)}\exp(-\beta\Delta E_I)\right] \qquad (1.4)$$

where $z = \exp(\beta\mu)$ and $\beta = 1/k_b T$

Similarly, particle deletion is accepted with a probability given by;

$$P_{acc}(N \longrightarrow N - 1) = min \left[1, \frac{N}{zV}\exp(-\beta\Delta E_D) \right] \qquad (1.5)$$

where E_D is the energy change for removing a particle.

In addition to particle insertion/deletion moves, there is also implicit particle displacement. This ensemble for MC simulations was originally designed considering adsorption experiments wherein the adsorbed gas is in equilibrium with a reservoir gas (Figure 3). The adsorbed gas has volume V and the volume of the reservoir is given by V_0-V, where there is exchange of particles between the two volumes. The reservoir sets the temperature and chemical potential of the system. This method has been extensively used for the determination of phase coexistence properties.
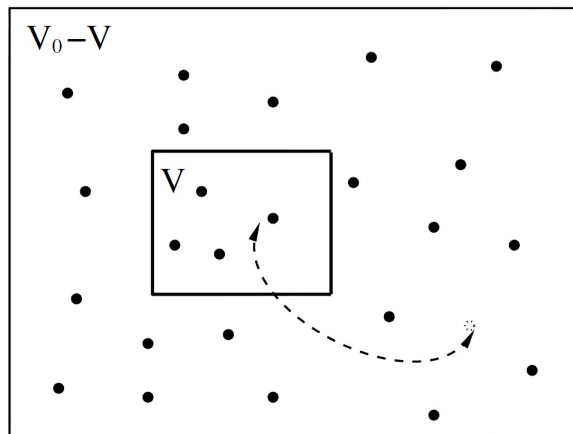
Figure 3. Setup for GCMC technique showing exchange of particles to ensure a constant chemical potential.

GCEMC uses the transition matrix or histogram reweighting technique (non-Boltzmann sampling method used to evaluate averages for a state of interest from a trajectory or a single simulation run) to obtain information from a single simulation and to sample all states with equal probability.[30] This makes the method suitable for studies where a large amount of phase equilibria data is needed. The main observables (variables) for these simulations are the number of particles and the configurational energy that are easily accessible during the course of the simulation. Although this method demands that the chemical potential of both

phases be specified, it is more accurate than the GEMC method.[30,31] Varying the number of particles implies fluctuation of the density $\rho = N/V$. A plot of the probability density $p(\rho)$ function versus the density can be used to obtain information on the nature of the phase coexistence (Figure 4). Because separate
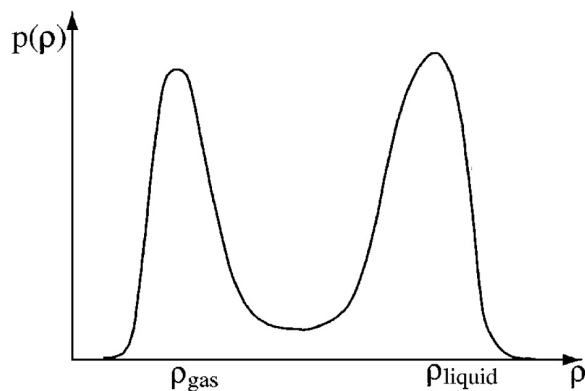
Figure 4. Variation of the probability density $p(\rho)$ and density at the liquid-vapor phase boundary.

simulations are run for the gas and liquid phases, the location of the liquid-vapor equilibrium point is discerned through continuous evaluation of the ρ and T thermodynamic properties of the individual phases, until the integrated weight or area under each peak is equal. Since the liquid-vapor coexistence is determined by the equal peak weight criterion, the process must be repeated until the point of coexistence is found.[14] The complexity of the procedure, coupled with the difficulties associated with obtaining the chemical potential data held back the study of phase equilibria via this molecular simulation technique.[32] Using the method, it is difficult and at times impossible to insert large chain molecules during the simulation, and gradual insertion methods fail when using the histogram reweighting method. Also, more simulations are required for large systems to be able to overlap the histograms to obtain the liquid-vapor phase boundary.

1.3.2 Gibbs Ensemble Monte Carlo

The development of the Gibbs ensemble sampling method helped revitalize studies of phase properties via molecular modeling.[17] Based on this method, the

phase coexistence properties could be investigated in a single simulation without the need to specify the chemical potentials. The Gibbs ensemble method, developed by Panagiotopoulos, has been widely used in the study of phase coexistence because of its simplicity and applicability to a large range of systems.[31,33,34] This method simulates phase behavior by following the evolution of a system composed of two distinct regions in phase space. Each region represents a small volume of a homogeneous phase. There is no physical interface separating the two phases in the system.[34]
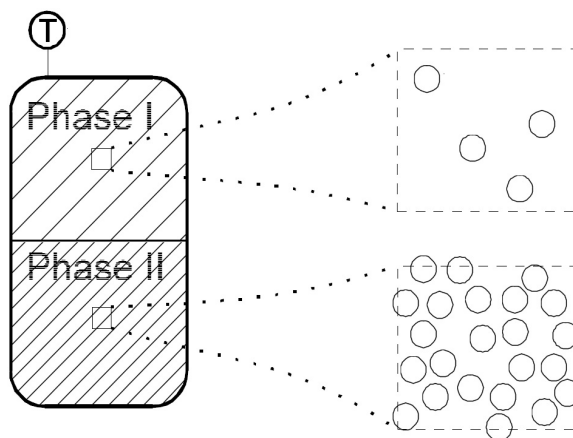
Figure 5. Simple illustration of Gibbs sampling technique, phase I and II represent the vapor and liquid states respectively.

The two phases may be represented in two separate boxes as shown in Figure 5 from which three types of moves can be performed to meet the conditions for equilibrium. While particles displacement inside each separate box ensures that there is internal equilibrium, random volume changes between the two boxes satisfy the condition for equality of pressure, and particle exchange between the two boxes ensures that the chemical potentials of all the components are equal.[35] Although there is movement of particles within and between the two regions as well as volume changes, the total number of particles, volume and temperature are constant. Thus the Gibbs ensemble method can be construed to be a variation of the canonical ensemble where the number of particles, volume and temperature are fixed. However, the Gibbs ensemble differs from the NVT ensemble in that particle exchange and volume changes are performed between the subsystems (boxes), while

keeping the total number of particles and volume constant.
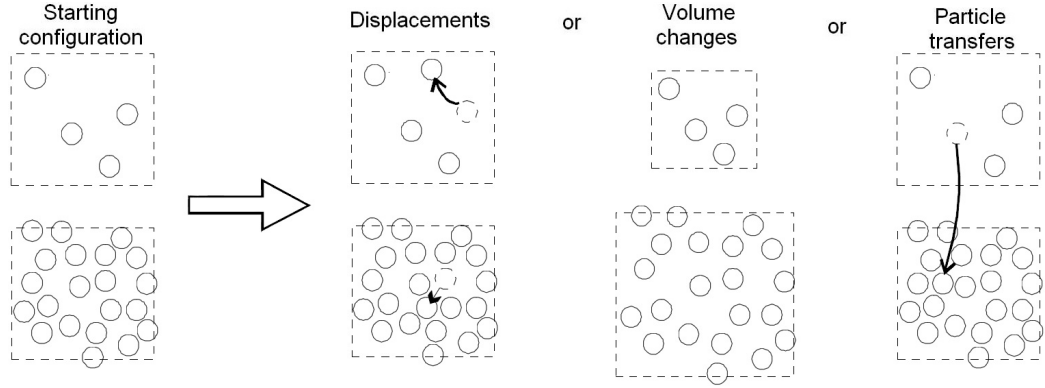
Figure 6. Characteristic moves in a typical Gibbs sampling technique.

If a one-component system at a constant temperature T, having a total volume V and total number of particles N, is divided into two regions, the volume and number of particles in each region will be as follows; V_I and N_I and $V_{II} = V - V_I$, and $N_{II} = N - N_I$ for regions one and two respectively. The partition function for this system Q_{NVT} is given by:

$$
\begin{aligned}
Q_{NVT} \;=\; & \frac{1}{\Lambda^{3N} N!} \sum_{N_I=0}^{N} \frac{N_I}{N_I N_{II}} \int_0^V dV_I \; V_I^{N_I} V_{II}^{N_{II}} \\
& * \int d\xi_I^{N_I} \exp\left[-\beta U_I(N_I)\right] \int d\xi_{II}^{N_{II}} \exp\left[-\beta U_{II}(N_{II})\right]
\end{aligned}
\tag{1.6}
$$

where Λ is the thermal de Broglie wavelength, $\beta = 1/k_B T$, ξ_I and ξ_{II} are scaled coordinates of the particles in both regions and $U(N_I)$ is the total interaction potential of N_I particles.

This partition function has been used with the free-energy minimization procedure to illustrate that the Gibbs ensemble technique gives accurate results of equilibrium densities for first order phase transitions. The partition function represented by Equation 1.6 has a probability density $\rho(N_I, V_I; N, V, T)$ given by;

$$\rho\left(N_I V_I; NVT\right) = \frac{N!}{N_I! N_{II}!} \exp\left(N_I \ln V_I + N_{II} \ln V_{II} - \beta(U_I(N_I) - \beta U_{II}(N_{II}))\right) \quad (1.7)$$

Since each type of move within the system results in a new configuration, the acceptance for the three different moves can be derived from Equation 1.7. Thus, for displacement of particle within either region or box the acceptance probability is:

$$\rho_{displ} = min\left[1, \exp\left(-\beta \Delta U\right)\right] \quad (1.8)$$

where ΔU is the configurational energy change associated with particle displacement.

This acceptance criteria is the same as that for conventional NVT ensemble simulations. For a change in volume, since the total volume is constant, if the size of box I is increased by ΔV, there is a corresponding decrease for box II and the acceptance probability is:

$$\rho_{volume} = min\left[1, \exp\left(-\beta \Delta U_I - \beta \Delta U_{II} + N_I \ln\frac{V_I + \delta V}{V_I} + N_{II} \ln\frac{V_{II} - \delta V}{V_{II}}\right)\right] \quad (1.9)$$

Equation 1.9 indicates that the sampling is performed uniformly in the volume itself. Consequently, the volume change is effected by generating a uniformly distributed random number between 0 and 1 (ξ), making sure that a negative volume does not result from any change.

$$\Delta V = \xi \Delta V_{max} \text{ x } min\left(V_I, V_I\right) \quad (1.10)$$

where ΔV_{max} is the maximum fractional volume changed allowed. It is adjusted to obtain the desired acceptance rate. Finally, the acceptance criterion for the particle transfer from box II to box I is:

$$acc_{transf} = min \left[1, \frac{N_{II}V_I}{(N_I + 1)V_{II}} \exp\left(-\beta \Delta U\right) \right] \quad (1.11)$$

where $\Delta U = \Delta U_I + \Delta U_{II}$

When the two phases coexist at temperatures and pressures away from the critical point, the equilibrium densities and compositions can be calculated by averaging the variables after equilibration. However, since there are three different types of moves to be performed throughout the simulation, each of them will therefore have a criterion for accepting a new configuration. Also, for simulations of a multicomponent system, the pressure could be specified and the system simulated with a constant number of particle, pressure and temperature (NPT) ensemble. As such, the probability density and the acceptance criteria are modified.[35]

Although the GE method does not require prior knowledge of the chemical potential for the two phases at coexistence, the exchange of particles between the two regions could be burdensome in the case of high density liquids such as melted metals. The transfer from low density to high density states could often be rejected due to the highly unfavorable energetic states (particles overlap) in the liquid phase after the transfer. Configurational bias Monte Carlo techniques and the Gibbs-Duhem method are used in the simulation to enhance the acceptance rate for particle swaps between the two phases.[32,34]

1.3.2.1   Limitations of the Gibbs Ensemble Method

The dependence of the Gibbs ensemble on particle exchange to achieve a balance in chemical potential between the coexisting phases introduces a number of limitations:[30,34]

1. Because of the low particle acceptance probability, it may not be easily applied to high density fluids such as the case of fluid-solid equilibria.

2. It becomes inaccurate in the vicinity of the critical point, this makes it

inappropriate for study of phase properties near the critical point in either pure fluids or mixtures. This has been the subject of a number of recent studies that have shown that the inaccuracy is due to interfacial simulation between the two boxes.

3. For simulations of a multicomponent system that is dilute in one component the number of particles in one box could become zero due to successive transfer from the same box. In such a situation the probability of a transfer from the empty box is zero, which limits the transfer probability.

CHAPTER II

PHASE TRANSITION

2.1   Introduction

Phase transitions refer to the changes of the states of matter from one form to the other across a phase boundary. Phase transitions are ubiquitous in nature and have been explored by engineers as well as scientists for numerous applications. The most common phases are solid, liquid and gas; in rare cases however, there exist a plasma phase that is considered the most abundant state of matter in the universe (Figure 7). The plasma phase is a high energy electrically charged mixture of ions and electrons that exist at very high temperatures.
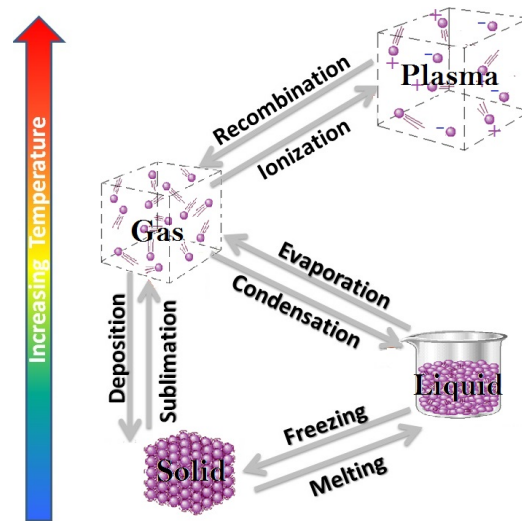
Figure 7. Different phases and the processes associated with the change from one phase to the other.

In addition to observing phase transitions between the different forms of matter, phase transitions can also occur within the same form of matter. For example diamond and graphite are two polymorphic forms of carbon. They are

physically different due to their difference in molecular arrangement and the conversion from one form to the other is described as solid-solid transition. However, for clarity, within this dissertation phase transition will refer to the changes from one state of matter to the other, known as classical phase transitions.

Different thermodynamic parameters can be used to describe the states of a simple and pure one component system such as water. These include density ρ, energy E, temperature T, pressure P, and chemical potential μ. A phase diagram (Figure 8) is the easiest way of representing the phases of a pure system using two of the thermodynamic parameters.[36,37] A common example is the PT phase diagram of water (Figure 8). For mixtures and complex systems, the phase diagrams can be very complex. Phase diagrams aid in the understanding of the behavior of single and multicomponent systems.
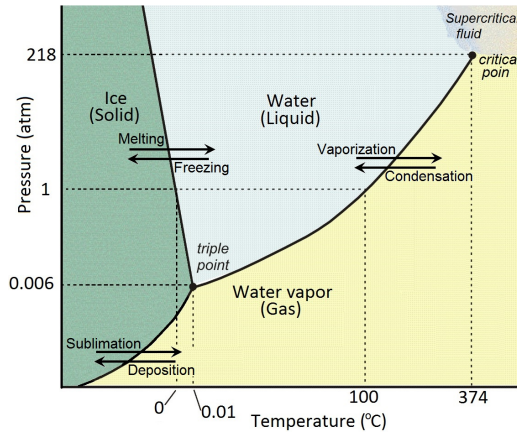
Figure 8. Simple temperature and pressure phase diagram.

It has been established that phase transitions are a consequence of competition between the internal energy E and the entropy S of the system.

$$F = E - TS \tag{2.1}$$

In the definition of the free energy (equation 2.1), E favors order while S favors disorder and depending on the value of the temperature, one of the terms becomes dominant and thus determines the stable phase.[36] Therefore to attain equilibrium,

the chemical potentials of the coexisting phases must be equal.

2.2 Classification of Phase Transitions

Phase transitions can be classified based on a singularity in the thermodynamic potential (Gibbs free energy) and/or variation of one of its derivative at the point of a phase change.[36] This classification method is referred to as the Ehrenfest classification of phase transitions. Based on this scheme, phase transitions are named relative to the lowest free energy derivative that has a discontinuity at the transition point.

2.2.1 First-Order Phase Transition

The equations of state for different phases of a pure substance like water are well-defined, regular, and continuous functions, with continuous derivatives. For a first-order phase transition, the functions of a given phase undergo a sudden change to the functions of a new phase. This results in a discontinuity in the first derivative of the bulk Gibbs free energy of the system as it crosses the phase boundary.[38] This type of transition involves the absorption and release of heat (latent heat) with no observable change in the phase of the system, leading a mixed-phase regime.[38,39] In the mixed-phase region the two phases coexist in equilibrium, i.e., part of the system that has completed the transition exists in the new phase and the other part yet to complete the transition still exists in the old phase as illustrated in Figure 9.[39]

$$S = -\left(\frac{\partial G}{\partial T}\right)_p \qquad V = \left(\frac{\partial G}{\partial p}\right)_T \qquad H = \frac{\partial (G/T)}{\partial (1/T)} \qquad (2.2)$$
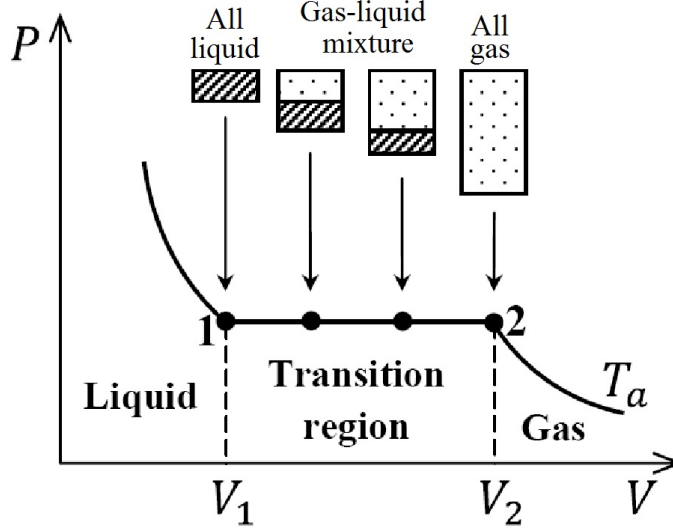
Figure 9. Representation of Ehrenfest first-order phase transition.[39]

2.2.2   Second-Order Phase Transition

Second-order phase transitions can be identified by a continuous first derivative of the Gibbs free energy and at least one discontinuous second derivative. It does not involve latent heat as for example, in the ferromagnetic phase transition in iron.[39] Here magnetization, which is the first derivative of the free energy with respect to the applied magnetic field strength, increases continuously with a decrease in temperature across the phase boundary, while the response functions (susceptibilities) are discontinuous.

$$C_P = -T\left(\frac{\partial^2 G}{\partial T^2}\right)_p \qquad \kappa_T = -\frac{1}{V}\left(\frac{\partial^2 G}{\partial p^2}\right) \qquad \beta = \frac{1}{V}\left(\frac{\partial^2 G}{\partial P \partial T}\right) \qquad (2.3)$$

Ehrenfest system of classification gives the impression that higher order phase transitions can be deduced based on the discontinuity of higher derivatives.[38,39] However, this method cannot be extended consistently. Besides, the method is limited since it depends on the mean field theory which itself fails in the vicinity of phase transitions. For example, the Ehrenfest classification is invalid for systems that show divergences rather than finite discontinuities in the response functions
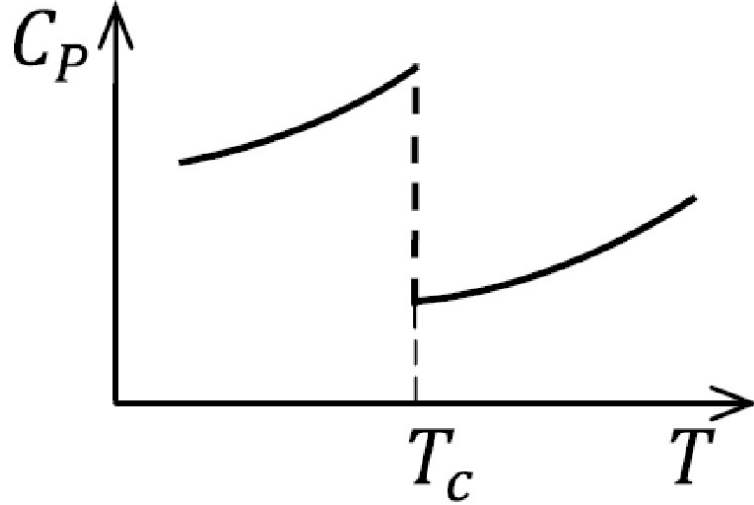
Figure 10. Second-order phase transition according to Ehrenfest classification showing discontinuity in the heat capacity C_P (second derivative of Gibbs free energy) as a function of the temperature T).[39]

and are not first-order transitions. Moreover, this method of classification tends to neglect the role of thermodynamic fluctuations given that some systems appear to undergo first-order phase transition for a specific temperature as depicted in Figure 11(a). But when the temperature is increased, the discontinuity vanishes and the system then appears to undergo second-order phase transition instead (11(b)). This phenomenon is common with several systems found in nature and needs to be accurately classified for a clear understanding phase transitions.
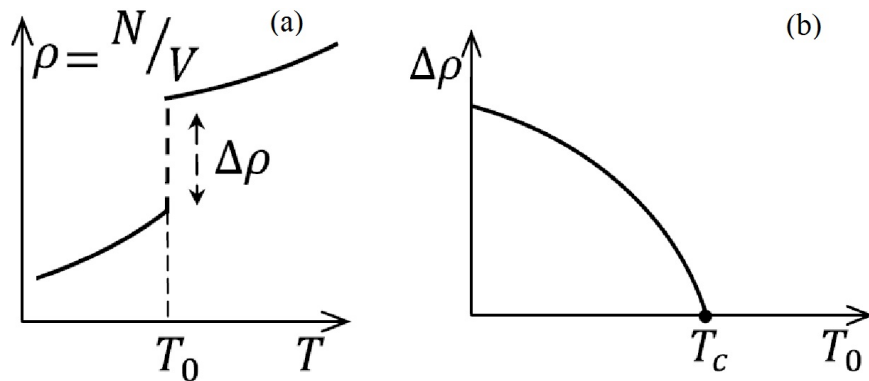
Figure 11. Pictorial representation of the limitation of the Ehrenfest classification of phase transitions.[39]

Two main classes of phase transition are exemplified in the modern classification of phase transitions namely: First-order and second-order phase transitions or discontinuous and continuous phase transitions. Unlike the Ehrenfest classification, the modern classification is based on the order parameter. The Landau theory is a modern classification scheme that uses the order parameter to distinguish between transitions.

2.3.1   Order Parameter

An order parameter ϕ is an extensive thermodynamic variable used to distinguish between phases. It is a measure of the degree of symmetry in the ordered phase where it takes a non-zero value (usually one) and vanishes in the disordered phase.[36] Most systems have a natural or particular parameter that can function as the order parameter (Table 1). Modern classifications of phase transitions are based on whether the order parameter ϕ is a scalar or vector quantity or has a tensor character.

Table 1. Examples of order parameters for different systems and their associated phase transitions[36,38]

System	Transition	Order parameter
Liquid-solid	Melting/crystallisation	Density ρ_G G=reciprocal lattice vector (real scalar)
Liquid-gas	Condensation/evaporation	Density $\Delta\rho = \rho_{liquid} - \rho_{gas}$ (real scalar)
Magnetic solid	Ferromagnetic (T_C)	Spontaneous magnetization M (vector)
	Antiferromagnetic (T_N)	Sublattice magnetization M_S (vector)
Dielectric solid	Ferroelectric (T_C)	Polarization P (vector)
	Antiferroelectri (T_N)	Sublattice polarization P_S (vector)
Quantum liquids	Normal fluid$\longleftrightarrow$ superfluid	Wavefunction ψ (complex scalar)

Landau's theory is the most popular modern classification scheme for phase transitions. It assumes that the free energy of a system can be given as a power series of the order parameter.[38] For example, in simple systems with a scalar order parameter, the free energy proposed by Landau has the form of Equation 2.4.

$$G = a(T) + \frac{1}{2}r(T)\phi^2 + d(T)\phi^3 + u(T)\phi^4 \tag{2.4}$$

If the coefficients are functions of temperature, a stable phase is observed when

$$\frac{\partial G}{\partial \phi}\Big|_{\phi_0} = 0, \qquad \frac{\partial^2 G}{\partial \phi^2}\Big|_{\phi_0} > 0 \tag{2.5}$$

Following this theory, the high symmetry phase is stable only if the linear term in ϕ in Equation 2.4 is absent and r is positive. If r is negative, the system is distorted. Equation 2.4 is the simplified Landau expression for free energy. However, if ϕ is a vector, the dot product should be used, i.e, $\phi^2 = \phi.\phi$.

For a symmetric system, at high temperatures $\phi = 0$, implying that the free energy minimum is at $\phi = 0$ and symmetry implies the free energy is symmetric, i.e, G(ϕ, T) = G(-ϕ, T). Thus the free energy as a function of ϕ becomes;

$$G = a(T) + \frac{1}{2}r(T)\phi^2 + u(T)\phi^4 + h(T)\phi^6 + ... \tag{2.6}$$

A phase transition will occur if one or more of the expansion coefficient changes sign as the temperature decreases.

2.3.3 *First-Order Phase Transition*

Considering the case in which the second non-trivial coefficient u(T) changes sign while the others maintain their signs. First-order phase transitions, or discontinuous phase transitions, have stable phases when

$$0 = \partial_\phi G(\phi, T) = r\phi + u\phi^3 + h\phi^5 + ... \tag{2.7}$$

Neglecting higher powers of ϕ, and assuming that $\phi = 0$ is a solution of Equation 2.7 as well as a local minima, two other minima would occur if Equation 2.8 has non-zero solutions $\phi = \phi_\pm \neq 0$.

$$G(\phi, T) - G(0, T) = 0 = \frac{1}{2}r\phi^2 + u\phi^4 + h\phi^6 + ... \tag{2.8}$$

This implies that Equation 2.8 simplifies to:

$$u^2 = 16rh, \qquad \phi_\pm^2 = \frac{-c \pm 3\sqrt{c^2 - 16rh}}{4h} > 0 \tag{2.9}$$

The transition temperature is given by

$$u^2(T_c) = 16r(T_c)h(T_c) \tag{2.10}$$

for which u$(T_c) < 0$. Thus the order parameter just below T$_c$ is given by

$$\phi_0 = \pm\sqrt{-\frac{u(T_c)}{4h}} \neq 0 \tag{2.11}$$

The stability of the low-temperature phase, i.e., at $T < T_c$ with respect to the order parameter, is given by

$$\phi_0^2 = \frac{a}{4u}(T_c - T) \tag{2.12}$$

2.3.4 Second-Order Phase Transition

For a continuous phase transition, G must increase with $|\phi|$, at T$_c$, r=0, d=0, and u>0. Considering that r(T) approaches zero at $T = T_c$ while the other
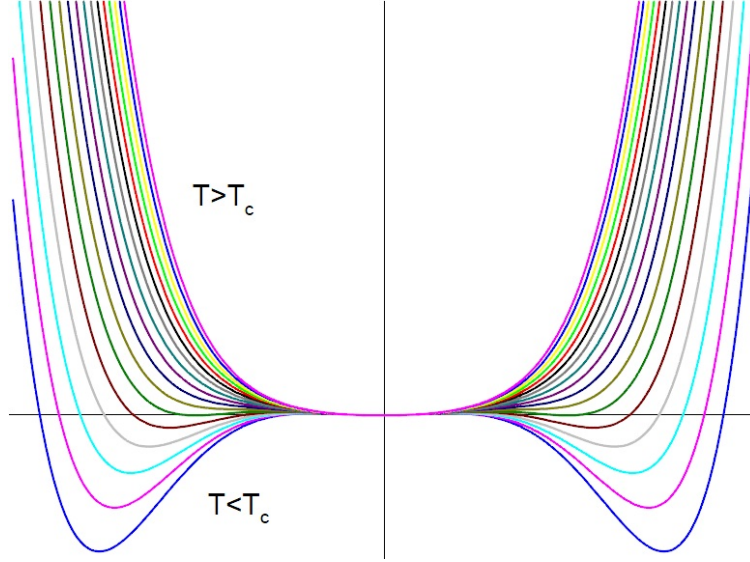
Figure 12. Variation of Gibbs free energy with the order parameter at different temperatures for a discontinuous phase transition.[38]

coefficients are positive, r can be written as a function of T near T_c.

$$r(T) = r_0(T - T_c) \tag{2.13}$$

The coefficient u is independent of temperature for temperatures very close to T_c. The free energy can then be rewritten as

$$G(\phi, T) = \frac{r_0}{2}(T - T_c)\phi^2 + u\phi^4 + h\phi^6 + ... \tag{2.14}$$

As T goes below the critical temperature, the extreme at $\phi = 0$ becomes an unstable minimum. Two other minima appear at $\pm\phi_0$ and the order parameter increases continuously from zero as the temperature is lowered from the critical point. This type of transition is a second-order phase transition or continuous phase transition. The order parameter can be determined by applying the condition for a minimum.

$$\frac{\partial G}{\partial \phi} = 0 = r_0(T - T_c)\phi + u\phi^3 + ... \tag{2.15}$$

23

The solution of Equation 2.15 as $T\to T_c$ becomes

$$|\phi| = \sqrt{r_0(T_c - T)/d} \qquad (2.16)$$

This affords the critical scaling property

$$\phi \sim |T - T_c|^\beta \qquad (2.17)$$

Given that the critical exponent $\beta = 1/2$, the specific heat capacity is obtained from

$$C = T\partial_T S = -T\partial_T^2 G \qquad (2.18)$$

For $T\to T_c + 0_+$ and $\phi = 0$

$$C = -Ta"(T)\to - T_c a"(T_c) \qquad (2.19)$$

For $T\to T_c\text{-}0_+$ and $\phi^2\to - r_0(T - T_c)/d$

$$C = -Ta"(T) - Tr'(T)(\phi^2)" - Td(T)(\phi^4)"\to - T_c a"(T_c) + T_c r_0^2/(2d) \qquad (2.20)$$

This leads to the scaling property

$$C \sim |T - T_c|^{-\alpha} \qquad (2.21)$$

The critical exponent $\alpha_\pm = 0$, for $T\to T_c \pm 0_+$.

In simple systems phase transitions can be classified or identified based on the sign of the coefficient u in the Landau expansion. When $u > 0$, a continuous or second-order phase transition is observed, while if $u < 0$ it indicates a discontinuous or first-order transition, and at $u = 0$ there is the tricritical point (only observed for mixtures).

A common feature of all phase transitions is the nucleation process. The phase
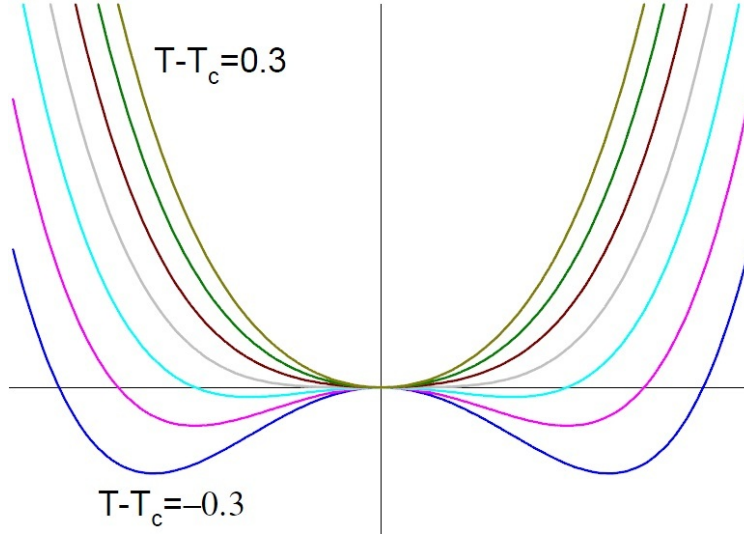
Figure 13. Variation of Gibbs free energy with the order parameter at different temperatures for a continuous phase transition.[38]

boundary in a phase diagram is characterized by the critical nuclei whose direct observation is often difficult. This is because before the nuclei are big enough to be visible, they have already passed the critical stage. The characteristic properties of critical nuclei of different fluids as well as their mechanism of growth have been extensively studied through simulations and advanced microscopy.[13] These mechanisms are governed by the classical nucleation theory (CNT).[40]

2.4   Classical Nucleation Theory

2.4.1   Definition

Nucleation is the process by which nuclei are formed from solution. It is the first irreversible formation of a nucleus of the new (equilibrium) phase.[41] The term "nucleus" refers to the smallest ensemble of atoms, molecules or ions of the new phase formed during precipitation and which is capable of spontaneous growth. Examples of nucleation processes include the condensation of a vapor to a liquid droplet, or the formation of gas bubbles from boiling water. In both processes only physical changes are involved and no chemical reaction.

The role of nucleation in the dynamics of most first-order phase transitions and its application in many industrial processes has greatly influenced research interest in the nucleation phenomenon.[42] Crystal nucleation is an activated process that requires the handling of less frequent events that occur for a very short time at a specific location of a liquid sample.[43,44] The understanding of the theory of nucleation has been based on the classical nucleation theory (CNT) for decades. This is because CNT, though developed using the liquid droplet model, captures the qualitative features of the nucleation process[45] and predicts the nucleation rate based on bulk material properties.[42]

CNT contains two ingredients: the first being a thermodynamic estimate of the reversible work needed to make a critical nucleus (i.e., a nucleus that is equally likely to dissolve as it is to grow to macroscopic size). The second ingredient of CNT is an estimate of the rate at which critical nuclei transform into macroscopic crystallites (growth).[46]

A system that contains a critical nucleus is said to be at a local free-energy maximum. The critical nucleus has a high free energy, which makes it less likely of forming. Thus the time scale for nucleation is much larger than the characteristic time scale for the microscopic dynamics of the system.[44] The nucleation step is the rate limiting step in a phase transition and a rare event on the timescale of simulations. As such, special techniques are required for its investigation. Ngale *et al.*, for example, have used the umbrella sampling technique and hybrid Monte Carlo simulations to study nucleation in different systems.[47]

2.5   Theory

The CNT gives the link between the observable quantity (number of crystal nuclei formed per unit time per unit volume) and the surface free energy.[46] It is the simplest and most widely used theory that describes the process of nucleation, originally derived for condensation of a vapor into liquid. By analogy, it has also

been employed to explain precipitation of crystals from supersaturated solutions and melts.[40] Crystallization is importance in many naturally occurring processes, as well as in the chemical, pharmaceutical, and food industries.[48] Gibbs was the first to attempt a thermodynamic description of the nucleation process in the late 19th century. He showed that the free energy change for the formation of clusters was made up of two parts. The free energy change for phase transformation (ΔG_v) and the free energy change for the formation of a surface (ΔG_s).[48,49] That is, there is a cost associated with the creation of a new phase, the interface energy. This is a penalty term which becomes smaller as the particle surface to volume ratio decreases. It accounts for the stability of the new phase (solid phase), and is proportional to the volume of the nucleus. This term also known as the bulk term, is equal to the number of spheres in the nucleus, n, times the chemical potential difference $\Delta \mu$.[50] In a metastable system this leads to a critical size of fluctuation beyond which growth is favored.

$$\Delta \mu = \mu_{eq} - \mu_m \tag{2.22}$$

where $\mu_e q$ defines the chemical potential of the coexisting equilibrium fluid and solid phases, and μ_m the chemical potential of the metastable fluid phase which contains the nucleus.

The other term describes the free energy needed to create a solid/liquid interface. It is given a positive sign and proportional to the surface area of the nucleus.[46] This surface term is given by the surface area of the nucleus times the surface tension γ of the bulk interface between the coexisting solid and fluid phases. Here any difference between the spherical interface created by the solid nucleus and the surrounding metastable fluid phase, and the flat interface between the coexisting solid and fluid phases is ignored.[50]

These two terms were used by Gibbs to develop an expression for the (Gibbs) free energy of a spherical nucleus of radius R in the form
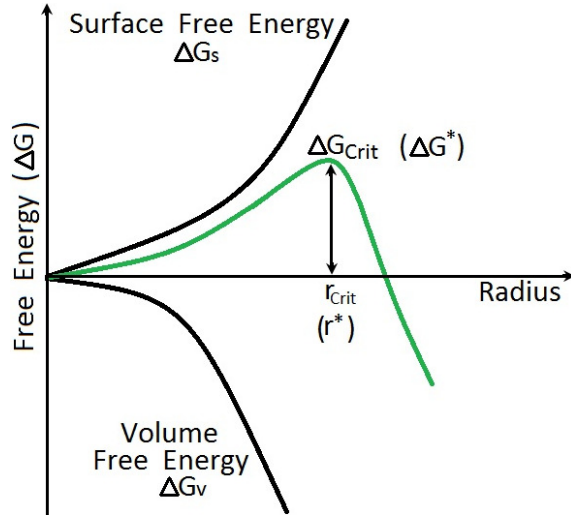
Figure 14. Free energy diagram for nucleation.[51]

$$\Delta G = 4\pi R^2 \gamma - \frac{4}{3}\pi R^3 \rho_s \Delta\mu \tag{2.23}$$

Where ρ_s is the number density of the bulk solid, $\Delta\mu$ the difference in chemical potential between the solid and the liquid, and γ is the solid/liquid surface free energy density.

It is important to observe that the free energy change for a phase transformation (ΔG_v) of the volume term decreases linearly with n, while the free energy change for the formation of a surface or the surface term increases as $n^{2/3}$. Thus, the function ΔG has a maximum at $R = 2\gamma/(\rho_s|\Delta\mu|)$ denoted by ΔG^* which defines the height of the nucleation barrier given by

$$\Delta G* = \frac{16\pi}{3}\frac{\gamma^3}{(\rho_s|\Delta\mu|)^2} \tag{2.24}$$

A nucleus with free energy equal to ΔG^* also has n^* particles and is known as the critical nucleus (has equal chance of growing or going into solution). There are two classes of nucleation processes: homogeneous and heterogeneous nucleation.

The nucleation theory expresses the rate J of nucleation as the product of an exponential factor and a prefactor.

$$J = K exp(-\Delta G^* / k_B T) \tag{2.25}$$

where ΔG^* is the free energy cost of creating the nucleus at the top of the barrier (critical nucleus), k_B is the Boltzmann constant and T the absolute temperature. K is the kinetic prefactor which is composed of three terms, i.e.

$$K = \rho Z f_c^+ \tag{2.26}$$

Z is the Zeldovich factor defined as;

$$Z = \sqrt{\frac{\beta |\Delta \mu|}{6 \pi n^*}} \tag{2.27}$$

f_c^+ is the rate at which molecules attach to the critical nucleus given by

$$f_c^+ = \frac{< [n^*(t) - n^*(0)]^2 >}{2t} \tag{2.28}$$

and ρ is the number density of sites for nucleation as the nucleus can form around any molecule. The product of Z and f_c^+ defines the rate at which the nucleus at the top of the barrier actually crosses it. [44]

Volmer and Weber developed the first expression for the nucleation rate where they assumed it was proportional to a Boltzmann factor, [52] while Farkas provided an expression for the pre-exponential factor. [53] Farkas considered equilibrium reactions and assumed that every collision of molecules is a potential start toward nucleus formation and that every molecule that collides with a growing nucleus sticks to it. [44,45]

2.5.1 Homogeneous Nucleation

Homogeneous nucleation is a spontaneous process that occurs in a uniform solution (form in the bulk). Although it is spontaneous, it is a consequent of a response to change in some intensive properties such as temperature or pressure.[54] The CNT was developed for homogeneous nucleation, wherein it assumes that the embryo (nucleus) formed from the bulk fluid (liquid) is spherical and possesses properties of the bulk liquid phase.[55] The energy needed to create a droplet of critical size, is given by ΔG^* as shown in Equation 2.24, and the rate of nucleation is given by Equation 2.25.

2.5.2 Heterogeneous Nucleation

Heterogeneous nucleation is sometimes referred to as binary or multiple nucleation. It is important for many processes such as cloud formation and emulsion polymerization. It involves the promotion of nucleation by insoluble particles or impurities in solution or the walls of the container.[44] Condensation processes of practical interest, in fields like atmospheric science, are usually heterogeneous or ion-induced. Although this type of nucleation process is more common and tends to occur much more quickly than homogeneous nucleation, it is believed to proceed through a more complex mechanism of nucleation.[55] Heterogeneous nucleation from the vapor on atomic size particles as studied with the interaction site model shows that it is highly dependent on the nature of the condensed fluid and the size of the seed. These factors induce unexpectedly high surface adsorptions that reduce the barrier to nucleation.[56] Thus the nucleation rate near a surface or induced by some impurities can be many orders of magnitude higher than in the bulk. Consequently, in many commonly encountered processes heterogeneous nucleation dominates while homogeneous nucleation turns to be irrelevant.[44] The surface of the impurities was considered as being smooth and flat by Volmer in the late 1920s, from which he was able to extend the classical nucleation theory by developing an expression for the
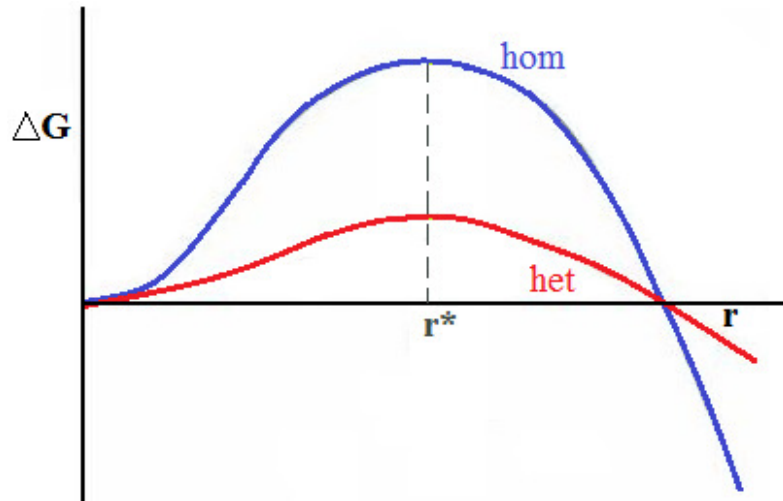
Figure 15. Free energy diagram illustrating the difference between homogeneous and heterogeneous nucleation.

free energy of heterogeneous nucleation as:[52]

$$\Delta G_{hetero} = \Delta G_{homo} * f(\theta) \tag{2.29}$$

The main differences between homogeneous and heterogeneous nucleation are the presence of nucleating agents such as impurities and/or the container walls, and the reduction in the nucleation barrier for heterogeneous nucleation (Figure 15).

2.6   Assumption of the Classical Nucleation Theory

During the development of the classical nucleation theory a number of different assumption were made. Some of these assumptions have been shown to be irrelevant while others either fail after a certain critical value or the shape of some parameters are met. One of such assumptions is that the crystal nucleus is incompressible, that has been shown to be irrelevant.[46]

Another assumption is that the structure of the crystal nucleus is that of the stable bulk phase at coexistence. In the presence of a metastable solid phase, this

31

assumption is violated as shown by the Ostwald's step rule.[43,57] This is most easily seen by considering the density of crystal nuclei as a function of their size.

The CNT assumes that the shape of the nucleus is spherical, in order to minimize the surface energy, and that it possesses the properties and the structure of the stable crystal phase. However, studies have shown that the shape of the nucleus is not always spherical. Valeriani *et al.* for example, showed that NaCl nucleates into cubic shaped crystallites.[43]

CNT assumes uniform composition throughout the droplet. However, it is believed that at the surface of mixed solutions such as alcohol-water and acetone-water, clusters can have considerable difference in composition compared to that of the bulk due to the surface enrichment effects.[48]

2.7   Limitations of the Classical Nucleation Theory

The derivation of classical nucleation theory gives a false estimate of the pressure inside the critical nucleus. This result in failure of CNT to predict the metastable phases during the nucleation process.[46] The pathway for crystal nucleation can be strongly influenced by the presence of metastable phases, as can be shown from the Ostwald's rule which states that most compounds do not always nucleate in the stable form but in the form for which the free energy barrier is the lowest.[43]

CNT fails systematically in predicting the temperature dependence of the nucleation rates for most substances, and the behavior of strongly polar fluids. As a result, nucleation rates predicted by CNT are 1-2 order(s) of magnitude higher than those reported from experiments.[48] CNT ignores molecular level effects relevant to the homogeneous and heterogeneous nucleation of clusters of only a few molecules, and is incapable of explaining the observed sign preference in ion-induced nucleation of dipolar molecules.[56]

The classical nucleation theory derived for a vapor/liquid condensation system is inapplicable to crystallization in solution. This is explained as being due to the use of the contact angle concept of the Young's equation (Equation 2.30) in the description of the interaction between substrate and nucleus by the CNT.

$$cos\,\theta_C = \frac{\gamma_{SG} - \gamma_{SL}}{\gamma_{LG}} \qquad (2.30)$$

where γ_{SG}, denotes the solid-vapor interfacial energy, γ_{SL}, the solidliquid interfacial energy, γ_{LG}, the liquid-vapor interfacial energy (surface tension), and θ_C the equilibrium contact angle.

This concept is considered crude. However, there are no theoretical developments in the microscopic direction and the contact angle concept provides little kinetic information about heterogeneous nucleation. Gibbs free energy on the other hand ignores the free energy of the electrical double layer that is spontaneously formed with the production of the embryo where the surface and solution are in contact.[58]

CNT fails in the prediction of the absolute nucleation rates since the pre-exponential factor in the kinetic (rate) equations remains undetermined.[48] It cannot also explain polymorphism and cross nucleation since it assumes uniform composition. But it is known that a lot of compounds can exist in the solid state with more than one crystalline form.[43]

The classical theory does not predict nucleation differences due to ion polarity. Although studies illustrate that water vapor nucleates much more readily around negative ions than in the presence of positive ions, whereas alcohols and carboxylic acids, have a preference for positive ions.[59]

2.8 Steps Toward Improving the Limitations of the Classical Nucleation Theory

The Gibbsian droplet model makes a correction regarding the incompressibility of the crystal nucleus assumed by the CNT model by considering that the critical

nucleus is at equilibrium with the parent phase. This suggest that the the critical nucleus and the parent phase must have the same chemical potential. It introduces the Laplace pressure which is always positive and predicts that the small nuclei are denser than the corresponding bulk phase. However, this model cannot be applied to crystallites because the excess pressure is not equal to $2\gamma/r_s$.[46]

Molecular dynamics studies have been used to show that the obtained nuclei present anisotropic shapes in opposition to the spherical assumption of the CNT that they are spherical.[43] Some theories that have been used in an attempt to correct CNT end up producing similar results. For example, it was suggested that the use of viscosity in CNT instead of considering the interfacial activation energy could be a source of error for the theory. Conversely, a study by Tolman and collaborators gave results closer to CNT than with experiments which indicated that other problems exist with the classical nucleation theory.[60] A number of models have been put in place in attempts to make corrections to some of the drawbacks of CNT.

2.8.1   The Self-Consistent Classical Theory (SCCT)

SCCT tries to correct the assumption of uniform composition from the CNT model by distinguishing the monomers of the new and parent phase. This adjusts the nonzero free energy of the monomers in an *ad hoc* way by subtracting the free energy of the monomer from all cluster sizes. This model, which appears to underestimate the height of the nucleation barrier, still gives improved agreement between theory and experiment in the case of homogeneous vapor condensation.[57]

2.8.2   The Phenomenological Diffuse Interface Theory (DIT)

DIT takes into account atomistic simulations results, which show that the solid-liquid and vapor-liquid interfaces extend to several molecular layers. It assumes that bulk crystal properties exist at the center of the nuclei. This approach

considers a curvature dependent interfacial free energy (surface tension) and usually improves significantly the agreement between theory and experiment for both vapor condensation and crystal nucleation.[57,59]

2.8.3   The Phase Field Models (PFTs)

PFT has two variant forms that rely on either the double-well and interpolation functions (denoted by PFT/S1 and PFT/S2), or on a Ginzburg-Landau expanded free energy that reflects the crystal symmetries (denoted by PFT/GL1 and PFT/GL2). The double-well variation of PFT has a double-well free energy density, with minima representing the newly formed and the parent phases. PFT/S1, and PFT/S2 models underestimate the height of the nucleation barrier while PFT/GL1, and PFT/GL2 models predict it fairly accurately.[57]

2.8.4   Density Functional Theory (DFT)

Density functional theory has been used in the last several years to develop a nonclassical approach to nucleation. The properties of the critical nucleus are obtained from the structure of the free energy of a nonuniform fluid by assuming that any nucleating system has an inhomogeneous structure, thus eliminating the basic assumptions of the capillarity approximation. It introduces the temperature dependence by considering that the free energy of a nonuniform system is a unique functional of the average density whose minima determine the thermodynamic states at a given temperature. The results follow the experimental trends more closely. But the effect of the dipole moment on the free energy was quite small compared to the experimental results for the study of Stockmayer fluids, which consist of point dipoles embedded in Lennard-Jones particles. The free energy of the

fluid in a weighted density approximation may be expressed as follows;

$$
\begin{aligned}
\beta_0 F[\rho_\alpha(r)] = \sum_\alpha \int dr \rho_\alpha(r) &- \int \int dr\ dr' s(|r - r'|) f_1(r) f_2(r') \\
&+ \int dr \Psi[\bar\eta(r)] \rho_s(r) + \frac{\beta_0}{2} \sum_{\alpha,\beta} \int \int dr\ dr' \phi_p^{\alpha,\beta}(|r - r'|) \rho_\alpha(r) \rho_\beta(r') \\
&+ \beta_0 \sum_\alpha \int dr V_{ext}^\alpha(r) \rho_\alpha(r) \quad (\alpha, \beta = 1, 2)
\end{aligned}
\tag{2.31}
$$

The interaction site model together with the DFT incorporates terms for most of the possible interactions that may occur in a solution during nucleation. This is done by introducing the first four terms in Equation 2.31, which accounts for different contributions to the free energy of the system. The first term takes care of the ideal free energy of a binary mixture of isolated atoms. The decrease in entropy due to chemical bonding in the formation of a molecule is included separately and represented by the second term. Short-range repulsive interactions between molecules are introduced by the third term using a weighted density approximation, and the fourth term compensates for the long-range part, $\phi_p^{\alpha,\beta}$, of the site-site interaction potential in a classical mean-field approximation. The atoms in this model are assumed to interact via a Lennard-Jones type potential with the additional coulombic interaction of embedded point charges.[56]

2.9   Conclusion

CNT is based on the continuum thermodynamic treatment of clusters by imposing the capillarity approximation, which means that small clusters are considered to have the same properties as the bulk material. The validity of continuum thermodynamics appears to be doubtful. However, CNT describes basic principles of nucleation processes and has been successfully used in many cases.

The exponential dependence of nucleation rate makes nucleation very sensitive to even slight changes in the experimental conditions. This makes the direct

experimental observation of nucleation difficult, given that the critical nucleus is small.

Models used to correct the limitations of CNT, either produce the same results or underestimate the barrier of nucleation. Nonetheless, others have been very successful giving improved agreement between theory and experiment.

CHAPTER III

STATE OF THE ART IN MOLECULAR SIMULATIONS

3.1 Statistical Mechanics

Statistical mechanics deals with the bulk properties of a system and tries to bridge the gap between simulations and experiments. It achieves this by expressing the bulk properties as a sum over the properties of the individual constituents.[61,62] Molecular simulations provide details such as the position and momentum of all particles within the system. With the help of statistical mechanics these properties are translated to macrostate properties through a set of state variables such as the number of particles, volume, and energy of the system. Statistical mechanics therefore allows for a connection between the microscopic states of a system and the macroscopic (observable) thermodynamic properties.[63] Let $\Gamma = \Gamma(q_i....q_{3N}; p_i...p_{3N})$ specify the microstate of a classical system of independent particles in equilibrium at time t. Γ will evolve in time in accordance with Newton's laws and the value of a particular thermodynamic quantity, A_{obs}, is considered to be the long time average of some analogous microscopic value $A(\Gamma)$, such that

$$A_{obs} = \langle A \rangle_{time} = \langle A(\Gamma(t)) \rangle_{time} = \lim_{t_{obs} \to \infty} \frac{1}{t_{obs}} \int_0^{t_{obs}} A(\Gamma(t)) dt \qquad (3.1)$$

The principles of statistical mechanics can be explained under two main headings: Lagrangian mechanics and Hamiltonian mechanics.[61,62] These will be presented in the subsequent sections together with the explanation/definition of some common terms in statistical mechanics.

3.1.1 Lagrangian Mechanics

Lagrangian mechanics provides a convenient way to study the trajectory of a system of particles in configuration space.[63–65] The Lagrangian is defined as

$$\mathcal{L} = \mathcal{T} - \mathcal{V} \tag{3.2}$$

where $\mathcal{T}$ is the kinetic energy of the system and $\mathcal{V}$ is the potential energy.

For a single particle in three dimensions, the Lagrangian in Cartesian coordinates can be written as

$$\mathcal{L}(\mathbf{x}, \dot{\mathbf{x}}) = \frac{1}{2}m\dot{\mathbf{x}}^2 - \mathcal{V}(\mathbf{x}) \tag{3.3}$$

where the bold characters indicate 3D vectors.

The trajectory of the system can be found by solving the Euler-Lagrange equation of motion for the system,[64]

$$\frac{\mathrm{d}}{\mathrm{d}t}\left(\frac{\partial \mathcal{L}}{\partial \dot{x}_i}\right) - \frac{\partial \mathcal{L}}{\partial x_i} = 0 \tag{3.4}$$

where $i = 1, 2, 3$ and indicates the three Cartesian directions.

By substituting in the Lagrangian, one gets

$$\frac{\partial \mathcal{L}}{\partial x_i} = -\frac{\partial \mathcal{V}}{\partial x_i} \tag{3.5}$$

and

$$\frac{\partial \mathcal{L}}{\partial \dot{x}_i} = \frac{\partial}{\partial x_i}\left(\frac{1}{2}m\dot{\mathbf{x}}^2\right)$$
$$= \frac{1}{2}m\frac{\partial}{\partial x_i}(\dot{x}_i\dot{x}_i)$$
$$= m\dot{x}_i$$

$$(3.6)$$

therefore

$$\frac{\mathrm{d}}{\mathrm{d}t}\left(\frac{\partial \mathcal{L}}{\partial \dot{x}_i}\right) = m\ddot{x} \tag{3.7}$$

Substituting Equation 3.5 and 3.7 into 3.4 gives

$$m\ddot{x}_i + \frac{\partial \mathcal{V}}{\partial x_i} = 0 \tag{3.8}$$

$$m\ddot{x}_i = -\frac{\partial \mathcal{V}}{\partial x_i} \tag{3.9}$$

Ignoring all i, one gets

$$m\ddot{\mathbf{x}} = -\nabla\mathcal{V} \tag{3.10}$$

Defining force $\mathbf{F}$ as

$$\mathbf{F} = -\nabla\mathcal{V} \tag{3.11}$$

implies that

$$\mathbf{F} = m\ddot{\mathbf{x}} \tag{3.12}$$

The use of scalars (T and V) in the Lagrangian formulation instead of vectors makes it simple.[65]

Hamiltonian Mechanics is an alternative theoretical formulation for describing a system. This has several advantages. Instead of requiring that the trajectory of the system be found by solving a series of second order differential equations, it defines the dynamics of the system with twice (6N) as many first order equations. The Hamiltonian formalism uses the idea of generalized coordinates $(q, \dot{q})$.[62,63] In some cases, like an isolated system of classical particles, normal Cartesian coordinates can be used as the generalized coordinates. The most general expression of the Lagrangian of a system in generalized coordinates is given by

$$\mathcal{L}(q_i, \dot{q}_i, t) = \sum_i \left(\frac{1}{2} m (\dot{q}_i)^2 - \mathcal{V}(q_i) \right) \tag{3.13}$$

The variation of Equation 3.13 with time is

$$d\mathcal{L} = \sum_i \left[\frac{\partial \mathcal{L}}{\partial q_i} dq_i + \frac{\partial \mathcal{L}}{\partial \dot{q}_i} d\dot{q}_i \right] + \frac{\partial \mathcal{L}}{\partial t} dt \tag{3.14}$$

This can be simplified by noting that

$$\frac{\partial \mathcal{L}}{\partial \dot{q}_i} = m\dot{q}_i = p_i \tag{3.15}$$

where p_i is the generalized momentum coordinate.

Substituting this expression into the Euler-Lagrange Equation 3.4 (written with generalized coordinates) and rearranging gives

$$\frac{\partial \mathcal{L}}{\partial q_i} = \dot{p}_i \tag{3.16}$$

Substituting Equation 3.15 and 3.16 into 3.14 yields

$$d\mathcal{L} = \sum_i [\dot{p}_i dq_i + p_i d\dot{q}_i] + \frac{\partial \mathcal{L}}{\partial t} dt \qquad (3.17)$$

Understanding that

$$p_i d\dot{q}_i = d(p_i \dot{q}_i) - \dot{q}_i dp_i \qquad (3.18)$$

and applying this in Equation 3.17, one gets

$$d\mathcal{L} = \sum_i [\dot{p}_i dq_i + d(p_i \dot{q}_i) - \dot{q}_i dp_i] + \frac{\partial \mathcal{L}}{\partial t} dt \qquad (3.19)$$

Finally, the derivative of the product can be moved to the left side of the equation, and multiplying both sides by -1 to arrive at

$$d\left(\sum_i p_i \dot{q}_i - \mathcal{L}\right) = \sum_i [-\dot{p}_i dq_i + \dot{q}_i dp_i] - \frac{\partial \mathcal{L}}{\partial t} dt \qquad (3.20)$$

The term in brackets on the left hand side of Equation 3.14 is defined as the Hamiltonian of the system, $\mathcal{H} = \mathcal{H}(q_i, p_i, t)$. The explicit time derivative is

$$d\mathcal{H} = \sum_i \left[\frac{\partial \mathcal{H}}{\partial q_i} dq_i + \frac{\partial \mathcal{H}}{\partial p_i} dp_i\right] + \frac{\partial \mathcal{H}}{\partial t} dt \qquad (3.21)$$

Comparing the terms of Equations 3.14 and 3.15, one gets Hamilton's equations

$$\frac{\partial \mathcal{H}}{\partial q_i} = -\dot{p}_i, \qquad \frac{\partial \mathcal{H}}{\partial p_i} = \dot{q}_i, \qquad \frac{\partial \mathcal{H}}{\partial t} = -\frac{\partial \mathcal{L}}{\partial t} \qquad (3.22)$$

For a system comprised of independent classical particles, i.e., in the absence of any external field, the Hamiltonian is just the total internal energy of the system.[61,63] Recall that the Hamiltonian is defined by a Legendre transformation of the Lagrangian

$$\mathcal{H} = \sum_i p_i \dot{q}_i - \mathcal{L} \tag{3.23}$$

where p_i is the one dimensional linear momentum for particle i, or mv_i, and m is the particle mass.

The term $\dot{q}_i$ is the velocity of the particle along the same dimension. The product of p_i and $\dot{q}_i$ can be written as mv_i^2 and the sum over all i yields twice the kinetic energy of the whole system, $2T$.[64] The Hamiltonian is thus

$$\mathcal{H} = 2\mathcal{T} - L = 2\mathcal{T} - (\mathcal{T} - \mathcal{V}) = \mathcal{T} + \mathcal{V} \tag{3.24}$$

The first of Hamilton's equations can now be used to obtain Newton's second law. In this system, $\mathcal{T} = \mathcal{T}(p)$ and $\mathcal{V} = \mathcal{V}(q)$, so one would have

$$\frac{\partial \mathcal{H}}{\partial q_i} = \frac{\partial \mathcal{V}(q_i)}{\partial q_i} = -\frac{d}{dt} p_i = -\frac{d}{dt}(mv_i) = -ma_i \tag{3.25}$$

Ignoring all i, one can write

$$\sum_i \frac{\partial \mathcal{H}}{\partial q_i} = \nabla \mathcal{V} = -\mathbf{F} = -m\mathbf{a} \tag{3.26}$$

which yields Newton's law upon dividing by -1

3.1.3   Phase Space Distribution and Liouville's Equation

When using the Hamiltonian formalism, the state of a system of N independent, classical particles at time t is specified by 3N generalized coordinates $(q_1...q_{3N})$ and momenta $(p_1...p_{3N})$ of the particles. The set of q and p accessible to the system describes the system's phase space. Because both p and q are functions of time, a phase space distribution can be defined, $\rho = \rho(q, p, t)$, which gives the probability that the system occupies each infinitesimal hypervolume element $(d^{3N}q \, d^{3N}p)$ of the phase space. Here, q and p represent the set of all 3N generalized coordinates and

momenta, respectively. While this distribution may change with time, no new states (i.e. points in the phase space) are ever created or destroyed.[66] The time evolution of the distribution must satisfy the continuity equation

$$\frac{\partial \rho}{\partial t} + \sum_{i=1}^{3N} \left(\frac{\partial(\rho \dot{q}_i)}{\partial q_i} + \frac{\partial(\rho \dot{p}_i)}{\partial p_i} \right) = S \tag{3.27}$$

where S is the rate at which new states are created and thus is equal to zero.

Applying the chain rule for the derivation of the products, one gets

$$\frac{\partial \rho}{\partial t} + \sum_{i=1}^{3N} \left(\frac{\partial \rho}{\partial q_i} \dot{q}_i + \frac{\partial \rho}{\partial p_i} \dot{p}_i + \rho \frac{\partial \dot{q}_i}{\partial q_i} + \rho \frac{\partial \dot{p}_i}{\partial p_i} \right) = 0 \tag{3.28}$$

Via Hamilton's equations, $\dot{q}_i$ and $\dot{p}_i$ can be replaced in the last two terms of the sum to get

$$\frac{\partial \rho}{\partial t} + \sum_{i=1}^{3N} \left(\frac{\partial \rho}{\partial q_i} \dot{q}_i + \frac{\partial \rho}{\partial p_i} \dot{p}_i + \rho \frac{\partial}{\partial q_i} \frac{\partial \mathcal{H}}{\partial p_i} + \rho \frac{\partial}{\partial p_i} \left(\frac{-\partial \mathcal{H}}{\partial q_i} \right) \right) = 0$$

$$\frac{\partial \rho}{\partial t} + \sum_{i=1}^{3N} \left(\frac{\partial \rho}{\partial q_i} \dot{q}_i + \frac{\partial \rho}{\partial p_i} \dot{p}_i + \rho \frac{\partial^2 \mathcal{H}}{\partial q_i \partial p_i} - \rho \frac{\partial^2 \mathcal{H}}{\partial p_i \partial q_i} \right) = 0 \tag{3.29}$$

Because the partial derivatives are equal, the last two terms will cancel out for each i to afford

$$\frac{\partial \rho}{\partial t} + \sum_{i=1}^{3N} \left(\frac{\partial \rho}{\partial q_i} \dot{q}_i + \frac{\partial \rho}{\partial p_i} \dot{p}_i \right) = 0 \tag{3.30}$$

This equation is the total time derivative of $\rho(q, p, t)$, so it can be simplified to

$$\frac{d\rho(q, p, t)}{dt} = 0. \tag{3.31}$$

This is Liouville's equation which essentially asserts the conservation of phase

space density. The special case which occurs for conservative and isolated systems where $\frac{\partial \rho}{\partial t} = 0$, is of particular importance to this work. Here, the phase space distribution for the system is not explicitly dependent on time but is stationary. Equation 3.30 becomes

$$\sum_{i=1}^{3N} \left(\frac{\partial \rho}{\partial q_i} \dot{q}_i + \frac{\partial \rho}{\partial p_i} \dot{p}_i \right) = 0 \tag{3.32}$$

one solution to which is the famous Maxwell-Boltzmann distribution

$$\rho \propto exp(-\frac{\mathcal{H}}{kT}) \tag{3.33}$$

3.1.4 Ensembles, Ergodicity, and Thermodynamics

As mentioned above, a given system of classical particles (distinguishable, non–relativistic) is defined by the accessible phase. The set of all points in this phase space (each one of which represents a unique state of the system) is called an *ensemble*. The statistical properties of an ensemble are described by its normalized phase space distribution. The normalization factor for the distribution is called the partition function, and provides the thermodynamic potential which connects statistical (microscopic) and classical (macroscopic) thermodynamics.[66–68] There are a number of commonly used ensembles, each characterized by different fixed macroscopic quantities of a system, like the microcanonical ensemble, with N, V, and E fixed, the canonical wherein N, V, and T are constant, and the isobaric-isothermal that has N, P, and T fixed. The quantities N, V, E, T, and P, refer to the number of particles, volume, total internal energy, temperature, and pressure respectively. The relevant aspects of the different ensembles, including the phase space distribution, partition function, and appropriate thermodynamic potential, will be discussed briefly in the next section.

3.1.4.1 Microcanonical Ensemble, NVE

The microcanonical ensemble describes a thermally isolated system where the number of particles (N) and the volume they occupy (V) remain fixed.[61,62] Because the system is thermally isolated, it will not exchange energy with an external environment and the Hamiltonian will remain fixed as well. The phase space density for the microcanonical ensemble is

$$\rho_{NVE} \propto \delta(\mathcal{H}(q,p) - E) \tag{3.34}$$

where δ is the Dirac delta function.

The Hamiltonian is not explicitly time dependent because the distribution is stationary. The probability of finding the system in a randomly chosen state is zero for those values of $\mathcal{H} \neq E$ and it is equal for all other states. The notion that an isolated system in equilibrium is found with equal probability in all of its accessible microstates is called the equal *a priori* probability postulate and is one of the cornerstones of statistical mechanics.[69] A normalization factor is needed to ensure that the probability of finding the system *anywhere* in phase space is equal to one. This normalization factor is called the partition function and is essentially a sum over states

$$Q_{NVE} = \int \delta(\mathcal{H}(q,p) - E)d^{3N}q\,d^{3N}p \tag{3.35}$$

For the microcanonical ensemble, the partition function is simply the number of microstates accessible to the system. Since the statistical entropy of a system is a function of the number of microstates,

$$S = k_B \ln Q_{NVE} \tag{3.36}$$

where k_B is Boltzmann's constant.

Equation 3.36 is the thermodynamic potential that provides the link between the microscopic states of a system in the microcanonical ensemble and its bulk thermodynamic properties. Additional properties are derived through classical thermodynamic relationships between the fixed parameters and the entropy.[66]

3.1.4.2 Canonical Ensemble, NVT

The canonical ensemble describes a system with NVT fixed. The phase space distribution and partition function for the canonical ensemble are typically arrived at by considering two systems: the system of interest or concerned, which is designated C, and a much larger system R.[61,62] These two systems are subject to the constraints

$$
\begin{aligned}
C &\ll R \\
E_T &= E_C + E_R
\end{aligned}
\tag{3.37}
$$

where E_T is the total energy, E_C is the energy of the system and E_R that of the larger system which will be called the reservoir.

Because the system and reservoir can be considered as being independent, the number of states possible (Ω) for the entire system is given by

$$
\Omega_{C+R} = \Omega_C \Omega_R
\tag{3.38}
$$

If a particular microstate, i, of the system with energy E_i is chosen, then $E_R = E_T - E_i$. The probability of finding the system at this state can be expressed by considering the total number of states possible in R with C at energy E_i divided by the sum of the total number of states for the reservoir for all possible values of E_i. This can be expressed as

$$p_i = \frac{1 \times \Omega_R(E_T - E_i)}{\sum_j \Omega_R(E_T - E_j)} \qquad (3.39)$$

The denominator is the canonical partition function, sum over all possible energy levels of the system, with each energy level supported by multiple states. It should be noted that in a system of classical particles, the available energy levels are continuous, and the positions and momenta of the particles themselves are continuous. Therefore both the denominator and numerator would need to be coarse grained and the given expressions replaced with an equivalent integral formulation.[61,62] For clarity, however, one can continue assuming that the system can be described by discrete and countable states, and provide the corresponding integral expression at the end. Now, entropy relates to the number of microstates by Equation 3.36 which can be re-written here using Ω

$$S = k_B ln(\Omega) \qquad (3.40)$$

Solving for Ω gives

$$\Omega = e^{\frac{S}{k_B}} \qquad (3.41)$$

Substituting this into Equation 3.33 and adding subscripts to differentiate our systems and energy levels yields

$$P_i = \frac{1 \times \exp(\frac{S_R(E_T - E_i)}{k_B})}{\sum_j \exp(\frac{S_R(E_T - E_j)}{k_B})} \qquad (3.42)$$

This is rather cumbersome and can be made simpler via an appeal to the first law of thermodynamics which provides the relationship between entropy, temperature and energy:

$$dE = TdS - PdV \qquad (3.43)$$

Where E is the total internal energy of the system, T temperature, and P the pressure.

In the canonical ensemble, the volume is fixed and so the last term vanishes. Integrating both sides of the resulting differential equation and solving for S with limits 0 to T and 0 to S for the temperature and entropy respectively, yields

$$S = \frac{E}{T} \tag{3.44}$$

Substituting this into Equation 3.42 gives

$$P_i = \frac{1 \times e^{\frac{E_T - E_i}{k_B T}}}{\sum_j e^{\frac{E_T - E_j}{k_B T}}} \tag{3.45}$$

Introducing the inverse temperature, $\beta = \frac{1}{k_B T}$

$$P_i = \frac{1 \times e^{\beta(E_T - E_i)}}{\sum_j e^{\beta(E_T - E_j)}} \tag{3.46}$$

Since E_T is a constant, it can factor out of both the numerator and denominator to give

$$P_i = \frac{1 \times e^{-\beta E_i}}{\sum_j e^{-\beta E_j}} \tag{3.47}$$

Notice that the probability as given here does not depend on the total energy of the combined system, but only on the specific energy of the smaller system that is immediately being considered. Thus, for system $\mathcal{C}$, the probability of finding it in state i is proportional to $e^{-\beta E_i}$, which means

$$\rho \propto e^{-\beta E_i} \propto e^{-\frac{\mathcal{H}_i}{k_B T}} \tag{3.48}$$

and the partition function is

$$Q_{NVT} = \sum_j e^{-\beta E_j} = \sum_j e^{-\frac{\mathcal{H}_j}{k_B T}} \tag{3.49}$$

Recall however that this formulation assumes countable energy levels. For a system of particles with continuous energy levels the partition function becomes

$$Q_{NVT} = \int e^{-\frac{\mathcal{H}(q,p)}{k_B T}} d^{3N}q \, d^{3N}p \tag{3.50}$$

The relevant thermodynamic potential in the canonical ensemble is the Helmoltz free-energy, $\mathcal{A}$

$$\mathcal{A} = -k_B T \ln Q_{NVT} \tag{3.51}$$

3.1.4.3 Isothermal-Isobaric Ensemble, NPT

The isothermal-isobaric (NPT) ensemble is a statistical mechanical system that maintains constant temperature and pressure in addition to the number of particles. In this ensemble, the energy and volume of the system are allowed to fluctuate. It is important for clear definitions of thermodynamic states of a simulated system and permits direct comparison with experiments.[70] The NPT ensemble has been extensively used with MC considered the method of choice for processes that require long relaxation time such as phase transition.[71] As a result, the NPT ensemble is said to be the natural ensemble for the study of first order phase transitions that involve drastic change in the density of the system.[72]

The NPT ensemble can be construed as a modification of the canonical (NVT) ensemble by replacing volume with pressure. As such the NPT partition function is defined in terms of the canonical partition function rather than the basic microcanonical (NVE) ensemble. Consider a system in contact with an infinitely large energy and volume reservoir, then the probability that the system is in a microstate m is given by:

$$
\begin{aligned}
\wp_m \quad &\propto \quad \Omega_B(E_B, V_B) \\
&\propto \quad \Omega_B(E_T - E_m, V_T - V_m) \\
&\propto \quad \exp[S_B(E_T - E_m, V_T - V_m)/k_B]
\end{aligned}
\tag{3.52}
$$

where V_T and E_T are the total and constant volume and energy respectively. Applying Taylor's expansion on Equation 3.52 gives

$$
\wp_m \quad \propto \quad \exp\left[\frac{S_B(E_T, V_T)}{k_B} - \frac{E_m}{k_B}\frac{dS_B(E_T, V_T)}{dE_B} - \frac{V_m}{k_B}\frac{dS_B(E_T, V_T)}{dV_B} + ...\right]
\tag{3.53}
$$

Treating the first term in the exponential as a constant since it is independent of m and simplifying the derivatives of the entropy base on its relation to temperature and pressure results to

$$
\wp_m \propto \exp\left[-\beta E_m - \beta P V_m\right]
\tag{3.54}
$$

The probability normalization factor isothermal-isobaric partition can now be introduced to give

$$
\wp_m = \frac{\exp\left[-\beta E_m - \beta P V_m\right]}{\Delta(NPT)}
\tag{3.55}
$$

$$
\Delta(NPT) = \sum_V \sum_{\text{all n at } V,N} \exp\left[-\beta E_n - \beta P V\right]
\tag{3.56}
$$

where the first sum is over all possible volumes of the system while the second sum is over all microstates at constant V and N. Also notice that the $\Delta(NPT)$ is a

function of N, P, and T only since the volume varies.

Thus if the pressure term is factored out from the second sum equation 3.56 becomes;

$$\Delta(NPT) = \sum_V \exp\left[-\beta PV\right] \sum_{\text{all n at } V,N} \exp\left[-\beta E_n\right] \tag{3.57}$$

Recognize that the second sum is the canonical partition function. Changing the first sum to an integral with respect to the volume of all possible microstaes leads to the expression of the isothermal-isobaric partition.

$$
\begin{aligned}
\Delta_{NPT} &= \int_0^\infty e^{-\beta PV} Q_{NVT} dV \\
&= \frac{1}{\Lambda(T)^{3N} N!} \int_0^\infty e^{-\beta PV} Z_{NVT} dV
\end{aligned}
\tag{3.58}
$$

where Z represent the configurational integral of the system.

The corresponding thermodynamic potential in the isothermal-isobaric ensemble is the Gibbs free energy G.

$$G_{NPT} = -\frac{1}{\beta} ln\Delta(NPT) \tag{3.59}$$

In a MC simulation, fluctuation in energy is accomplished through particles displacement (same as in the NVT ensemble) while volume fluctuation is achieved by using volume scaling moves. For a given volume change ΔV the new volume is given by $V \leftarrow V + \Delta V$. For the study of phase coexistence, the volume fluctuations near the critical point can be large as the system move between both phases. In this case the log-volume scaling moves are used where the change in volume $\Delta V = ln\Delta V$. However after each volume change, the volume-dependent long range corrections must be recalculated.

The ergodic hypothesis is important because like statistical mechanics, it provides a second link between microscopic and macroscopic states of a system. An ergodic system is one with a stationary distribution ($\frac{\partial \rho}{\partial t} = 0$) that will sample all of its accessible phase space (regions where $\rho_{ens}(\Gamma)$ is non-zero) before ever repeating a state. Although ergodicity is difficult to prove for all but the simplest of mechanical systems, it is almost always assumed to be true-based in part on Liouville's theorem and the equal *a priori* probability postulate of statistical mechanics. If a system is ergodic, the time average of $A(\Gamma)$ as $t \to \infty$, or even as t approaches the Poincaré recurrence time (the time taken to complete one cycle through phase space) will be identical to the ensemble average of $A(\Gamma)$.[73]

$$\langle A \rangle_{ens} = \int A(\Gamma)\rho_{ens}(\Gamma)d\Gamma = \langle A \rangle_{time} = A_{obs} \qquad (3.60)$$

where $\langle A \rangle_{ens}$ indicates the ensemble average and $\rho_{ens}(\Gamma)$ the normalized probability density.

In general, the relationship between $\rho_{ens}(\Gamma)$ and the partition function Q_{ens} for a particular ensemble is

$$\rho_{ens}(\Gamma) = Q_{ens}^{-1} w_{ens}(\Gamma) \qquad (3.61)$$

where $w_{ens}(\Gamma)$ properly weights each value of Γ and for each ensemble it is the function proportional to ρ (i.e., Equation 3.42) such that

$$Q_{ens} = \int d\Gamma w_{ens}(\Gamma) \qquad (3.62)$$

The left piece of Equation 3.60 can be rewritten as

$$\langle A \rangle_{ens} = \int \frac{w_{ens}(\Gamma)A(\Gamma)}{\int w_{ens}(\Gamma)d\Gamma} d\Gamma \qquad (3.63)$$

The use of computer simulations to establish the properties of systems, can therefore be seen as a process of computing the average value of a given ensemble's relevant thermodynamic potential. Using this and other thermodynamic properties that are fixed in defining the ensemble, other thermodynamic quantities of interest can be calculated. Because of the direct relationship between the partition function and this thermodynamic potential in each ensemble, the work of simulation becomes the of estimating the partition function. This can be done either by letting the system evolve over some long enough timescale via MD simulation or by suitably sampling the phase space of the ensemble via MC techniques.[66]

3.2   Simulation Methods

Molecular Dynamics (MD) and Monte Carlo (MC) are two practically independent techniques. However, limitations of each method sometimes makes one suitable for a particular task over the other. They are both limited to the study of relatively small systems (on the order of 1000 particles or less). MD studies different systems as a function of time, typically in the order of 100 picoseconds. But for small systems, using restricted force fields, a time scale of up to 100 nanoseconds can be attained.[74] It is designed to work best in the microcanonical (NVE) ensemble. Consequently simulations in other ensembles such as the canonical (NVT), grand canonical (μVT) etc., cannot be performed with pure MD. In such situations, a combination of MD with other techniques can be used or it is replaced with MC. Conversely, MC can be employed to study many different ensembles such as NVT, μVT, isobaric-isothermal (NPT) ensembles but is not suitable for systems in the NVE ensemble. MD, on the other hand, gives details about the trajectory of the system, which is not possible with MC since it is a random (stochastic) technique.[61,62] A combination of both methods known as the used Hybrid Monte Carlo (HMC) has also been widely used in molecular modeling. HMC has been largely employed in the projects conducted for this dissertation and to a limited extent MC. In this chapter, the different simulation methods are discussed together

with some sampling techniques used to aid various simulations in sampling rare events accurately.

3.2.1 Molecular Dynamics

An MD simulation seeks to follow the trajectory of a system as it evolves over time via Newton's laws. If the state of an isolated system of N particles is specified by $q = (\mathbf{q}_1...\mathbf{q}_N)$ and $p = (\mathbf{p}_1...\mathbf{p}_N)$ where $\mathbf{q}_1$, $\mathbf{p}_1$ represent the 3-dimensional generalized position and momenta vectors associated with particle 1, then the Hamiltonian $\mathcal{H}(q,p)$ is

$$\mathcal{H}(q,p) = \mathcal{T}(p) + \mathcal{V}(q) \tag{3.64}$$

and Hamilton's equations are

$$\frac{\partial \mathcal{V}}{\partial q} = -\dot{p} \quad \text{and} \quad \frac{\partial \mathcal{T}}{\partial p} = \dot{q} \tag{3.65}$$

Using Cartesian coordinates ($\mathbf{r}$) in place of the generalized position coordinates and considering the ith particle, we have

$$-\nabla_{r_i} \mathcal{V} = \dot{\mathbf{p}_i} = \mathbf{f}_i \tag{3.66}$$

where $\mathbf{f}_i$ represents the force on the ith particle.
The evolution of the system is monitored by 3N first order differential equations.

For even smaller systems (N>3) in three dimensions, finding the exact solution of the system of differential equations is daunting task. Instead, simulations rely on numerically approximated solutions for solving this problem. Given a set of initial conditions for the system (q and p specified at t_0), the forces on each particle are calculated via Equation 3.66. This force is used to determine the instantaneous acceleration on each particle by

$$\mathbf{a}_i = \frac{\mathbf{f}_i}{m_i} \tag{3.67}$$

where the force and the acceleration are assumed to be constant over some short time interval, δt.

New positions and momenta of each particle at $t + \delta t$ are calculated and the system is advanced to the new point in phase space. The process is then repeated using the new configuration. This 'step-by-step' advancement of the system is ideally carried out using an algorithm that provides a step-wise trajectory through phase space that closely matches the actual (continuous) trajectory to a desired degree of accuracy. Before an algorithm is applied to a system that is not exactly solvable, it is tested on an analytically solvable system. There are several solvable two-dimensional systems that have been well studied[66] and are often used for this purpose. As a result, a host of schemes for integrating the equations of motion have been developed, including predictor-corrector algorithms, the Verlet algorithm, the leap frog, and the velocity-Verlet, discussed in detail below. In addition to closely approximating the true trajectory of a system, an integration scheme must also satisfy two important criteria, area preservation and time reversibility.

For isolated systems at equilibrium (where there is no explicit time dependence in the Hamiltonian), the Hamiltonian, which represents the total energy of the system, is a constant of motion. This result can be seen by considering the total time derivative of the Hamiltonian, $\mathcal{H}(q, p)$

$$\begin{aligned} \frac{d\mathcal{H}}{dt} &= \frac{\partial \mathcal{H}}{\partial q}\dot{q} + \frac{\partial \mathcal{H}}{\partial p}\dot{p} \\ &= \frac{\partial \mathcal{H}}{\partial q}\left(\frac{\partial \mathcal{H}}{\partial p}\right) + \frac{\partial \mathcal{H}}{\partial p}\left(-\frac{\partial \mathcal{H}}{\partial q}\right) \\ &= 0 \end{aligned} \tag{3.68}$$

Because $\mathcal{H}$ remains constant, the phase space that is accessible to the system must

remain constant as well, this is referred to as area preserving.[61,63] Any algorithm used to advance the system through time must do so in a way that neither increases nor diminishes the total energy (and thus the accessible phase space) of the system. Actual trajectories of systems are also time reversible. Systems evolve in such a way that each point in phase space is on exactly one trajectory through that space. By reversing the sign of t in the equations of motion, the exact trajectory is traced out in reverse. The analogy for a system of discrete sates is that each state (at say, $t = 0$) leads to exactly one future state (at $t = 1$). Going backwards in time must necessarily return to this original state.[61–63] An algorithm for which such a time reversal led to a state point that was different than the original, would indicate that two initial state points produced the same future state point - which would mean that 1) the system was not ergodic and 2) area preservation was violated.

Considerations for MD are numerous. To begin with, δt must be chosen based on balancing computational expense and simulation accuracy. δt is usually very short, much smaller than the time it takes individual molecules or atoms to move their own length,[66] but because classical systems are theoretically continuous, it is not bound by a lower limit. The smaller the time over which the potential (and thus the forces and accelerations) are assumed constant, the greater the accuracy with which the step-wise produced trajectory of the system match it's actual trajectory through phase space. The trade-off for choosing a small δt, however, is a greater computational expense required to explore the same phase space. Even when the goal of the simulation is not to obtain a thorough exploration of a system's phase space but rather a study of part of the trajectory itself, a similar trade off exists in terms of the cost per *length* of trajectory studied.[61–63] Choice of an algorithm is thus based on the following considerations:

1. It is area preserving

2. It is time reversible

3. It is accurate (as needed) for long δt

Simulations in this dissertation use the Velocity Verlet Algorithm to integrate the equations of motion. It is chosen for its area preserving and time reversible properties. It advances the positions and velocities of the system's particles using both full time steps (for positions) and half time-steps (for velocities). The details are as follows:

1. The position of the particles at time t are known.

2. The velocities of the particles at time t are known.

3. The particles' positions at time $t + \delta t$ are found by

$$\vec{r}_i(t + \delta t) = \vec{r}_i(t) + \vec{v}_i(\delta t)\delta t + \vec{a}_i\frac{1}{2}(\delta t) \tag{3.69}$$

   where $\vec{a}_i$ is found from Equation 3.66 and 3.67.

4. The velocity at half time-step is calculated from

$$\vec{v}_i(t + \frac{\delta t}{2}) = \vec{v}_i(t) + \frac{\vec{a}_i\delta t}{2} \tag{3.70}$$

   This essentially provides updated positions that are accurate to the degree that the velocities at the mid-point of the time step approximates the average velocities over the entire time step.

5. The forces and accelerations at $t + \delta t$ can be computed via Equation 3.66 and 3.67.

6. The new positions and the velocity at $t + \delta t$ are found by

$$\vec{v}_i(t + \delta t) = \vec{v}_i(t + \frac{1}{2}\delta t) + \vec{a}_i(t + \delta t)\left(\frac{1}{2}\delta t\right). \tag{3.71}$$

Molecular Dynamics simulations can be used effectively to study the behavior of systems in isolated systems far from equilibrium. In such cases, solutions to the

equations of motion provided by the chosen integration scheme provide a system trajectory that can then be studied. Typically, concerns about the assumption of ergodicity are less important here, as the initial conditions are chosen to ensure that the relevant phase space is explored. An example of MD thus applied is found in early research on the formation of fullerenes (C_{60}).[75] In the study, a system of 500 carbon atoms was evolved using the Brenner empirical bond-order potential (which will be discussed in detail later) and the Verlet algorithm (with a 0.5 femto-second (fs) time-step) for integration. Because the actual time scale for formation of C_{60} is in the order of a second, simulation of the entire process was not feasible as it would have required more than 10^{15} time-steps, each step in turn requiring the calculation of the gradient of a rather complicated potential function dependent on the position of 500 atoms. The researchers used several techniques to effectively 'compress' time - namely increasing the effective density of the simulation cell to promote interactions between the particles and adopting an 'annealing' strategy by which the simulation temperature was decreased at an artificial rate to mimic the cooling that actually happens at a longer time scale. After several simulations using different starting temperatures and annealing strategies, the researchers obtained results which demonstrated the formation of nearly closed cage-like clusters up to C_{70} in size. The larger of these structures were then traced backwards in time to provide clues as to the important dynamical aspects that led to their formation.

For a suitably small system at equilibrium, MD can also be used to determine statistical information about a particular ensemble described. Care must be used in describing such a system. The validity of the results depends on the system's assumed ergodicity and the notion that the calculated distribution (over the course of the simulation) of the parameter(s) to be studied will approximate the ensemble distribution. It is important to remember that evolution of a system governed by Newton's laws in the absence of an external field ($\mathcal{H}$ does not explicity depend on t) takes place entirely within the microcanonical (NVE) ensemble because of Equation 3.68. Study within the microcanonical ensemble is therefore relatively

straightforward. For example, the potential energy distribution of any isolated system at equilibrium could be derived via MD if the simulation ran long enough to generate enough system configurations to be representative of the ensemble as a whole. An example of generating a system average outside of the microcanonical comes from the work done by Even et al.[76] on the dynamics of noble gases encapsulated in fullerenes. The research entailed a number of MD simulations, each comprised of a single noble gas atom (Helium, Neon, Argon, Krypton, and Xenon) placed at the center of a fully formed C_{60} molecule. Each simulation was carried out in the canonical NVT ensemble and the potential was a combination of the Brenner empirical bond order potential and the Lennard-Jones potential (with mixed interaction parameters obtained by using the Lorentz-Berthelot mixing rules) to describe the carbon-carbon and carbon-noble gas interactions, respectively. Again the Verlet algorithm was used for integration and δt was 0.5 fs with a total simulation time of 500 picoseconds (ps), and five different temperatures, ranging from 160 K to 800 K, were simulated for each noble gas species. For each configuration, the distance between the central atom and the center of mass of the cage was calculated and the corresponding radial distribution function determined. In addition, carbon atom bond angle data was recorded and the bond angle distribution determined. The first of these distributions provides clues as to the role of the central atom's size (Van der Waals radius) in interactions between it and the cage itself, while the second gives information about stresses on the cage itself.

In this latter example, a thermostat is required in order to ensure that the system remains at a constant temperature as the simulation progresses. There are many types of thermostats that are typically used in NVT MD - each of which essentially ensures that the total kinetic energy of the system bears a particular relationship to the kinetic energy distribution that defines the fixed temperature in question. In the case of the above work, a technique called velocity rescaling was used to rescale the velocity of the central atom whenever the total kinetic energy of the system deviated from the average kinetic energy specified by the temperature at

which the simulation was being run.

One problem faced by MD simulations seeking to explore a representative phase space is that they are sometimes very dependent on initial conditions, particularly for large systems. If a randomized choice of initial state starts the system in a region of phase space that contributes little towards the average of the thermodynamic quantity of interest, repeated runs might not produce consistent results nor ones that are in agreement with known parameters of the system. In addition, if the system's phase space contains bottlenecks or cyclic trajectories an MD simulation beginning in such a regime will not be able to provide a representative sample of the ensemble, even when everything else is working flawlessly.[66] The technique to which we now turn provides an alternative method for estimating thermodynamic averages (via the partition function) that is not hampered by these considerations.

3.2.2   Monte Carlo Simulation

Monte Carlo simulation for a system of N particles uses an algorithm to randomly choose a string of 'states', Γ (where $\Gamma = \Gamma_{\mathbf{q,p}}$, with $\mathbf{q}=\vec{q}_1...\vec{q}_N$ and $\mathbf{P}=P_1...P_N$ in the phase space (domain) of a system based on a probability distribution. Quantities of interest are calculated for each of these points (which represent individual microstates accessible to the system). The averages of these quantities converge to the actual values of their corresponding thermodynamic parameters, with an error that diminishes with increasing N. Because of the *equal a priori probability of states* hypothesis of statistical mechanics, in its simplest application to certain molecular systems (for example those in the microcanonical ensemble), the probability distribution which governs the random sampling is uniform. Equilibrium values for the quantities of interest will be 'supported' by the greatest number of states, however, which will ensure the convergence described.

In practice, there are drawbacks to using the above method. In even a simple system of 100 particles in three dimensions, the size of the domain is typically so

large that the number of configurations that need to be sampled can quickly become computationally prohibitive. Most modern MC simulations therefore use some type of importance sampling. In this method, the random generation of configurations is based on the importance of each configuration to the value of the overall integral (remember the goal here is essentially that of estimating the value of the partition function of the system). The partition function is thought of as a weighted distribution (of integral contributions) of the accessible states, $\rho(\Gamma)$. If we are seeking the thermodynamic average of some quantity $\mathcal{A}(\Gamma)$, one can write

$$\langle\mathcal{A}\rangle_{ens} = \int \mathcal{A}(\Gamma)\rho_{ens}(\Gamma)\mathrm{d}\Gamma \qquad (3.72)$$

where $\rho(\Gamma)_{ens}$ is the probability distribution for the ensemble.

As mentioned, simply sampling the phase space randomly is undesirable - a great many configurations will provide little or no contribution to the integral. If we instead sample based on the weighted distribution, we obtain

$$\langle\mathcal{A}\rangle_{ens} = \left\langle \frac{\mathcal{A}(\Gamma)\rho_{ens}(\Gamma)}{\rho(\Gamma)} \right\rangle_{\tau} \qquad (3.73)$$

where τ is used to indicate the total number of trial states.

The widely used Metropolis method makes use of the fact that for most systems, in obtaining the thermodynamic parameters of interest, the biggest contributions to the integral come from states that are also the most probable. It chooses $\rho(\Gamma) = \rho_{ens}(\Gamma)$ to yield

$$\langle\mathcal{A}\rangle_{ens} = \langle\mathcal{A}\rangle_{\tau} \qquad (3.74)$$

In other words, we seek to generate (randomly) a chain of states, each member of which occurs with the the appropriate probability. This is accomplished by producing a Markov chain which has the equilibrium distribution of the ensemble, $\rho_{ens}(\Gamma)$, as its limiting distribution.

3.2.2.1 Markov Chains and the Metropolis method

A Markov chain is produced by the following conditions: each trial move must produce a state which is a member of a finite set of outcomes (in our case the phase space of the system being considered); and the move to each state must only be dependent on the state immediately preceding it. If we label the ith state Γ_i, then we can define the probability that the chain will move from state n to state m (called the transition probability) as π_{mn}. Any probability distribution, $\rho(\Gamma)$ satisfying the condition of detailed balance (also known as the condition of microscopic reversibility), also satisfies the relation

$$\rho_m \pi_{mn} = \rho_n \pi_{nm} \tag{3.75}$$

where ρ_m gives the probability of being in Γ_m as a stationary distribution for the Markov chain.

If operating in the canonical ensemble, for example, we therefore want $\rho(\Gamma)$ to be

$$\rho(\Gamma) = \frac{e^{-\frac{\mathcal{H}(\Gamma)}{k_B T}}}{\int e^{-\frac{\mathcal{H}(\Gamma)}{k_B T}} \, d\Gamma} \tag{3.76}$$

or

$$\rho(\Gamma) = \frac{e^{-\frac{\mathcal{H}(\Gamma)}{k_B T}}}{Q_{NVT}} \tag{3.77}$$

The solution to Equation 3.75 that provides the transition probability for this choice of ρ is given by

$$\pi_{mn} = \alpha_{mn} \quad \text{for } \rho_n \geq \rho_m \quad m \neq n$$

$$\pi_{mn} = \alpha_{mn} \left(\frac{\rho_n}{\rho_m} \right) \quad \text{for } \rho_n \leq \rho_m \quad m \neq n$$

$$\pi_{mm} = 1 - \sum_{n \neq m} \pi_{mn} \qquad\qquad m = n \qquad\qquad (3.78)$$

where π_{mm} ensures that it is possible for the system to remain in the same state and α_{mn} is a symmetrical stochastic matrix[66] that provides the probability that a particular move is attempted.

These rules are referred to as the acceptance criteria and for our example in the canonical ensemble would typically be written as

$$acc \; o \to n = min \left[1, \frac{\dfrac{e^{-\frac{\mathcal{H}(\Gamma_n)}{k_B T}}}{Q_{NVT}}}{\dfrac{e^{-\frac{\mathcal{H}(\Gamma_o)}{k_B T}}}{Q_{NVT}}} \right] \qquad (3.79)$$

which gives the probability of acceptance of a trial move from an old configuration to a new configuration as the minimum of two functions. It simplifies to

$$acc \; o \to n = min \left[1, \frac{e^{-\frac{\mathcal{H}(\Gamma_n)}{k_B T}}}{e^{-\frac{\mathcal{H}(\Gamma_o)}{k_B T}}} \right] \qquad (3.80)$$

and, is conveniently independent of Q_{NVT}. In general, the Metropolis acceptance criteria for a simulation in an ensemble with an equilibrium distribution is

$$\rho_{ens} = \frac{\sigma_{ens}}{Q_{ens}} \qquad (3.81)$$

where σ_{ens} the unnormalized distribution (which typically is known *a priori*) is thus

$$acc \; o \to n = min \left[1, \frac{\sigma_n}{\sigma_o} \right] \qquad (3.82)$$

In essence, any trial move will be accepted if the new configuration is more

64

probable (or equivalently in the canonical ensemble when it has less total energy, $\mathcal{H}$) than the old configuration. When the new configuration is less probable, it will be accepted with a probability equal to the ratio between the new and old probabilities. To create the Markov chain then, a sample simulation proceeds as follows:

1. For a given system, a random point in phase space is chosen. This is Γ_1

2. Based on the defining distribution of the system, $\sigma(\Gamma_1)$ is determined

3. A randomly selected particle is moved a randomly selected distance, as determined by α, to generate $\Gamma_{2\,trial}$

4. $\sigma(\Gamma_{2\,trial})$ is calculated and the acceptance criteria applied to the attempted move

5. If the minimum is 1, the move is accepted and Γ_{2trial} becomes Γ_2

6. Otherwise a randomly generated number between 0 and 1 is compared to $\frac{\sigma(\Gamma_{2\,trial})}{\sigma(\Gamma_1)}$. If the number is less than the ratio the move is accepted as above. If it is greater than the ratio, it is rejected

7. In the case of a rejected trial move, the system remains at the same point in phase space and $\Gamma_{2\,trial}$ becomes Γ_2

The Monte Carlo technique based on Metropolis type acceptance criteria (also known as Boltzmann sampling) is one of the most widely used techniques in molecular simulation.[77] In particular, it allows for relatively quick determination of average values for system parameters which are dependent only on particle positions in the canonical ensemble. It enables researchers to predict likely conformations of complex molecules (such as protein chains).

MC simulation also forms the foundation for the process of simulated annealing,[78] which seeks to predict the configurational structure of systems that form through cooling. An example is provided by the work of Tomanek, *et al.*,

which examines the growth regime of carbon clusters.[79] The work uses a standard MC approach with Metropolis acceptance criteria in the NVT ensemble. However, rather than seeking to adequately explore regions of relevant phase space, it simply allows the random downhill walks in potential energy to produce more stable configurations. After some specified time, the configuration is stored and used as the initial configuration for a second simulation at a reduced temperature. The process continues until the effective temperature is zero and thus the particle positions are essentially fixed in the configuration of (approximately) absolute lowest energy for the system.

One drawback of MC comes from this trend towards areas of high density (probability) phase space. It cannot be effectively used (without modification) to explore regions of phase space which represent states that are unlikely for a given system in equilibrium, or to probe high energy states.[80] As such, if used to study a system where there were regions of phase space separated by an energy barrier (for example a liquid and vapor at coexistence) it would make the simulation extremely sensitive to initial conditions. The simulation would remain in the bulk phase in which it begins and leave a large area of phase space unexplored. This difficulty can be overcome, however, by adapting the MC scheme to sample uniformly along some chosen physical parameter,[81] such as density. There are several ways to accomplish uniform sampling, one of which is the recently developed Wang-Landau method[82] which is used here and is discussed in detail below. Many additional problems faced by straight MC sampling have been overcome by combining certain facets of MC with other techniques, including MD. In fact, most studies adapt the relevant principles of both MD and MC in such novel and specific ways that makes most simulation details unique.

3.2.3   Hybrid Monte Carlo Method

HMC was originally developed for Quantum Chromodynamics (QCD). It is now proposed as a method to improve the traditional Markov Chain Monte Carlo

(MCMC) algorithm.[83] However, the theoretical understanding of the phenomenon is limited and, as such, it is not very popular in statistical applications. HMC involves globally updating the MC algorithm by introducing momenta conjugate to the system coordinate variables followed by MD integration of the associated Hamiltonian equations of motion to generate new coordinates of the system.[84]

HMC is known to allow for partial momentum updates to keep more dynamic information between Monte Carlo steps. This requires a momentum flip in case of generalized HMC. This momentum reversal does not arise with standard HMC since the momentum vector is replaced by a new random sample after each constant energy molecular dynamics Monte Carlo step.[85] This implies that HMC takes global moves based on deterministic Hamiltonian dynamics.[83]

HMC is a modification of Markov Chain Monte Carlo applicable to continuous state space that makes use of gradient information to reduce the random walk behavior.[86] The gradient guides the sampling by showing the location of states with high probability. The use of "hybrid" in the name of the algorithm comes from the fact that different algorithms are used for different parts of the partition function.[87] The HMC algorithm is a mixture of molecular dynamics (MD) and Monte Carlo (MC) algorithms. It therefore combines the advantages of MD and MC methods.[88,89]

- It allows for global moves, which consist in integrating the system through phase space.

- HMC is an exact method; i.e., the ensemble averages do not depend on the step size chosen.

- Algorithms derived from the method do not suffer from numerical instabilities due to finite step size as MD algorithms do.

- Temperature is incorporated in the correct statistical mechanical sense.

- Samples efficiently all configurations of the system since large time steps and therefore long MD trajectories are used to generate new configurations,

- It samples very efficiently the high-density configurations since it allows for global and concerted moves of the molecules,

- It satisfies the criterion of robustness since the method can be applied "as is" to any molecular fluid or systems, however complicated the hamiltonian $\mathscr{H}$ may be.

The idea behind HMC is simple as seen in its method of handling symplectic integrations. Furthermore, the series of random moves in MC (translations, rotations and conformational changes) are replaced by a single MD trajectory in the NVE ensemble. The HMC algorithm is ergodic with respect to the positional density.[90] This ensures that the configurations of the system are efficiently sampled.[89]

HMC is based on the hamiltonian function

$$\mathscr{H}(q,p) = \tfrac{1}{2}\langle p, \mathscr{M}^{-1}p\rangle + \mathscr{V}(q)$$

where $\mathscr{M}^{-1}$ is the matrix of inverse masses, $\tfrac{1}{2}\langle p, \mathscr{M}^{-1}p\rangle$ is the kinetic energy, $\mathscr{V}$ is the potential energy, q the positions and p the momenta. The replacement of conventional MC moves by long MD trajectory permits the system to relax along a long MD trajectory due to the ease of calculations in the MD method. Differentiating the hamiltonian yields the equations of motion

$$\dot{q} = \frac{d\mathscr{H}}{dp} = \mathscr{M}^{-1}p \qquad\qquad \dot{p} = -\frac{d\mathscr{H}}{dq} = -\mathscr{V}(q) = F[q(t)] \qquad (3.83)$$

where $\mathscr{V}(q)$ is the derivative of potential energy $\mathscr{V}$ with respect to q and F is a conservative force field.

In the HMC scheme, global moves can be made while keeping the average acceptance probability, P_A, high. HMC is a valuable method when many degrees of

freedom are coupled and single variable updates are not feasible. It starts with enlarging the partition function by momenta whose variables are refreshed following a Maxwellian distribution at the desired simulation temperature.[91] A total of N_{MD} MD steps are then executed using a timestep δt. The change in the total Hamiltonian, $\Delta \mathscr{H}$, is recorded and the "move" is accepted with a probability $P_{acc} = \min [l, \exp(-\Delta \mathscr{H}/k_B T)]$. Notice that this acceptance rate decays exponentially with the size of the system. This constitutes one global MC step (Figure 16). Irrespective of whether the move has been accepted or not, the momenta must always be refreshed before continuing with the next MC step. This is essential if detailed balance is to be obeyed, as is the use of a time-integration scheme for the MD integration which is both area-preserving in phase space and time-reversible.[84] It is important to note that the acceptance criteria are dependent on the timestep (δt), which is given by the total time or trajectory length t and the number of MD steps N_{MD}. Therefore, increasing N_{MD} increases the accuracy within the MD part of HMC, which in turn, increases the acceptance rate. The leap frog variant of the Verlet integrator is mostly used for HMC because it is known to satisfy the conditions for a detailed balance.

Another important aspect of HMC, like any other simulation technique, is the development of realistic and efficient potential models for the molecular interactions. HMC methods are unbiased since they do not show any systematic discretization errors; the only errors are of statistical origin because of the use of numerical method in solving the equations of motion. These errors can be minimized by increasing the number of samplings.[93] HMC is a popular method to conduct sampling from the constant temperature ensemble for molecular systems as such we use it with the NPT ensemble in the study of the nucleation and growth of C_{60} nanoparticles from the supersaturated vapor and from the undercooled liquid discussed in Chapter 4, where the system is studied under conventional experimental conditions.[47,85]

Despite the numerous advantages, HMC has a few limitations. It mostly suffers from inappropriate sampling of the conformational space due to lack of good energy
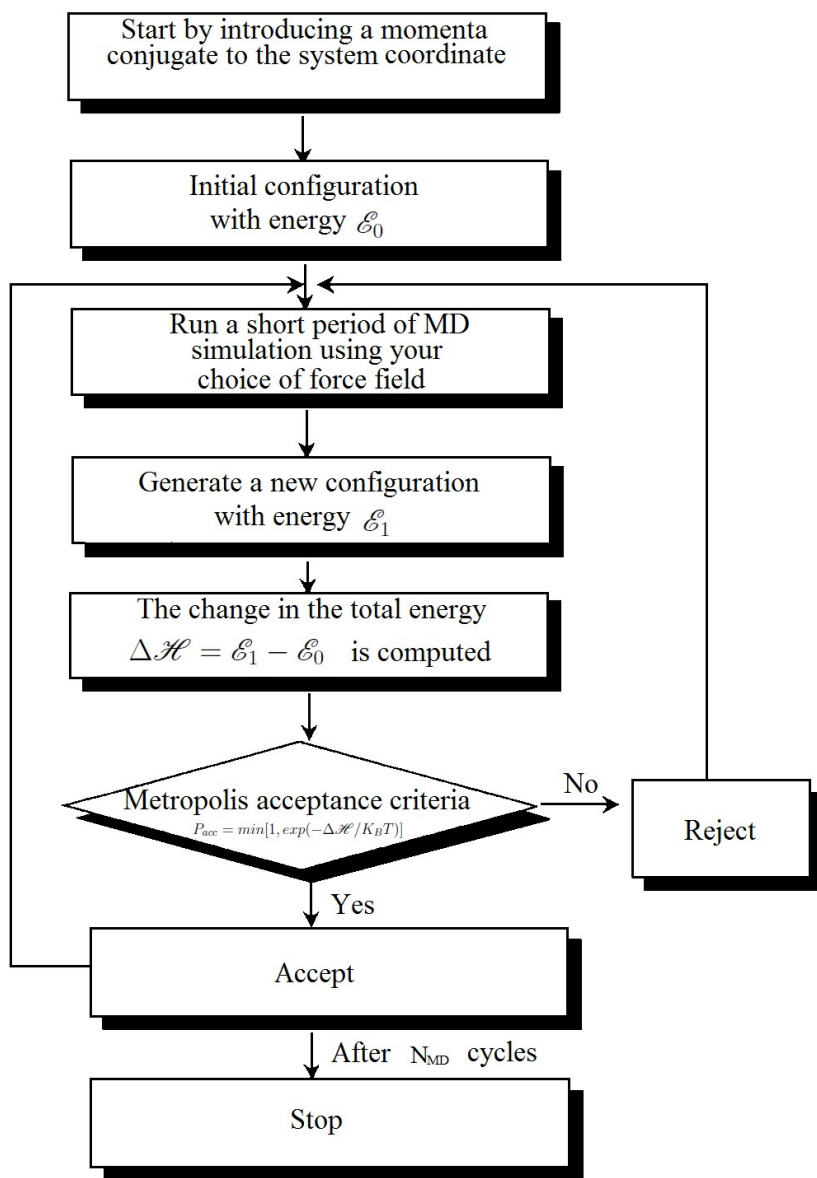
Figure 16. Steps require for an HMC algorithm.[92]

functions. As such, it works by rejecting moves with high fluctuations in the energy.[90,92] The normal hybrid Monte-Carlo methods break down if the hamiltonian $\mathscr{H}$ is discontinuous. In such cases, the functional space is divided into various homotopy classes, each being defined by its own winding number and surrounded by a potential wall. In situations where HMC faces such complications, the acceptance probability is lowered. It should be noted that it is the MD part of the HMC that encounters severe problems with the discontinuity. In order to tunnel through this topological sector barrier with a high acceptance rate, a number of modifications to the standard HMC algorithm are required.[94] Some of these modifications use the idea that HMC has an advantage that it can easily be combined with other techniques. For example, HMC has been combined with techniques such as parallel tempering, dynamical spatial warping, Wang-Landau, and umbrella sampling, to increase sampling rates in case of high energy barriers between molecular conformations.[47,85,89]

CHAPTER IV

SAMPLING THE LIQUID-SOLID TRANSITION

4.1   Introduction

Crystallization is the process whereby crystalline solids are formed from solution, melt or vapor. The latter process (deposition or the opposite process to sublimation) is possible but rarely observed. This is because of the high free energy difference involved for the direct transformation of matter from the vapor phase to the solid (crystalline) phase. Crystallization processes are observed commonly in our everyday life for example, formation of snowflakes, Figure 17, and ice crystals. This process is rampant in the pharmaceutical and most chemical industries.[11] While crystallization is more popular with the pharmaceutical industries, precipitation is common amongst the chemical industries where it is commonly used to refer to fast and uncontrolled crystallization.[95,96] Crystallization and precipitation are at times used interchangeably. Although crystallization result from variation in solubility or concentration while precipitation results from a chemical reaction. Crystallization is useful as a process of separation and purification in industry. As a result, an understanding of the process of crystallization is necessary to obtain the desired products with the required purity as well as for process efficiency.[96] The practice of modifying a crystallization method in order to change the physical properties of the crystals is referred to as particle engineering.[97]

A crystal is a three dimensional (3D) solid in which the structural building blocks (monomers) are arranged in a regular repeating pattern such that the environment of each monomer is the same throughout the crystal. The monomer may be an atom, a molecule, group of atoms or group of molecules. There are three

72
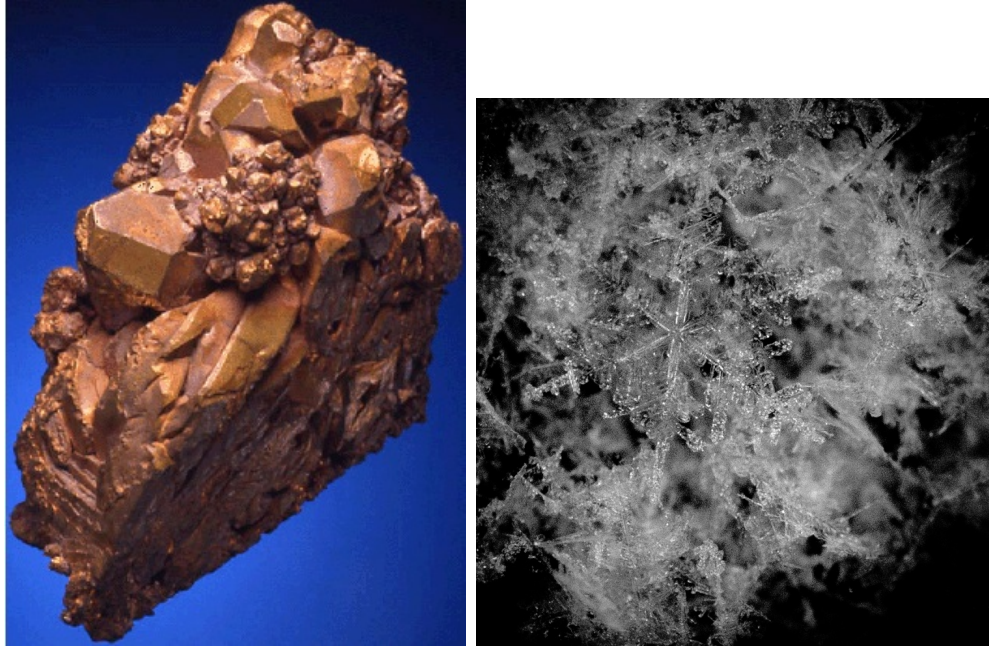
Figure 17. Examples of crystals from copper (showing a wide variety of crystal forms) and snowflake.[98]

main common arrangement of atoms in a crystalline solid, namely: body centered cubic (BCC), face centered cubic (FCC), and hexagonal close packed (HCP) (Figure 18). The green colored sphere in the BCC structure represents the atom in the
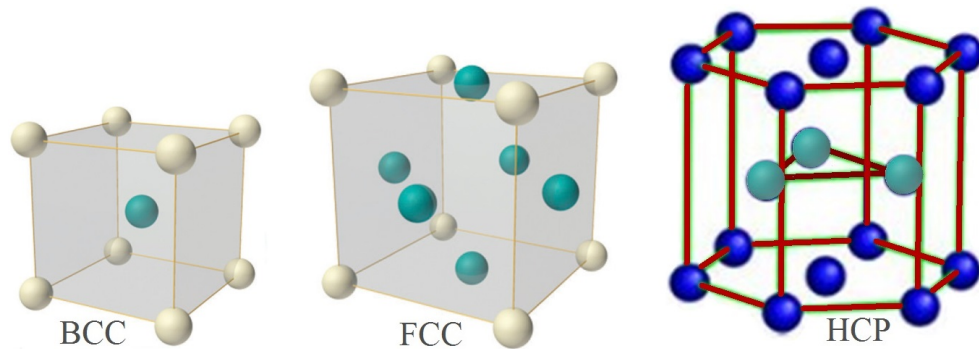
Figure 18. Common crystalline solid structures.

center while in the FCC the green spheres represent the atoms in the six faces.

4.2   Umbrella Sampling

Umbrella sampling is a thermodynamic, non-Boltzmann sampling technique developed by Torrie and Valleau for free energy calculations.[99] It has become a very popular sampling technique used in the sampling of rare events (energy barrier significantly larger than $k_B T$), where conventional sampling methods fail.[100] It has also been applied to small systems to examine the height of the free energy barrier and the transition from nucleation to spinodal decomposition.[101] The development of the umbrella sampling was based on Monte Carlo simulation methods but more recently it's being frequently used with MD simulations.[102] This has been attributed to the efficiency of the method in the calculation of free energy and potential of mean force (PMF) used to obtain accurate measures of a free energy barrier.[103] This technique has been used in a variety of studies of liquids, solids, and small molecules, not leaving out the application to structure, dynamics, and energetics of biological macromolecules.[104]

Another technique also used to evaluate the free energy is thermodynamic integration. However, Kastner *et al.* showed that when thermodynamic integration is performed along a reaction coordinate, it can be said to be a special case of umbrella sampling.[105] Free energy difference is the driving force of most chemical and biochemical systems. This makes calculating the free energy difference central in molecular simulations.[100] Conventional sampling methods fail or inadequately sample areas with high energy. This leads to poor estimates of the free energy, since high energy regions are also important to accurately trace the free energy profile within the available computational time.[106,107]

The umbrella sampling technique can be applied to both equilibrium and nonequilibrium situations for phenomena that require extremely long simulation time to be observed.[108,109] In the case of equilibrium processes, the application of bias potentials that are functions of some order parameter enhance the sampling of phase space that would otherwise be inadequately sampled.[107] On the other hand,

umbrella sampling does not respect the condition for microscopic reversibility (detail balance); consequently, using it for nonequilibrium systems is difficult. In such situations, it is necessary to divide the reaction coordinate into several small windows (Figure 19) that are sampled independently using a specific biased potential for each window (Figure 20).
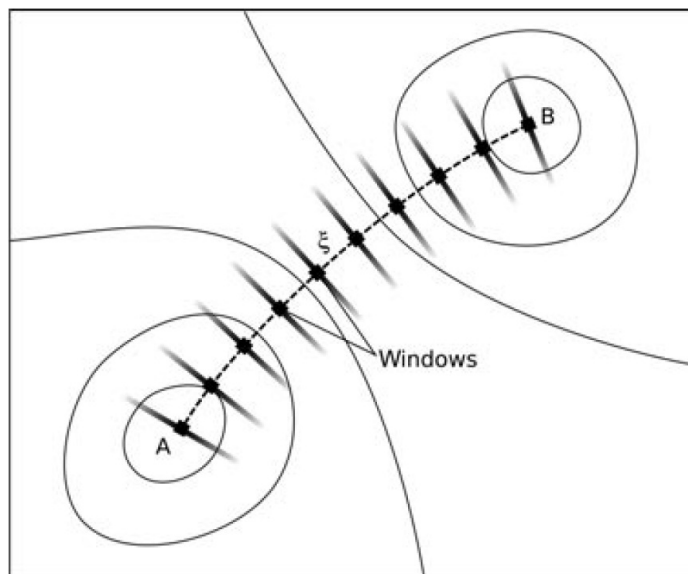
Figure 19. Splitting of the reaction coordinate (ξ) shown in dotted line between two different states (A and B) into several distinct windows.[100]

Each window is assigned an arbitrary center based on the reaction coordinate and sampled such that information about the probability and free energy can be transfered between connected windows. This procedure is sometimes also applicable to equilibrium studies.[109] This technique of splitting the energy profile into several small windows (Figure 19), performing different biased umbrella samplings (Figure 20) and recombining the results is the strength of the umbrella sampling scheme and the origin of the name umbrella sampling.[100,106] During the sampling, the biased potential helps keep the system within the center of the different windows.

This technique entails the use of the potential energy in the presence of an additional or extra potential energy term known as a biased potential (ω).[100,106,107] The sampling is done along a chosen reaction coordinate (ξ) or order parameter. The reaction coordinate can be single or multidimensional; for the specific case of
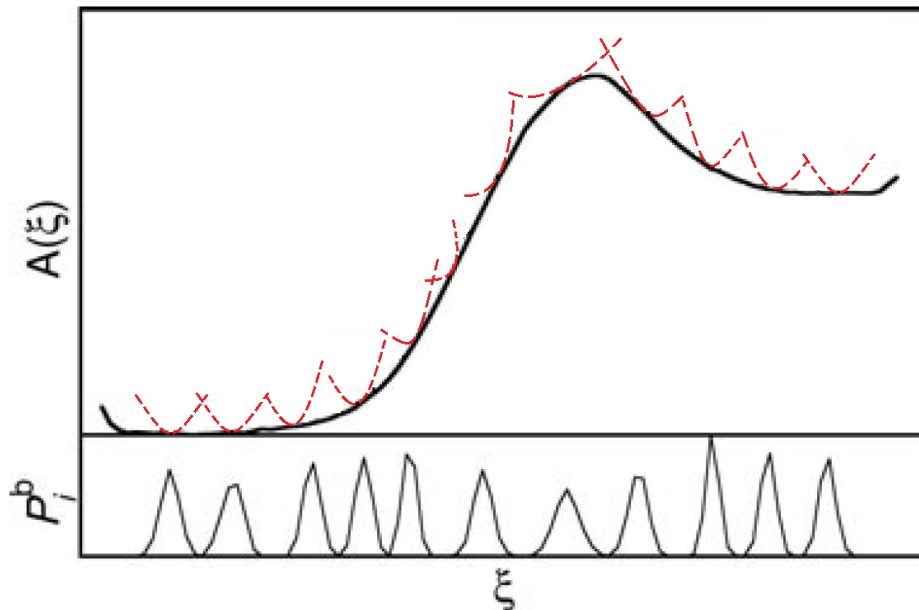
Figure 20. An illustration of how individual windows of free energy profile (solid black curve) are independently sampled (red dash curves) and the bias distribution obtained at the end of the simulation (bottom black curves).[100]

umbrella sampling, one has at most two dimensions. The form of the bias potential has to restrict the variation of the coordinate within a small interval around the region of interest to ensure efficient sampling of the configurational space.[108,109] The strength of the bias potential is very important; a strong bias will confine the sampling very close to the center that would call for more simulations before the system converges. Conversely, if the bias is too weak the system will converge after fewer simulations. But it may fail to sample the region of interest and does not ensure the sampling of the unfavorable areas (such as those with high energy) in the phase space. Considering that the reaction coordinate is divided into several small windows, the bias potential (ω_i), of each window i is an additional potential energy term that depends only on the reaction coordinate.[100,102,110] Then the bias free energy function is given by

$$U^b(r) = U^u(r) + \omega_i(\xi) \tag{4.1}$$

where the superscripts b and u denote biased and unbiased respectively.

Subsequently, $U(r)$ will be used for the unbiased potential.

Upon the completion of a simulation, the unbiased free energy needs to be evaluated to obtain the true Helmholtz free energy $A_i(\xi)$ for the window. This requires an unbiased distribution function along the coordinate ξ that can be derived from the Boltzmann weighted average.

$$\langle \rho(\xi) \rangle = P_i^u(\xi) = \frac{\int \exp[-\beta U(r)] \, \delta[\xi'(r) - \xi] d^N r}{\int \exp[-\beta U(r)] d^N r} \tag{4.2}$$

where $U(r)$ is the total energy of the system as a function of some coordinate r and $\xi'(r)$ is a function that depends on a few or several degrees of freedom N (for example $\xi'(r)$ may be an angle, a distance, or a complex function of the Cartesian coordinates of the system).[106]

Equation 4.2 gives the probability density as a function of the reaction coordinate ξ and it is the basis of the umbrella method.

Simulation of the biased system yields the biased distribution P_i^b along the reaction coordinate. For an ergodic system (every point in the phase space is visited during the simulation), the biased probability is defined by Equation 4.3.

$$P_i^b(\xi) = \frac{\int \exp[-\beta U^b(r)] \, \delta[\xi'(r) - \xi] d^N r}{\int \exp[-\beta U^b(r)] d^N r} \tag{4.3}$$

Substituting for the biased potential from Equation 4.1 in 4.3 and replacing $\omega_i(\xi)$ with $\omega_i(\xi'(r))$, since the integration is performed over all the degrees of freedom except ξ, gives

$$P_i^b(\xi) = \frac{\int \exp\{-\beta[U(r) + \omega_i(\xi'(r))]\} \, \delta[\xi'(r) - \xi] d^N r}{\int \exp\{-\beta[U(r) + \omega_i(\xi'(r))]\} \, d^N r} \tag{4.4}$$

Since the bias potential depends only on the reaction coordinate ξ and the integration in the numerator of Equation 4.4 is performed over all the degrees of freedom except ξ, the biased distribution can be rewritten as shown in Equation 4.5.

$$P_i^b(\xi) = \exp[-\beta\omega_i(\xi)] \times \frac{\int \exp[-\beta U(r)] \, \delta[\xi'(r) - \xi]d^N r}{\int \exp\{-\beta[U(r) + \omega_i(\xi'(r))]\} \, d^N r} \tag{4.5}$$

By comparing Equation 4.2 and 4.5 and solving for the unbiased distribution yields

$$P_i^u = P_i^b(\xi) \, \exp[\beta\omega_i(\xi)] \times \frac{\int \exp\{-\beta[U(r) + \omega_i(\xi(r))]\} \, d^N r}{\int \exp[-\beta U(r)] \, d^N r}$$

$$= P_i^b(\xi) \, \exp[\beta\omega_i(\xi)] \times \frac{\int \exp[-\beta U(r)] \, \exp\{-\beta\omega_i[\xi(r)]\} \, d^N r}{\int \exp[-\beta U(r)] \, d^N r}$$

$$= P_i^b(\xi) \, \exp[\beta\omega_i(\xi)] \, \langle \exp[-\beta\omega_i(\xi)] \rangle \tag{4.6}$$

The Helmholtz free energy $A_i(\xi)$ is determined from Equation 4.6 as

$$A_i(\xi) = -(1/\beta) \, ln P_i^b(\xi) - \omega_i(\xi) + F_i \tag{4.7}$$

where the biased distribution $P_i^b(\xi)$ is obtained from the MD/MC simulation of the biased system, $\omega_i(\xi)$ is determined analytically and $F_i = -(1/\beta) \, ln \, \langle \exp[-\beta\omega_i(\xi)] \rangle$ is an undetermined constant that is independent of ξ and represents the free energy associated with introducing a window potential.

A limitation to the umbrella sampling method is the necessity for an *a priori* choice of the reaction coordinate along which to sample.[111] Also a miss of some vital structural changes by the choice of the reaction coordinate may lead to an artificial lowering or raising of the umbrella sampling results. Similarly, a significant change in a degree of freedom not accounted for by ξ may result in jumps of the root mean square difference between average properties of subsequent umbrella sampling windows.[112]

4.2.1   Choice of the Bias Potential

The bias potential has to be such that the sampling along the entire range of the reaction coordinate is uniform. Thus the ideal choice of the optimal bias potential is $\omega_{opt} = -A(\xi)$. However, the free energy is not known prior to the simulation as it is to be determined with the use of umbrella sampling. There are mainly two forms of the bias potential; harmonic and adaptive bias.[100]

4.2.1.1   Harmonic Bias Potential

The most used biased potential for umbrella sampling takes the form of a harmonic function, Equation 4.8. The use of this form of the bias produces a sampling that is confined to a very small region. Therefore, the range of interest of ξ is divided into a number of small windows. The bias in each window keeps the sampling around the reference position ξ_i^{ref} within each respective window i.[100,106]

$$\omega_i(\xi) = \frac{1}{2}K(\xi - \xi_i^{ref})^2 \tag{4.8}$$

where K represents the strength of the bias and can be window dependent; ξ_i^{ref} is a reference point on the reaction coordinate.

The references ξ_i^{ref}, for each window, are usually evenly distributed along the reaction coordinate. The more windows there are, the more accurate the estimate of the free energy. Nonetheless, the time for equilibration increases with the number of windows. The different windows are sampled independent of each other. Accordingly, the simulations can be run simultaneously in parallel. Different bias potentials are used for different windows to sample the configurational space since the bias potential is gradually increased to force the system over the energy barrier.[110]

The main critical parameter of the harmonic biased potential is the strength K of the potential. A strong bias will confine the sampling very close to the center

thus requiring more simulations and over representing configurations of higher energy; whereas, if the bias is too weak it will sample outside the region of interest. A balance on the strength is vital to carry the system over the potential barrier. Depending on the method employed for the analysis of the results from respective umbrella sampling, another critical parameter is that the individual umbrellas have to overlap. This is pivotal if the weighted histogram analysis (WHAM) method is to be applied for the analysis.[71] Though this requirement is not necessary for the umbrella integration analysis method, it can be advantageous. If it is discovered that the series of windows leave a large separation between the distributions, additional windows can be inserted in the course of the simulation.[100]

4.2.1.2 Adaptive Bias Potential

The adaptive bias potential is a method aimed at selecting a bias potential that samples evenly the entire range of interest of the reaction coordinate in one simulation.[71] This is done by choosing $\omega(\xi)$ such that

$$\omega(\xi) = -A(\xi) \tag{4.9}$$

The free energy $A(\xi)$ is not known before the start of the simulation, thus the process starts with an estimate of $\omega(\xi)$ generating an initial estimate of the free energy. The process then iterates with the negative of the generated free energy until adequate sampling is obtained. This approach flattens the energy surface between two minima resulting to uniform sampling of ξ without the addition of a bias potential.[100,113] A drawback with this method is that only the last simulation result is preserved for the final estimate of the free energy, the rest are discarded.

4.3 Nucleation and Growth of C_{60} Nanoparticles

Molecular simulation was used to study the molecular mechanisms of nucleation and growth of C_{60} nanoparticles from the supersaturated vapor and from the undercooled liquid. The interest in this study stems from the importance of polymorphism in the properties and applications of nanoparticles as well as the potential use of C_{60} in cancer treatment.[114,115]

C_{60} is a member of the family of compounds known as fullerene. Fullerenes are molecules made up entirely of carbons and composed of an even number of carbon atoms, e.g. C_{60}, C_{70}, C_{76}, C_{84}. They can be of various forms such as spherical, ellipsoid or tube, etc. They are named based on their structures, for example

- Spherical: Buckyballs

- Cylindrical: Carbon nanotubes or buckytubes.[116]

C_{60} was the first member of the family to be discovered in 1985 by three scientists; Harold W. Kroto, Robert F. Curl and Richard E. Smalley.[116] C_{60} as the name implies, is composed of 60 carbon atoms arranged in a cage consisting of 20 hexagonal and 12 pentagonal rings.

Upon its discovery, C_{60} was thought to be the most stable molecule known at the time, with 12500 feasible resonance structures. However, only one of the resonance forms was found to be dominant because of the absence of pentagon strain, that is placement of one or more double bonds in pentagons.[117] The others are less stable, hence less prevalent.

4.4 Applications

Since its discovery, C_{60} has been shown to be promising in a wide variety of applications, which includes catalysis, electronic devices, material science and medicine.
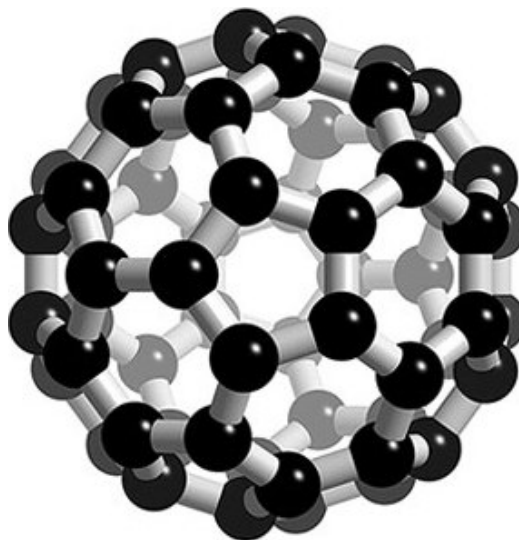
Figure 21. Structure of a Buckyminsterfullerene (C_{60})
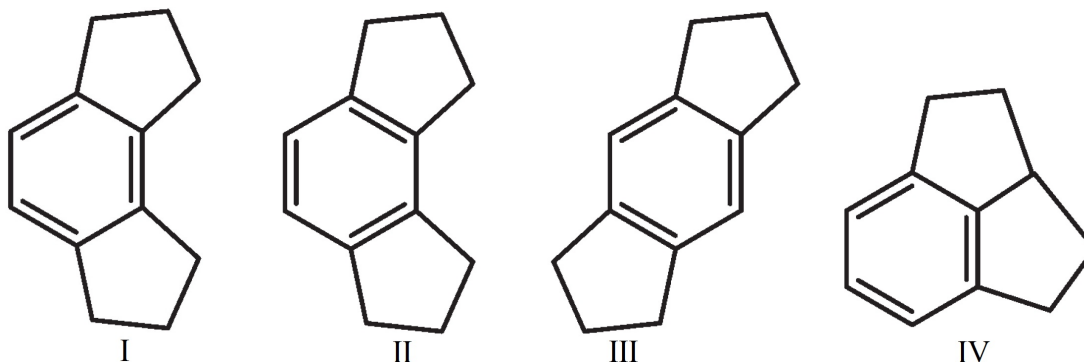
Figure 22. Possible double bond configuration in Buckyminsterfullerene, I is the stable configuration.[117]

- Due to its photosensitivity, it could be used as a vector for drug delivery as well as for the photodynamic treatment of cancer.[114]

- In material science, C_{60} nanowires have been envisioned as building blocks for the future of magnetism and photonic applications.[118]

- Their high degree of resonance projects them as good acceptors in polymer based solar cells, e.g., [6,6]-Phenyl C_{61} butyric acid methyl ester (PCBM).[119]

Several factors have hindered the advancement of research on fullerenes such as their insolubility in water, difficulty of obtaining high purity samples, and the construction of organized electroactive nanostructures by self-assembly.[120] Research

has shown that this difficulty is easily overcome by combining it with some biodegradable and water soluble polymers.[118] This has kept the search for molecular receptors for fullerenes as an active and challenging area of research since its discovery.[121]

To achieve this, the reactivity of C_{60} has been widely explored. In the formation of fullerene derivatives, large binding constants are essential for high stability in solution. A broad variety of molecular fragments that can form a positive noncovalent interaction with the outer surface of fullerenes have been explored. Nambo *et al.*[122] recently showed that an aziridine moiety on the fullerene core can serve as an aid for the controlled synthesis of a range of functionalized fullerene derivatives. It is important to mention here that addition on the fullerene surface can take place either across the 6,6-ring junction or the 5,6-ring junction.[118] In both cases there is either ring opening (expansion) fulleroids or the rings stay intact (closed). This often give rise to the four possible configurations shown in Figure 23. Due to the high reactivity of C_{60}, a photoactive polyvinyl alcohol PVOH/C_{60} nanohybrid with very low cytotoxicity, that is water soluble has been synthesized with very promising properties for the photodynamic therapy of cancer.[123]

Closed [6,6]   Closed [5,6]   Open [6,6]   Open [5,6]
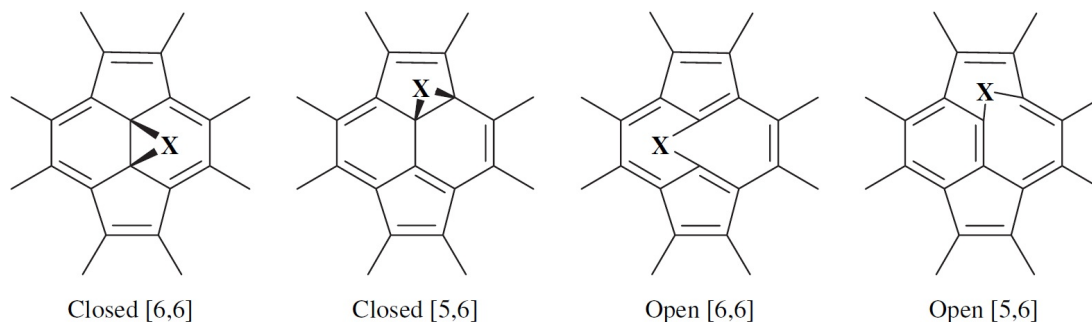
Figure 23. Possible modes of reactions on the C_{60} surface.[118]

Since the physical properties of nanoparticles strongly depend on their crystalline structure, it is important to understand and control the crystal structure or polymorphs in which C_{60} crystalizes, the nanostructures they form and the underlying mechanism. Polymorph selection is a complex process resulting from the interplay between kinetics and thermodynamics. A complete understanding of this

process is still not clear.[47]

Research has shown that the growth of C_{60} from the supersaturated vapor at temperatures above room temperature yielded both face centered cubic (FCC) and hexagonal close packed (HCP) crystalline structures. In contrast the growth of C_{60} solids from solutions of various organic solvents gave some unusual crystal morphology such as hexagonal nanosheets and orthorhombic nanowire.[124]

4.5 Simulation Process

At temperatures above 300 K, C_{60} molecules rotate freely, thus they may be treated as physically interacting spheres. Based on this property, Girifalco developed a pair potential (Equation4.10) describing the interaction between two C_{60} molecules.[125]
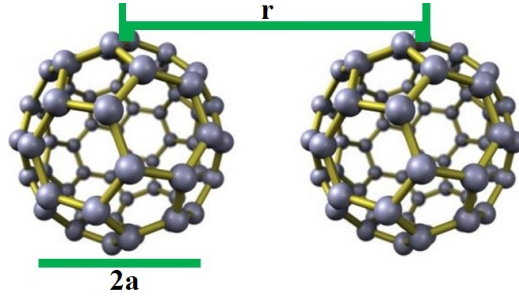
Figure 24. A sketch of the parameters as used in the pair potential described by Girifalco.

$$\phi(r) = -\alpha \left[\frac{1}{s(s-1)^3} + \frac{1}{s(s+1)^3} - \frac{2}{s^4} \right] + \beta \left[\frac{1}{s(s-1)^9} + \frac{1}{s(s+1)^9} - \frac{2}{s^{10}} \right] \quad (4.10)$$

where $s = r/2a$ is the distance between two C_{60} molecules, scaled by the diameter (2a) as shown in Figure 24, α and β are constants described by Girifalco, which can be determined experimentally by computing the energy for the FCC crystal.

The process of crystallization takes place in two steps: nucleation (an activated process involving a large free energy barrier) and growth that occur under

unconstrained molecular dynamics(MD) simulation. The growth step may sometimes be complex and thus proceed by a complex mechanism known as cross nucleation.[126,127] A schematic representation of the crystallization pathway is shown in Figure 25.
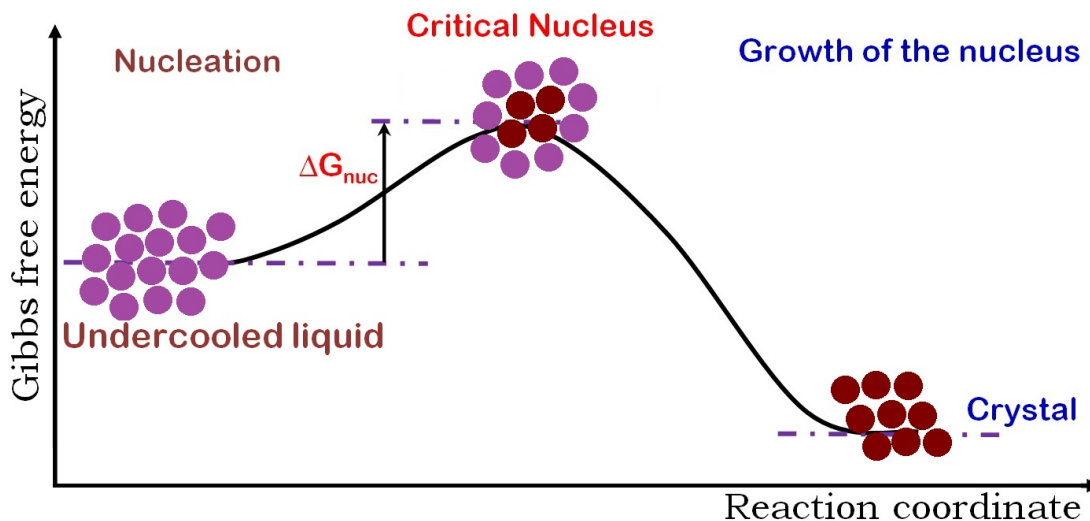
Figure 25. Annotated representation of crystallization.

The study of C_{60} crystallization involves three different polymorphs; FCC (considered the most stable) and two metastable forms, HCP and BCC. HCP has almost the same free energy as FCC while BCC is the least stable.

4.5.1   Nucleation

Nucleation is the early stage of crystallization involving a large free energy barrier. C_{60} nucleation is studied from the undercooled liquid at a pressure of 4.6 MPa and a temperature of 1425 K (25% below the melting temperature). First, the simulation of a critical nucleus at a temperature 25% below the melting point is performed. At this stage, there is a large free energy barrier. Molecular simulation studies show that the time scale for the nucleation process is much longer than that associated with MD simulations. To overcome this energy barrier, a series of hybrid Monte Carlo (HMC) simulations together with the umbrella sampling bias potential are carried out on a system of 3,000 C_{60} molecules. This bias potential imposes a

fixed value for the global order parameter, Q_6, to the system, which allows it to overcome the free energy barrier of nucleation.[128] It should be noted that this bias potential takes the same value for FCC, BCC and HCP polymorphs and therefore does not favor the formation of any particular crystal.[129] By gradually increasing the imposed value of Q_6, a critical nucleus is formed.

The nucleation starts with the formation of small clusters of the HCP polymorph (yellow spheres in Figure 26). The stable FCC polymorph starts nucleating from the metastable HCP. The FCC polymorph increases gradually until it reaches 42% in the critical nucleus made up 294±10 C_{60} molecules for the supersaturated vapor and 45% in the critical nucleus containing 361±21 C_{60} molecules for the undercooled liquid.

(a)
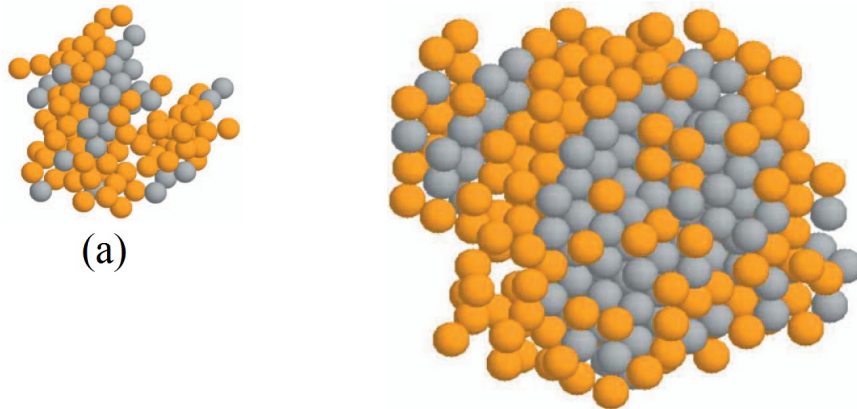
Figure 26. Structure of the pre-critical nucleus (a) and the critical nucleus.

4.5.2 Growth

Once the critical nucleus has been formed, its evolution is followed in the absence of the bias potential through a series of steps. First, the system of 3000 C_{60} molecules containing the critical nucleus is embedded in an undercooled liquid of 22,000 C_{60} molecules. Next, the new system of 25,000 molecules is equilibrated while maintaining the bias potential on the central subsystem of 3000 molecules. Configurations of the system are stored every 1,000 time steps during the equilibration run, and finally, the bias potential is switched off, letting the system

evolve freely during a molecular dynamic trajectory at fixed temperature and pressure. For each set of conditions, 20 MD trajectories are generated. These are employed to check if the critical nucleus formed is genuine. This is done by verifying that for half of these MD trajectory the nucleus dissolves and for the other half the growth of the critical nucleus occur. This demonstrated that the critical nuclei obtained are genuine.

The growth process occurs through a complex mechanism known as cross nucleation. Cross nucleation, discovered by Yu in his experimental study of the crystallization of D-sorbitol and D-mannitol,[126] is a phenomenon in which an early nucleating polymorph may cross-nucleate another polymorph instead of consuming the entire liquid. This phenomenon has also been observed theoretically in Lennard-Jones fluids.[127]

Experiment D-mannitol   Lennard-Jones C_{60}

Threoretical
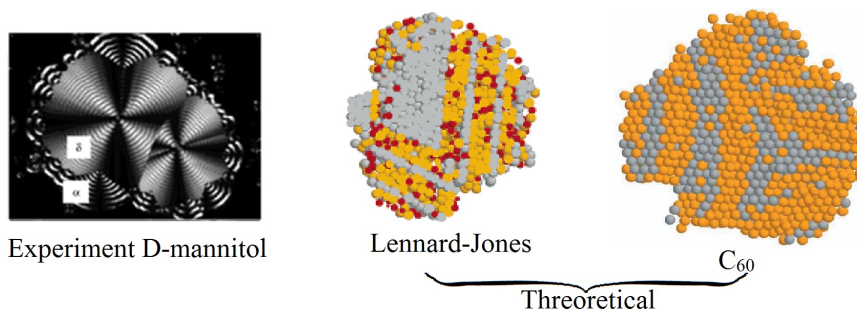
Figure 27. Cross-Nucleation in different systems.

Contrary to model fluids such as the Lennard-Jones fluid wherein cross nucleation leads to polymorph selection,[127] polymorph selection was not observed in the case of C_{60}. Instead, this resulted in a growth mechanism dominated either by the HCP or the FCC polymorph. This observation is consistent with experimental results on the crystallization of C_{60} from vapor, where FCC and HCP crystals were observed.[130]
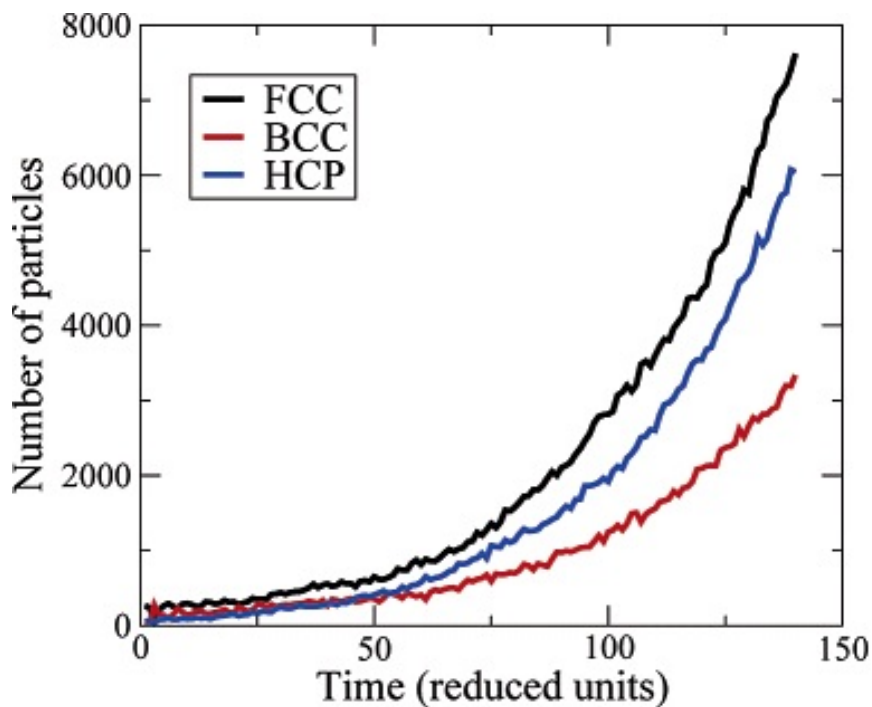
Figure 28. Growth mechanism in a Lennard-Jones system dominated entirely by the FCC polymorph (polymorph selection).[127]
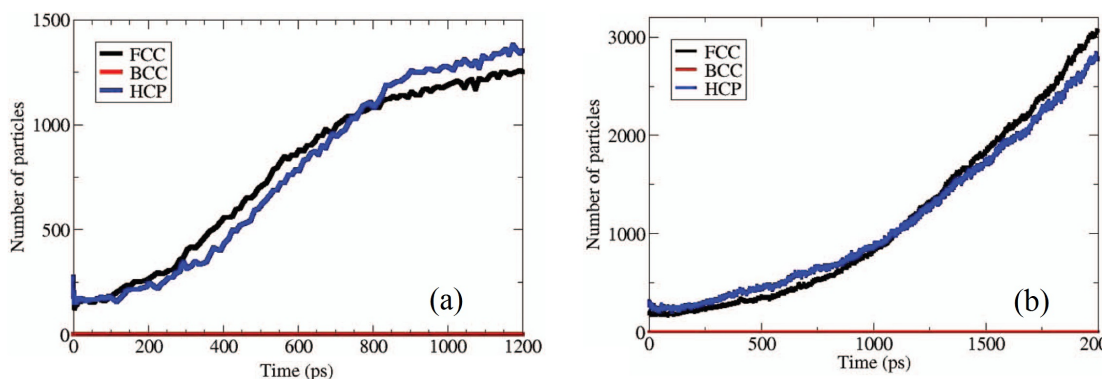
Figure 29. Growth mechanism in C_{60} dominated by the HCP polymorph (a) or by the FCC polymorph (b), absence of polymorph selection.[47]

4.6   Conclusion

Hybrid Monte Carlo simulation and the umbrella sampling bias potential have been used to elucidate the molecular mechanism underlying the formation of C_{60} nanocrystals from the undercooled liquid and the supersaturated vapor. During this study, it was observed that nucleation starts with the formation of small clusters of

the metastable HCP polymorph consistent with the Ostwald's step rule. Also the growth mechanism is found to occur through the complex mechanism known as cross nucleation, that has previously been reported for model fluids and from experiment. In addition, the growth step is either dominated by the stable FCC polymorph or the metastable HCP polymorph, consistent with the literature. Nevertheless, the metastable HCP polymorph observed here is different from the model fluids where the metastable polymorph is the BCC polymorph. Another difference observed during the study of C_{60} is that unlike the model fluids, where cross nucleation led to polymorph selection, C_{60} polymorph selection was not achieved.

These results demonstrate that cross nucleation is a more general phenomenon than previously anticipated. Due to the large size of the C_{60} molecule and the confinement of the liquid pocket of its phase diagram to a tiny temperature interval, only the FCC and HCP polymorphs which are closer in energy were observed. The BCC crystals were negligible.

CHAPTER V

SAMPLING THE VAPOR-LIQUID TRANSITION

5.1 Introduction

The term Vapor-liquid equilibria refer to the existence of a single liquid phase in equilibrium with its vapor. This occurs through the process of vaporization, i.e., the change from liquid to gas (vapor), and condensation, i.e., the change from vapor to liquid. These processes are commonly observed in our everyday life, for example, the presence of water droplets on grass (dew) or on the surface of water bottles see Figure 30.
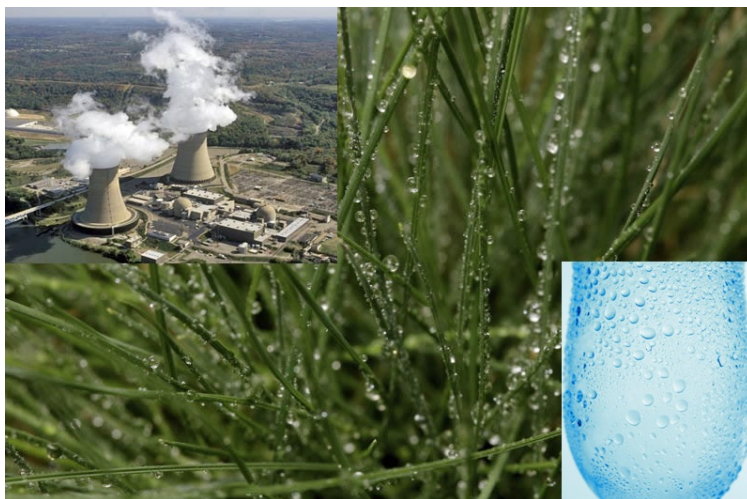
Figure 30. Common examples for the process of vaporization and condensation

Vapor-liquid equilibrium (VLE) is a vast research area in Chemical Engineering.[131] This is because a large number of industrial products and materials are marketed in the crystallized form, which makes crystallization an important industrial process. The purification of most of these products requires thermal separation, a non-equilibrium process. Non-equilibrium conditions are necessary

requirements for crystallization and require information about the VLE properties.

Describing the VLE for polyaromatic hydrocarbons and alkenes is a challenge for any given model. This is exemplified by the numerous attempts made to estimate the VLE of these systems, mainly because of poor and empirical prediction capacities of existing models.[26,132] During the last 25 years, a number of simulation methods have been developed to determine phase equilibria for various systems. Those techniques which rely on particle insertion/deletion schemes fail for large molecules.[133] Modification of these methods, for instance cavity bias or configurational bias, has been implemented to determine accurate critical properties of different molecular scaffolds.[134,135]

In the petroleum industry, for example, information on the VLE of hydrocarbon mixture is a cornerstone in process design.[136] This is because the design of new chemicals and processes is constantly carried out for economic vitality. The use of computational methods to understand phase properties minimizes traditional experimental methods, known for their expensive and length of time required. As a result, huge simulation projections for different systems have been made over the years. The prospect for numerical modeling is that it is likely to become more efficient over time.[132]

Knowledge of vapor-liquid behavior of fluids permits the determination of their distribution between the vapor and liquid phases. This can have a marked impact on the composition of circulating fluid mixtures in the atmosphere. For instance, burning of hydrocarbon remains such as tires release PAHs like chrysene (known to be carcinogenic) into the environment.[137]

Vapor-liquid equilibria are governed by some fundamental and simple laws, most of which are applicable only within certain limits.[136]

- Dalton's law describes the vapor phase

$$\frac{P_i}{P_t} = \frac{n_i}{n_t} \qquad (5.1)$$

where P is the pressure, n the number of moles, and the subscripts i and t component i and the total number of components respectively.

This law holds only for low pressures ($P_t < P_{cr}$, where P_{cr} is the critical pressure). At higher pressures the equation is written in terms of fugacity f as

$$f_i = y_i f_t \qquad (5.2)$$

where y_i is the molefraction of component i in the vapor phase.

- Raoult's law describes the liquid phase

$$P_i' = x_i P_i^0 \qquad (5.3)$$

where P_i' is the partial pressure of component i over the liquid mixture, and depends only on the vapor pressure of pure i and its liquid mole fraction. Raoult's law holds only for ideal mixtures. For nonideal mixtures, liquid phase behavior is described by replacing the mole fraction with the activity.

$$P_i' = \gamma_i x_i P_i^0 \qquad (5.4)$$

Both Equations 5.3 and 5.4 are only valid at temperatures below the critical point (T< T_{cr}).

- Henry's law is used at higher temperatures where Raoult's law fails

$$P_i' = H_{ij} x_i \qquad (5.5)$$

where H_{ij} is the Henry's coefficient for substance i in solution j.

Similar to Raoult's law, Henry's law is also valid only for ideal system. For nonideal mixtures, the equation is extended to include the activity coefficient

γ_i for the component of interest.

$$P_i^{'} = H_{ij}\gamma_i x_i \qquad (5.6)$$

The only logistical difference between Raoult's law and Henry's law is the proportionality constant.[138]

5.2   Wang-Landau Sampling

The Wang-Landau multiple-range random walk algorithm mostly referred to as the Wang-Landau sampling, was developed by Wang and Landau as a tool to study first and second order phase transitions of the two dimensional Potts and Ising model.[82] It allows for the efficient sampling of low probability states (low probability density region) that otherwise would not be visited by the Boltzmann scheme. This is achieved through the implementation of Monte Carlo simulations with concurrent or serial independent random walk, combined with a biased distribution.[82] The goal is to achieve a flat histogram of visited states and estimate a biasing function, which is essential in the calculation of thermodynamic properties at phase coexistence. A schematic representation is given in Figure 31.

The methodology in the isothermal isobaric ensemble was developed by Ganzenm$\ddot{u}$ller et $al.$[139] The NPT ensemble was chosen for simulations of VLE to avoid the particle insertion and deletion steps that significantly limit the acceptance rate in dense systems. In any given ensemble, the biasing function is dictated by the need to achieve a uniform sampling of an extensive variable which allows the sampling in both vapor and liquid phases. For a given variable X, the probability of finding X is defined by Equation 5.7.

$$p(X) = \int p(\Gamma, X)d\Gamma \qquad (5.7)$$

where Γ is a specific configuration and $p(\Gamma, X)$ is the joint probability of being in
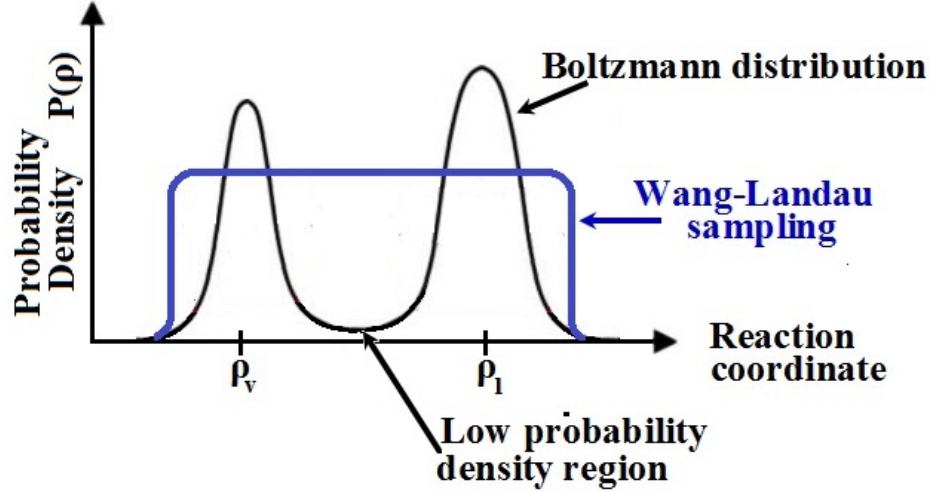
Figure 31. Boltzmann distribution (black line) and probability distribution obtained from Wang-Landau sampling (red curve), ρ_l is the density in the liquid phase and ρ_v the density in the vapor phase.

this specific configuration with a specific value of X.

The biased distribution, $p_{bias}(X)$, should be uniform, i.e., the probability of finding any of the states along the region comprising the vapor and the liquid state is equal. If the joint biased probability is defined by

$$p_{bias}(\Gamma, X) = \frac{p(\Gamma, X)}{p(X)} \tag{5.8}$$

then $p_{bias}(X)$ becomes one for any X

$$p_{bias}(X) = \int p_{bias}(\Gamma, X)d\Gamma = \int \frac{p(\Gamma, X)}{p(X)}d\Gamma = 1 \tag{5.9}$$

The detailed balance equation is then

$$p_{bias}(\Gamma_o, X_o)acc(o \to n) = p_{bias}(\Gamma_n, X_n)acc(n \to o) \tag{5.10}$$

where $acc(o \to n)$ is the acceptance probability of a trial move from an old (o) to a new (n) configuration.

The Metropolis solution becomes

$$acc(o \to n) = min\left[1, \frac{p_{bias}(\Gamma_n, X_n)}{p_{bias}(\Gamma_o, X_o)}\right] \tag{5.11}$$

The biased joint probability depends on the biasing function, that is estimated through the iterative scheme of the Wang-Landau method described below. The Boltzmann probability distribution $p(X)$ as well as thermodynamic properties are then found as a function of the biasing function.

5.2.1   Sampling in the Canonical Ensemble

The WL method was developed as an improvement of the conventional MC algorithm; therefore, it was originally designed to uniformly sample states in the canonical ensemble. The biased distribution is derived from the Boltzmann probability distribution in Γ

$$p(\Gamma) = \frac{V^N \exp[-\beta U(\Gamma)]}{N! \Lambda^{3N} Q(NVT)} \tag{5.12}$$

where $\Lambda = \sqrt{h^2/2\pi m k_B T}$ is the de Brogle thermal wavelength and $U(\Gamma)$ is the potential energy.

In the canonical ensemble the only variable is $U(\Gamma)$ (function of the particle positions), $p(\Gamma)$ can be considered as the joint distribution. The energy distribution should include those configurations with energy E

$$p(E) = \int p(\Gamma)\delta(U(\Gamma) - E)\mathrm{d}\Gamma \tag{5.13}$$

where δ is the delta Dirac function.

The density of states, with energy E, is given by

$$\Omega(NVE) = \int \delta(U(\Gamma) - E)\mathrm{d}\Gamma \tag{5.14}$$

and hence the energy distribution can be replaced with the following expression

$$p(E) = \Omega(NVE)\frac{V^N\exp[-\beta E(\Gamma)]}{N!\Lambda^{3N}Q(NVT)} \tag{5.15}$$

The biased probability is obtained by dividing Equations 5.12 and 5.15 as shown in Equation (5.8).

$$p_{bias}(\Gamma, E) = \frac{1}{\Omega(NVE)} \tag{5.16}$$

With this biased probability the final expression of the acceptance criterion can be derived, according to the detailed balance condition Equation (5.10).

$$acc_{o\to n} = \min\left[1, \frac{\Omega(NVE_o)}{\Omega(NVE_n)}\right] \tag{5.17}$$

The biasing function in the canonical ensemble is then the density of potential energy states with N and V fixed. The Boltzmann probability distribution $p(E)$ is found by performing a random walk. This gives a flat histogram since the acceptance probability is biased according to Equation (5.10). $\Omega(NVE)$ is modified systematically in order for the random walk over the allowed energy range to converge to the true value.

The simulation starts by assigning to all $\Omega(NVE)$ an arbitrary value ($\Omega(NVE)$=1 for all E). Microstates are visited by flipping randomly the spins for the 2D Ising model. Each time a spin is flipped, the corresponding new density of states is updated by multiplying the existing value with a modification factor f, such that $\Omega(NVE_n) \to f\Omega(NVE_n)$. During the first sweep, f can be as big as the Napier's number e. After each sweep the density of states converges to its true value with an accuracy proportional to lnf.

The walk in energy space continues with random flipping of the spins until all the states inside the allowed energy region are visited several times and the

accumulated histogram of visited states $H(E)$ is relatively flat. A flat histogram, as defined by Wang and Landau in their formulation, is such that the histogram $H(E)$ for all possible E is not less than 80% of the average one $< H(E) >$. f is then reduced and the random walk in energy space is repeated until the same flatness criterion is achieved. This step is performed several times until the Blotzmann distributions between the sweeps do not differ significantly. This is achieved when f becomes smaller than some predefined value, $f > 1$. f is reduced such that

$$f_n \rightarrow 1 \ \ \text{when} \ \ n \rightarrow \infty \tag{5.18}$$

where n is the sweep number.

The modification factor f is used as a control parameter for the accuracy of the density of states. The manner in which it is reduced should not allow it to become $f < 1$. In the original Wang-Landau sampling it is decreased by the square root of its predecessor after each sweep $(f \rightarrow \sqrt{f})$. Obviously, the closer f gets to unity (1), the more accurate $\Omega(NVE)$ becomes. At the end of the simulation, the $\Omega(NVE)$ obtained is rescaled by a factor of 2, corresponding to the Ising model (all spins are up or down).

The detailed balance condition for the Ising model, Equation 5.19, is not satisfied since the density of states is changed constantly during the random walk.

$$\frac{1}{\Omega(E_o)} acc_{o \rightarrow n} = \frac{1}{\Omega(E_n)} acc_{o \rightarrow n} \tag{5.19}$$

Nevertheless, after several sweeps $\Omega(E)$ quickly converges to its true value as f approaches 1. Accordingly, the detailed balance condition becomes satisfied at the end of the simulation, with an accuracy proportional to lnf.

5.2.2   Sampling in the Isothermal-Isobaric Ensemble

In the isothermal isobaric ensemble where the number of particles (N), pressure (P), and temperature (T) are fixed, the extensive variable that allows the sampling of the vapor-liquid region is the volume (V). Here, the joint probability distribution is given by Equation (5.20).

$$p(V, \Gamma) = \frac{V^N exp[-\beta U(\Gamma) - \beta PV]}{N!\Lambda^{3N}Q(NPT)} \tag{5.20}$$

where $Q(NPT) = \int_0^\infty Q(NVT)exp(-\beta PV)dV$ is the isothermal isobaric partition function and $Q(NVT)$ is the canonical partition function.

The integration of the joint probability over the possible configurations yields

$$p(V) = \frac{Q(NVT)exp(-\beta PV)}{Q(NPT)} \tag{5.21}$$

Substituting Equation 5.20 and 5.21 into the expression for the joint biased probability in equation (5.8), the joint biased probability in the isothermal isobaric ensemble is then given by

$$p_{bias}(V, \Gamma) = \frac{V^N exp[-\beta U(\Gamma)]}{N!\Lambda^{3N}Q(NVT)} \tag{5.22}$$

This leads to an acceptance probability

$$acc(o \rightarrow n) = min\left[1, \frac{Q(NV_oT)V_n^N exp[-\beta U(\Gamma_n)]}{Q(NV_nT)V_o^N exp[-\beta U(\Gamma_o)]}\right] \tag{5.23}$$

In Equation (5.23), the canonical partition function $Q(NVT)$ is the only unknown and it plays the role of the biasing function. Obtaining a good estimation of $Q(NVT)$ is the core of the simulation. Another important characteristic of the WL method in the NPT ensemble is that the pressure is not required in the acceptance criteria as shown in Equation (5.23). The coexistence pressure is found

after the simulation converges and does not have to be predetermined in advance.[140,141] This is important because the simultaneous prediction of the vapor pressure in the course of a simulation is a daunting task. First, because pressure is ignored in the development of most force fields and second, due to the limitations of the commonly used Lennard-Jones potential.[18]

In the classical Wang-Landau method with spherical particles in the NPT ensemble, two types of moves are performed. Random particle translational moves and volume changes. For this purpose, the volume domain comprising the volume and liquid range is divided into equal intervals in lnV. The simulation starts by attributing an arbitrary value of one to $Q(NVT)$. Each time a new volume interval is sampled, it is updated by a convergence factor $f(Q(NV_oT)) \rightarrow fQ(NV_oT)$, starting with $lnf = 1$.

The updated partition function is higher in value and thus, as it can be seen from Equation (5.23), the acceptance probability of visiting a new volume increases. This constant updating is the driving force behind the uniform sampling. Not only does it allow visits to the low probability volumes, but it also aids the partition function to converge towards its true value. Once all states in each volume interval are sampled for a certain amount of time (to ensure a reasonably flat histogram), another sweep is run with a lower convergence factor ($f_n = \sqrt{f_{n-1}}$). The convergence of the simulation is monitored by tracing the histogram of visited states and the running estimate of the partition function as shown in Figure 32.

The refinement of the convergence factor is necessary, as a better estimate of $Q(NVT)$ is obtained after each sweep. After each simulation run for a given value of f has converged, the random sampling of the volume interval starts all over. Estimates of the partition function are kept after each simulation has converged. The refinement of the convergence factor f is accompanied by a refinement in $Q(NVT)$ and when it has the allure of smooth and continuous function (dotted line in Figure 32), the simulation is over.
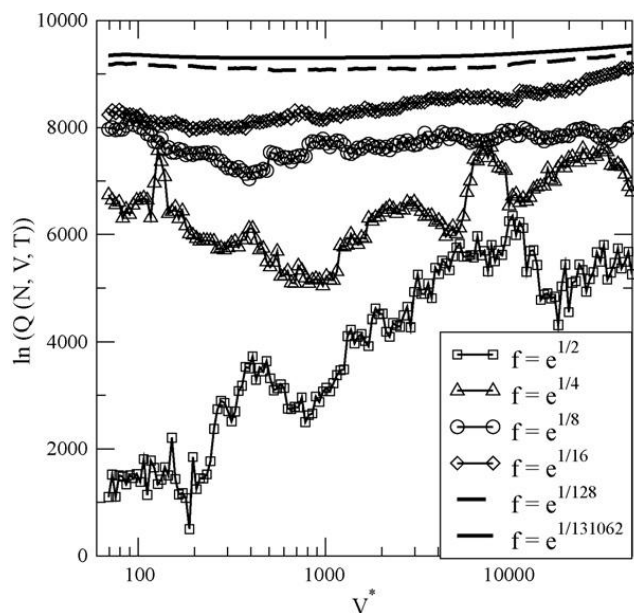
Figure 32. Variation of the canonical partition function Q(NVT) as a function of the reduced volume for different convergence factors f.

5.3 Determination of Critical Properties of Polyaromatic Hydrocarbons (PAHs)

5.3.1 Introduction

Polycyclic aromatic hydrocarbons (PAHs), sometimes referred to as polynuclear aromatic hydrocarbons, consist of fused aromatic rings with no substituents or heteroatoms. They occur naturally in oil, coal, tar deposits and are also byproducts of combustion.[142] PAHs have been extensively studied because they are potent atmospheric pollutants and known to be carcinogenic.[143,144]

PAHs are semi-volatile and are usually found sorbed to aerosol particles. Consequently, vapor-liquid, vapor-solid, and/or solid-liquid equilibrium data for these compounds are vital reducing their concentrations in the environment. But limited data is available for PAHs in the literature.[145] To circumvent this problem, molecular simulation appears to be a great tool to predict the critical properties of PAHs. Previous simulation methods have mostly been employed for phase equilibria of PAHs with two or three aromatic rings. This can be explained as being due to low acceptance probability for dense fluids and increasing molecular complexity.[23,141,146]

100

Wang-Landau sampling in the NPT ensemble was used to establish the vapor-liquid equilibria of three PAHs with 4 aromatic rings see Figure 33. Unlike prior methods,[133] working in the NPT ensemble does not require any insertion/deletion steps during the simulation. Another advantage is that knowledge of the pressure at coexistence is not required, since Wang-Landau scheme samples uniformly a wide range of volumes at a given temperature. Finally, only a single simulation at a fixed temperature is needed to provide an accurate estimate of the canonical and isobaric-isothermal partition functions, i.e., $Q(N, V, T)$ and $Q(N, P, T)$ respectively. Statistical thermodynamics enables estimates of densities and vapor pressures at coexistence from $Q(N, V, T)$. The scaling laws aid the evaluation of critical properties of the system. The obtained results are authenticated by comparing with the available data.
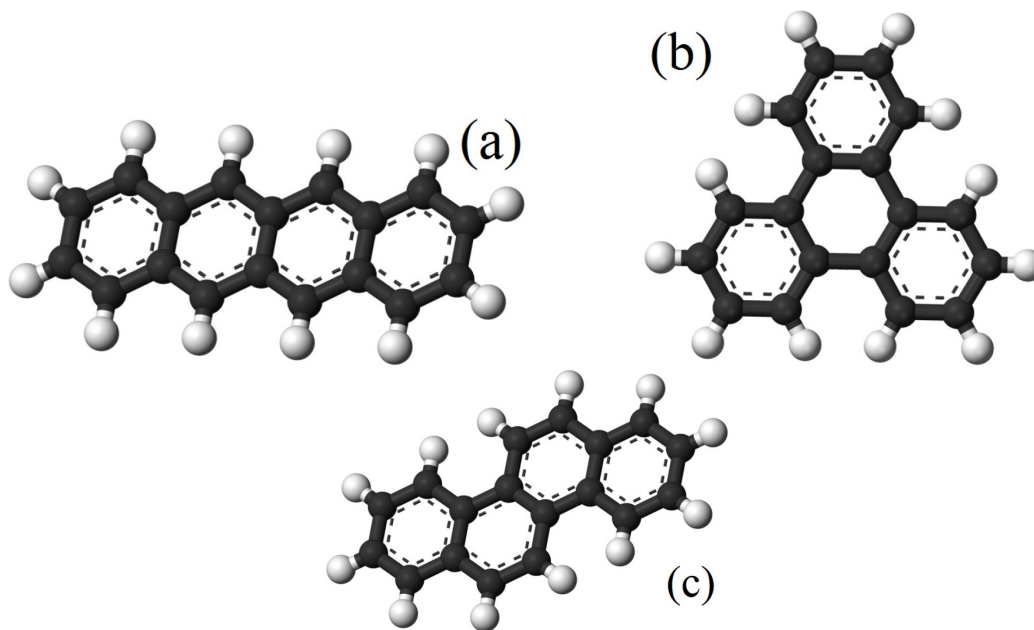
Figure 33. The three PAHs studied Naphthacene(a), Triphenylene(b), and Chrysene(c).

5.3.2 The Potential Energy Function or Potential Model

The accuracy of the potential model is a very vital component for any simulation scheme. The three PAHs studied here consist mainly of carbon atoms

and CH groups (Figure 33). The DHMD potential developed by Desgranges *et al.* in our research group[141] is employed to model the PAHs. The potential is a united atom model that treats each CH group as a single interaction site. This potential uses a Buckingham exponential-6 functional (Equation 5.24) to describe nonbonding interactions between two sites i and j belonging to different molecules, with the assumption that each molecule is rigid and planar. Details of this model can be found in references[141,147].

$$\phi(r_{ij}) = \frac{\epsilon_{ij}}{1 - (6/\alpha_{ij})} \left[\frac{6}{\alpha_{ij}} exp\left(\alpha_{ij} \left[1 - \frac{r_{ij}}{r_{ij}^m} \right] \right) - \left(\frac{r_{ij}^m}{r_{ij}} \right)^6 \right] \tag{5.24}$$

where ϵ represents the well depth, and r^m and α are fitting parameters.

The parameters for various interactions, given in Table 2, were obtained by running a simulation for napthalene at several temperatures and optimizing the results with experimental data.[141] Interactions between two unlike sites are modeled with the Lorentz-Berthelot mixing rules (Equation (5.25)).

$$
\begin{aligned}
\epsilon_{ij} &= \sqrt{\epsilon_{ii}\epsilon_{jj}} \\
r_{ij}^m &= \frac{1}{2}(r_{ii}^m + r_{jj}^m) \\
\alpha_{ij} &= \sqrt{\alpha_{ii}\alpha_{jj}}
\end{aligned}
\tag{5.25}
$$

Table 2. Parameters for the DHMD potential

	r^m(Å)	ϵ/k_B (K)	α
C	3.800	61.74	18.13
CH	4.067	74.06	20.00

The DHMD potential has recently been used to study the vapor-liquid equilibria of naphthalene, phenanthrene and anthracene with accurate results. This demonstrates the appropriateness of the model in predicting critical properties of PAHs. In this work, the bond length between carbon atoms for the three PAHs

studied was fixed to 1.40 Å. A cutoff radius of 11.13 Å is applied throughout the simulations together with the standard long-range corrections.[62]

5.3.3   Simulation Method

5.3.4   Wang-Landau Hybrid Monte Carlo Simulation

The phase behavior of three PAHs mentioned previously were explored by means of Hybrid Monte Carlo simulations and the Wang-Landau sampling technique. This method involves combining MD trajectories with WangLandau (WL) sampling. The choice of MD trajectory over MC random translation is to allow for concerted moves and to advance the system as a whole. From previous work, the probability of accepting a MD move from an old configuration o to a new configuration n is given by

$$acc(o{\rightarrow}n) = min\left[1, exp\left(-\frac{(E_{(n)} - E_{(o)})}{k_B T}\right)\right] \tag{5.26}$$

where E is the total energy given by the sum of the potential and kinetic energy for the system.

The equations of motion for translation was integrated by employing the velocity-Verlet algorithm while that for rotation was integrated using the scheme proposed by Matubayasi and Nakahara.[62,148]

The Wang-Landau flat histogram technique proposed by Ganzenmüller *et al.* was applied to uniformly sample the simulation volume (V) at a given temperature.[139] The density of the system was changed by varying the volume, and the simulation ran to determine the temperature at coexistence. The probability of accepting a volume change move from an old configuration o with coordinates Γ_o, V_o to a new configuration n with coordinates Γ_n, V_n is defined as in Equation 5.23. Recall that Equation (5.23) has no expression for pressure. In addition an estimate of the canonical partition function Q(N, V, T) was obtained at the end of the

simulation.

A system of 100 molecules PAHs was studied for each simulation. Throughout the simulation temperatures, the upper and lower bounds for the volume were chosen to correspond to densities of 0.001 and 1.05 g/cm_3 respectively. The volume was divided into 400 uniform intervals of $ln(V)$ instead of V for sampling convenience. This changes Equation 5.23 slightly as the factor V_N is replaced by V_{N+1}.

WL-HMC simulations consist of two types of moves, MD trajectories and random volume changes. One of the objectives of WL sampling in the NPT ensemble is to gain information on Q(N, V, T); each time an interval of volume is visited. The quality of the estimate of Q(N, V, T) was controlled by a convergence factor f in the simulation. At the start of the simulation, Q(N, V, T) was assigned a value of one and the initial value of f was obtained from $\ln f = 1$. For each value of f, the number of times a volume interval is visited was recorded in a histogram H(V) and Q(N, V, T) was adjusted by multiplying it by f. When the histogram H(V) was reasonably flat (in practice, it is accomplished when all intervals for the volume have been visited at least 500 times), the simulation had converged. f was reduced by $\sqrt{f}$ and all entries for the histogram were initialized. A new HMC-WL run was started with these new values of the convergence factor f and Q(N, V, T). This procedure was repeated until $\ln f = 10^{-5}$. Equation (5.27) is used to validate that the simulation has converged.

$$\Delta_n = \left| \frac{lnQ_{f_n}(N,V,T) - lnQ_{f_{n-1}}(N,V,T)}{lnQ_{f_n}(N,V,T)} \right| \tag{5.27}$$

where Q_{f_n}(N,V,T) is the running estimate for the canonical partition function for the convergence factor $f_n = e^{1/2n}$, and Δ_n is the relative error made for a convergence factor of $f_n = e^{1/2n}$ and a measure of convergence for the WL-HMC simulation.

Figure 34 shows data for Δ_n collected during the course of the WL-HMC

simulations for triphenylene at T = 700 K and T = 950 K.
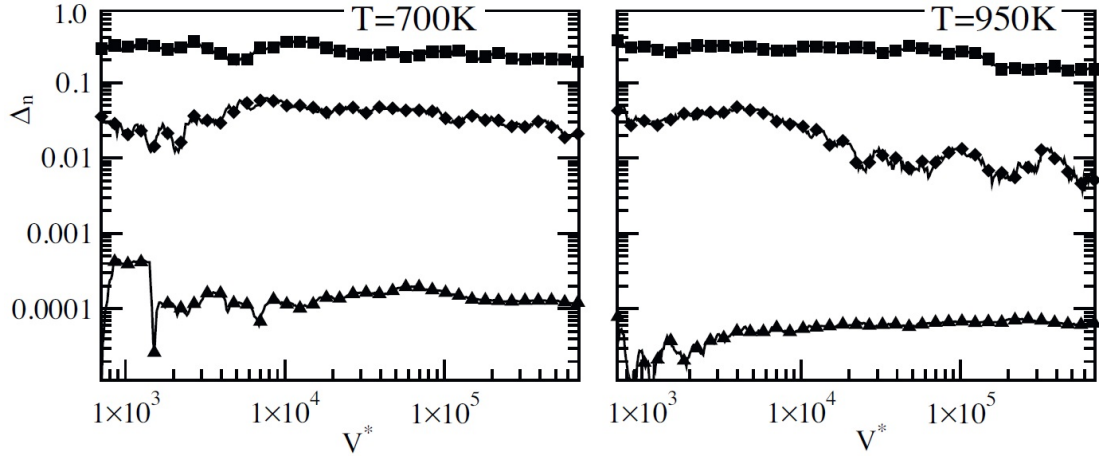
Figure 34. Relative error on the convergence factor for triphenylene at T=700 and 950 K

At the end of the simulation, the volume distribution was evaluated using the following equations

$$p(V) = \frac{Q(N,V,T)exp(-PV/k_BT)}{Q(N,P,T)} \tag{5.28}$$

and

$$Q(N,P,T) = \int_0^\infty Q(N,V,T)\ exp(-\frac{PV}{k_BT})dV \tag{5.29}$$

where Q(N, P, T) is the isothermal-isobaric partition function.

When the probability p_{liq} associated with the liquid phase is equal to the probability p_{vap} associated with the vapor phase, the saturation pressure P_{coex} was calculated. Then the densities for the two coexisting phases, i.e., (ρ_{vap}) and (ρ_{liq}) may be calculated by

$$\rho_{liq} = \frac{\int_0^{V_b} (N/V)V^N Q(N,V,T)\ exp(-(P_{coex}V)/(k_BT))dV}{\int_0^{V_b} Q(N,V,T)\ exp(-(P_{coex}V)/(k_BT))dV} \tag{5.30}$$

$$\rho_{vap} = \frac{\int_{V_b}^\infty (N/V)V^N Q(N,V,T)\ exp(-(P_{coex}V)/(k_BT))dV}{\int_{V_b}^\infty Q(N,V,T)\ exp(-(P_{coex}V)/(k_BT))dV} \tag{5.31}$$

105

Simulations in the NPT ensemble using the Wang-Landau sampling method resulted in the determination of the pressures at coexistence P_{coex}. This was obtained by equating the probability of the liquid and vapor phase $(p_{liq} = p_{vap}))$ and the densities of the coexisting phases ρ_{liq} and ρ_{vap} are obtained from Equation 5.30 and 5.31.

The critical parameters were estimated from the simulation results by fitting WL-HMC simulated vapor-liquid equilibria results with the density scaling law (Equation 5.32) and the law of rectilinear diameters (Equation 5.33) to determine the critical temperature (T_c) and the critical density (ρ_c) respectively.[89,149] The data obtained for the coexistence properties of the PAHs studied are polted in Figure 35.

$$\rho_l - \rho_v = B(T_c - T)^\beta \tag{5.32}$$

$$\frac{\rho_l + \rho_v}{2} = \rho_c + A(T - T_c) \tag{5.33}$$

where ρ_l and ρ_v are the liquid and vapor densities respectively, $\beta = 0.3265$ is the critical exponent that equals the three-dimensional Ising order-parameter, and A and B are fitting parameters.

The results for the pressure at coexistence were fitted to Antoine's law, Equation (5.34). Values of the Antoine's parameters A, B, and C in Table 3 are applied to estimate the critical pressure for the three PAHs. Plots of the fit to Antoine's law as a function of temperature are shown in Figure 36.

$$logP = A - \frac{B}{T + C} \tag{5.34}$$

The values of the various properties obtained during the simulations are shown in Table 4.
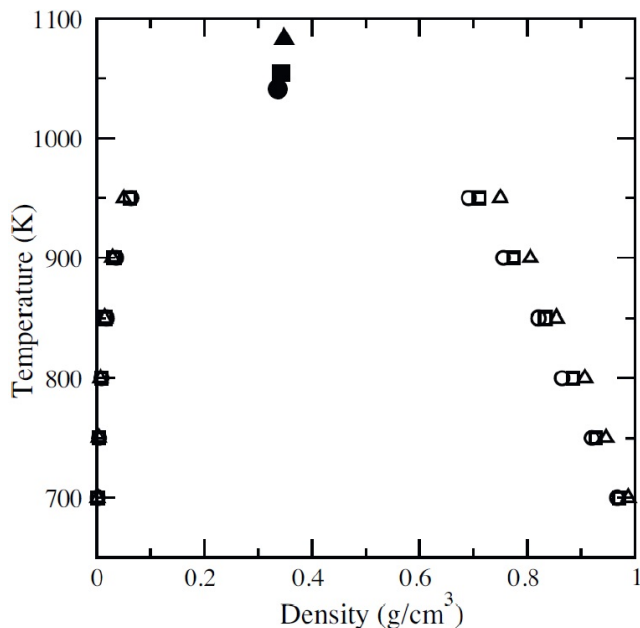
Figure 35. Vapor-liquid equilibria for naphthacene (circles), triphenylene (triangles) and chrysene (squares). The filled symbols represent the critical point.

Table 3. Antoine's parameters for the different PAHs.

	A	B	C
Naphthacene	11.1735	5428.61	410.184
Triphenylene	11.1643	5511.73	412.060
Chrysene	11.3757	5833.20	440.904

Table 4. Critical and boiling points for naphthacene, triphenylene and chrysene (standard deviations are of 5 K for temperatures, 0.50 bar for pressures and 0.010 g/cm^3 for densities).

	T_c (K)	P_c (bar)	ρ_c (g/cm^3)	T_b (K)
Naphthacene	1041	36.75	0.337	742
Triphenylene	1083	45.04	0.348	755
Chrysene	1054	39.93	0.342	747

Due to the scarcity of experimental data, a direct comparison of the critical properties predicted by the simulations with experimental data was not possible. However, a comparison of our results with those obtained via correlations from molecular structure are in close agreement and our boiling points also match those estimated from experiments.[150]
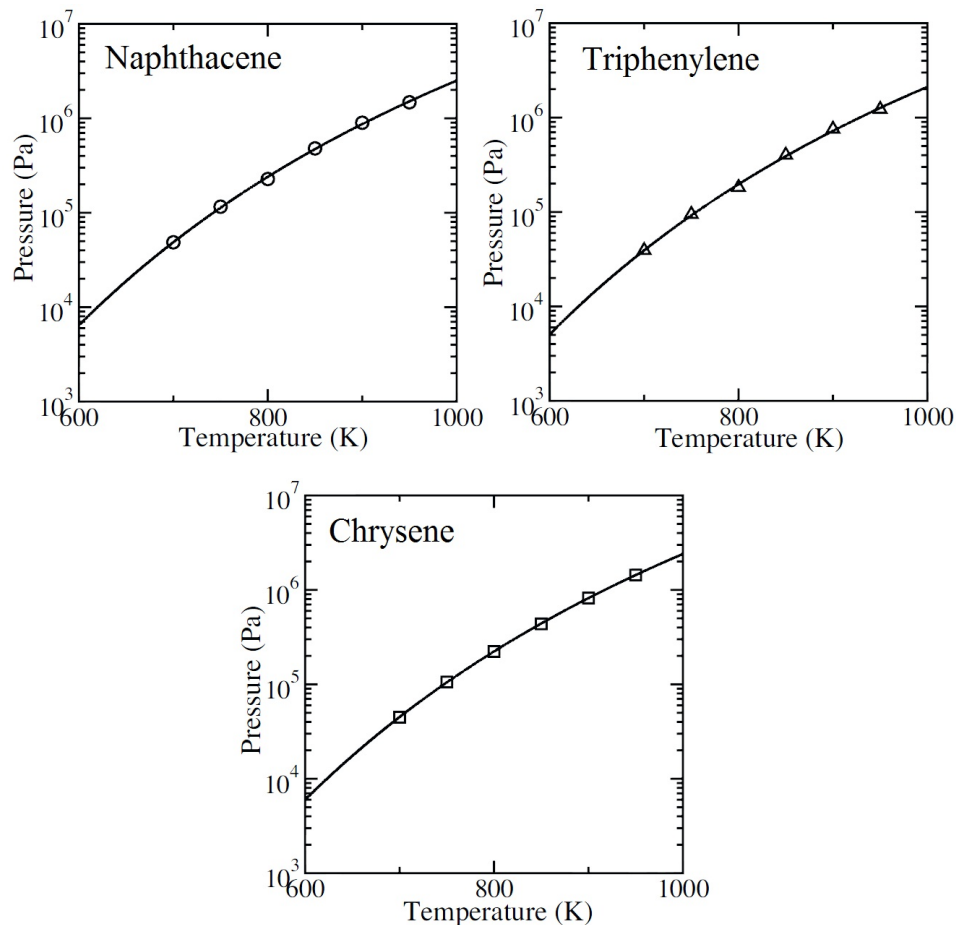
Figure 36. Saturated vapor pressures for the three PAHs. In all plots the lines represent Antoine fits.

5.4 Vapor Liquid Equilibria of Alkenes

5.4.1 Introduction

The phase behavior of hydrocarbons (alkanes and alkenes) is of importance in many applications, especially in the petrochemical industry for the separation of different hydrocarbon fractions. As a result, the critical properties of these flexible hydrocarbons have been extensively investigated by experiments and theory. These groups of compounds are explored in industries either as reactants, products or intermediates for the development of new products.[1,149,151]

The study of flexible molecules like alkanes and alkenes via molecular

simulations demands special care, especially in the selection of the simulation method. This is due to the possibility of conformational changes in addition to molecular overlaps when sampling between the different densities. Although Monte Carlo simulations are remarkable for their efficiency over MD methods when it comes to the study of phase properties, they suffer from low acceptance probabilities in dense fluids due to the large free-energy barrier separating the coexisting phases.[141]

Previous works on chain molecules have been done with the help of configurational-bias Monte Carlo (CBMC) simulation methods in combination with the very popular Gibbs ensemble Monte Carlo (GEMC)[71,133] and the cavity bias Monte Carlo developed by Mezei *et al.*[134] The former method is commonly referred to as configurational-bias Gibbs ensemble Monte Carlo (CB-GEMC). These methods rely solely on the implementation of a specific bias that has to be a function of the molecular structure. This bias may be difficult to obtain for some molecules, which hinders their application to such systems.[135] The accuracy of these methods also depends on the high acceptance rate for particle insertion and deletion Monte Carlo steps. The insertion and deletion Monte Carlo steps become difficult to achieve either at low temperatures when the liquid phase is very dense or for long alkanes.[152]

As a result of the enumerated difficulties, in this work GEMC was replaced with Wang-Landau sampling. The Wang-Landau CBMC (WL-CBMC) simulation in the NPT ensemble enabled the prediction of the vapor-liquid equilibria of four α-olefins, propene through hexene (C-3 to C-6).[153] WL-CBMC sampling provides a simple, improved and efficient technique of studying phase coexistence that resolves the low acceptance probability limitation of previous methods.[139] Using this approach, the chemical potential or any intrinsic properties at phase coexistence are not needed for the simulation. This work represents the first application of this method to molecular fluids and the results are in close agreement with both experimental and other simulation results.[89,140,141,151]

WL-CBMC simulation technique has mostly been applied to model

(Lennard-Jones) fluids. The study of α-olefins is in line with our previous work of estimating vapor-liquid equilibria of molecular fluids. This method is a simple handy tool suited for probing coexistence properties since it allows the system to easily overcome the free energy barrier between the equilibrium phases.[154,155]

5.4.2 Potential Model

The NERD force field developed by Nath and coworkers was used for this study.[21] This is a united atom model developed for alkanes; it has proven to be efficient for the study of both n-alkanes and branched alkanes.[26,89,151,156] The ability of the method to accurately describe flexible molecules motivated the parametrization of the potential for alkenes.[153] This was achieved with the parameters indicated in Equations 5.36 to 5.38 and Table 5.[153,157] Equation 1.1, defines the total energy of a system as

$$E_{total} = E_{internal} + E_{external}$$

where

$$
\begin{aligned}
E_{internal} \quad = \quad & Bond\ stretching\ potential \\
+ \quad & Bond\ bending\ potential \\
+ \quad & Torsional\ potential
\end{aligned}
\tag{5.35}
$$

The bond stretching potential is given by

$$V(r)/k_b \quad = \quad \frac{K_r}{2}(r - b_{eq})^2 \tag{5.36}$$

where $K_r \; = \; 96500 K/\mathring{A}^2, \quad b_{eq} \; = \; 1.34\mathring{A}\ (C=C), \quad and\ 1.54\mathring{A}\ (C-C)$

The bond bending potential is defined by

$$V(\theta)/k_b \quad = \quad \frac{K_\theta}{2}(\theta - \theta_{eq})^2 \tag{5.37}$$

110

where $K_\theta = 62500 K/rad^2$, $\quad \theta_{eq} = 124°Å$ $(C - C = C)$

And the torsional potential is given by

$$V(\phi)/k_b = V_0 + V_1(1 + cos\phi) + V_2(1 - cos2\phi) + V_3(1 + cos3\phi) \quad (5.38)$$

For $C - C - C = C$

$\quad V_0 = 47.97~K, \quad V_1 = 86.31~K, \quad V_2 = -109.71~K, \quad V_3 = 282.08~K$ and

$$E_{external} = 4\epsilon \left[\left(\frac{\sigma}{r} \right)^{12} - \left(\frac{\sigma}{r} \right)^6 \right] \quad (5.39)$$

Table 5. Lennard-Jones parameters.[153,157]

Propene (CH$_2$=CH-CH$_3$)

$\sigma CH_3(sp^3) = 3.85Å$	$\epsilon CH_3(sp^3) = 100.0$ K
$\sigma CH_2(sp^2) = 3.72Å$	$\epsilon CH_2(sp^2) = 92.5$ K
$\sigma CH(sp^2) = 3.77Å$	$\epsilon CH(sp^2) = 46.0$ K

For longer molecules

$\sigma CH_3(sp^3) = 3.91Å$	$\epsilon CH_3(sp^3) = 104.0$ K
$\sigma CH_2(sp^2) = 3.72Å$	$\epsilon CH_2(sp^2) = 92.5$ K

The parameters K_r, K_θ, and K_ϕ represent the bond, bond angle, and dihedral angle force constants, respectively; r, θ, and ϕ are the bond length, bond angle, and dihedral angle respectively. The Lennard-Jones 12-6 potential and Coulombic terms represent the external or nonbonding interactions, with the Lennard-Jones potential used for the van der Waals interactions. ϵ is the Lennard-Jones well depth, σ is the exclusion diameter, q$_i$ is the partial atomic charge, ϵ_0 is the dielectric constant, and r is the distance between Lennard-Jones interacting sites.[21,89]

5.4.3   Simulation Method

5.4.4   Configurational Bias Monte Carlo (CBMC)

Monte Carlo simulation technique, though simple and fast, is limited in the sampling of chain molecules. This is because it does not account for conformation changes. Efforts have been made in the past two decades to develop sampling schemes that can sample different conformations in chain molecules as established by Kremer and Binder.[158] One such sampling scheme involves the socalled reptation moves mostly common with polymeric molecules, where the molecular conformation changes with the movement of the entire molecule. This procedure necessitates the transfer of a monomer from one end of the molecule to the other and a rotation of the monomer as illustrated in Figure 37.
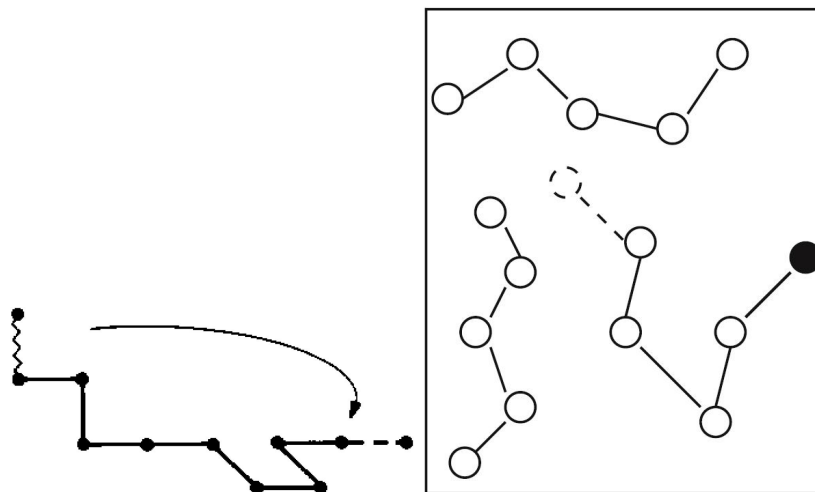
Figure 37. Examples of reptation moves. To the left the wavy bond is moved to a new position indicated as broken lines. The right figure indicates that the dotted cycle is an atom moved to a new position shown by the filled cycle.[158,159]

This approach cannot be used for monolayers where one end of the molecule is fixed. Another method suggested is to perform trial moves that involve cooperative bond rotations that can also incorporate the reassembling of the chain molecule either as a whole or in parts. However, the randomness of MC sampling method will result in the vast majority of moves being energetically unfavorable. Figure 38, illustrates that the fraction of chains without overlap decreases exponentially with

increasing chain length.[157] Siepmann and Frenkel proposed a method that generates
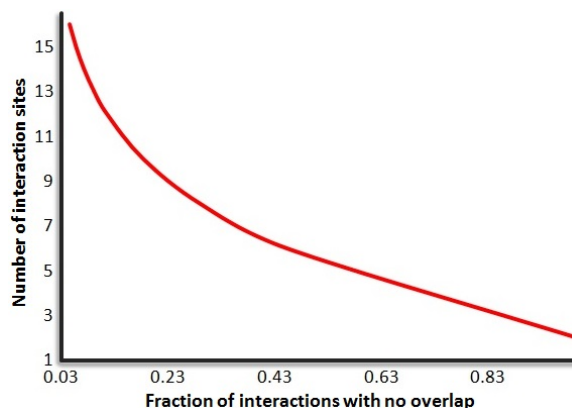
Figure 38. Variation of chain length (number of interaction sites) against the fraction of interactions without overlap.[157]

these trial moves with reassembling of the molecular framework in a smart way that prevents the molecule from overlapping with itself as well as other chains within the system. This happens, while taking into account intermolecular potentials such as *trans-gauche* torsional potential.[135] Siepmann and Frenkel researcher group modified the self-avoiding random walk proposed by Rosenbluth and Rosenbluth but kept the Rosenbluth ratio weighting factors as the acceptance criterion for accepting a new configuration.[135] In their scheme, many configurations are discarded before the complete construction of a chain. This makes the reptation method more efficient than conventional CBMC for long chains and high densities as indicated in Figure 39.[160]

Configurational Bias Monte Carlo (CBMC) allows all the conventional MC moves (translation and rotation) but introduces a new method of changing the configuration of the individual molecules. The process begins with a random selection of a chain molecule, say (i), and a segment of the molecule usually referred to as a bead (j). All the units in the molecule are discarded with indices larger than j or with a probability smaller than j. Each bead (or monomeric unit) is part of the molecule and can be considered as a single potential site interacting with its neighbors through intra- and inter-molecular forces. Next, the same chain length is regrown using the Rosenbluth self-avoiding random walk algorithm that has the
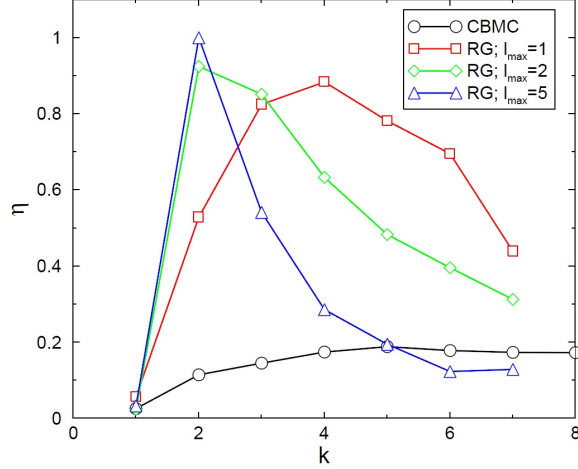
Figure 39. The efficiency of the regrowth (RG) scheme by Siepmann and Frenkel compared to the conventional CBMC method. l_{max}, indicates the maximum allowed recoil steps, and k the number of trial moves.[160]

following steps:

1. Check if any of the lattice sites neighboring the current end point of the growing chain are unoccupied. The chain growth can only continue if at least one neighboring position is not occupied either by other molecules in the system or by any previous unit of the trial chain that was grown.

2. From the available positions, one is chosen at random and the next segment of the trial conformation is added at that position. The new Rosenbluth weight for the trial conformation of length m is calculated following the original scheme, Equation 5.40.

$$W_m = \frac{n'}{n} W_{m-1} \qquad (5.40)$$

where n is the maximum number of choices (number of next-nearest neighbor sites except the one corresponding to the previous unit, which is dependent only on the type of lattice used in the simulation and the geometrical requirements for the test molecule), n' is the number of available sites for the walk, and m the number of the new unit. W_0 is the Rosenbluth weight at the start of the regrowth sequence and is equal to the Boltzmann factor of the

point where the regrowth starts.

In the case when no free neighbor sites are available, the corresponding weight for the trial attempt is zero and the attempt to grow a trial conformation has to be abandoned.

3. Otherwise proceed with steps 1 and 2 until the desired length of the trial chain is reached.

4. The new configuration of the self-avoiding random walk (SAW) is accepted or rejected based on two criteria. Better results are obtained with one of these criteria: namely, the one based on the ratio of the Rosenbluth weight of the trial conformation and the old conformations

$$P_{acceptance} = \frac{W_{trial}}{W_{old}} \tag{5.41}$$

Having accepted the SAW outcome of the trial move as a new configuration, the energy of the old and new configurations are evaluated. The standard Metropolis acceptance criterion is then applied to decide if the changes undergone by the system lead to a new configuration.

Step-by-step regrowing of the molecule by the insertion of one bead after the other results in the more probable configurations with a higher frequency. The regrowth starts with placing a new bead around the old position, first by considering the intramolecular interactions for the model. Figure 40 illustrates the regrowth process wherein a molecule is transferred from the gas phase to the liquid phase bead-by-bead. The three dark spheres show segments of the molecule that have been successfully grown in the liquid. The arrows represent trial moves to be performed for the insertion of the next bead. The energy change for each of the trial moves is calculated and the move with the right energy requirement is then accepted (here represented as the shaded sphere).[1]

The bond energy can be written as a sum of the vibrational, bending and
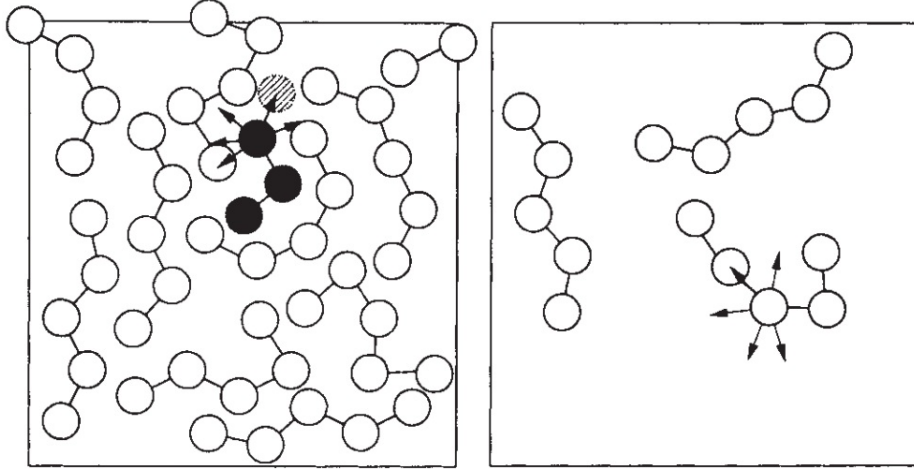
Figure 40. Regrowth process between vapor and liquid.[1]

torsional potentials

$$U_{bond}(r, \theta, \phi) = U_{vib}(r) \; + \; U_{bend}(\theta) \; + \; U_{tors}(\phi) \tag{5.42}$$

The length of the bond is often subjected to a harmonic potential with oscillations around an equilibrium distance. Thus the trial orientations can be distributed on an outer portion of a sphere, enclosed by two spherical surfaces with radii that are slightly bigger and slightly smaller than the equilibrium bond distance. Only a limited number of k trials are generated in order to speed up the simulation. The probability of generating a new position n from the set of trial configurations $\mathbf{r}$ is:

$$
\begin{aligned}
\rho_{n,bond}\mathrm{d}\mathbf{r} \;\; &= \;\; \frac{\exp\left[-u_{n,bond}(\mathbf{r})/k_BT\right]\mathrm{d}\mathbf{r}}{\int \mathrm{d}\mathbf{r}\,\exp\left[-u_{i,bond}(\mathbf{r})/k_BT\right]} \\
&= \;\; \frac{\exp\left[-u_{n,bond}(\mathbf{r})/k_BT\right]\mathrm{d}\mathbf{r}}{C}
\end{aligned}
\tag{5.43}
$$

where $u_{n,bond}$ is the bond energy of monomer n, and C is the normalization constant related to the bond energy.

Since r, θ and ϕ are used to represent the conformations of the molecule (see Figure 5.4.4), it is convenient to work with spherical coordinates:

116
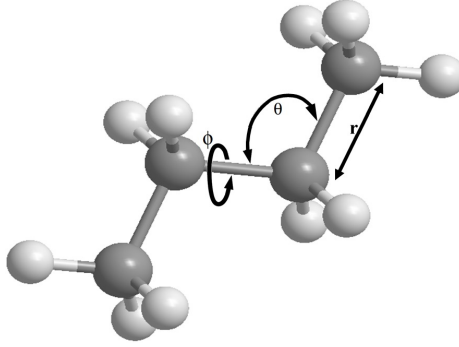
$$d\mathbf{r} = r^2 dr \, dcos\theta \, d\phi \tag{5.44}$$

The probability that this new trial position is generated then becomes:

$$\rho_{n,bond} d\mathbf{r} = \frac{\exp\left[-u_{n,vib}(r)/k_B T\right] \exp\left[-u_{n,bend}(\theta)/k_B T\right] \exp\left[-u_{n,tors}(\phi)/k_B T\right] r^2 dr \, dcos\theta \, d\phi}{C} \tag{5.45}$$

A new trial is obtained by generating a random vector within the portion of a sphere limited by the two radii and calculating the distance (r), bending (θ) and torsional (ϕ) angles. The distance and the angles are accepted with a probability according to Equation 5.45. If rejected, another vector is generated until one gets accepted. In case the new position corresponds to the second bead in the molecule, any random vector is accepted with a probability distribution according to the vibrational energy, since no bending or torsional restraints are present. The probability of generating the third bead is also simplified, given that no torsional changes are present.

$$\rho_{n,bond} d\mathbf{r} = \frac{\exp\left[-u_{n,vib}(r)/k_B T\right] \exp\left[-u_{n,bend}(\theta)/k_B T\right] r^2 dr \, dcos\theta \, d\phi}{C} \tag{5.46}$$

The next step is to calculate the external, nonbonding energy probability of the selected bead. At this point, selecting the new position depends on the interactions with the beads from the other molecules around and those from the same molecule

117

separated by more than 3 monomeric units

$$\rho_{n,ext}(\mathbf{r}_n) = \frac{\exp\left[-u_{n,ext}(\mathbf{r}_n)/k_BT\right]}{\sum_{i=1}^{k}\exp\left[-u_{i,ext}(\mathbf{r}_n)/k_BT\right]} \tag{5.47}$$

where $u_{n,ext}(\mathbf{r}_n)$ is the external energy for the new bead and the denominator represents its external configurational partition function. The latter term is given the symbol $w_{i,ext}(n)$

$$\rho_{n,ext}(\mathbf{r}_n) = \frac{\exp\left[-u_{n,ext}(\mathbf{r}_n)/k_BT\right]}{w_{i,ext}(n)} \tag{5.48}$$

Once the entire chain is regrown, the Rosenbluth factor is calculated:

$$W_{ext}(n) = \prod_{i=1}^{l} w_{i,ext}(n) \tag{5.49}$$

where, l is the number of beads regrown.

In order to compare the obtained new conformation to the old (o) one, it is necessary to repeat the same steps for the old chain. This time, the first step of evaluating the bonded probability is omitted as it does not influence the final acceptance criterion for accepting or rejecting the new structure. Each new-bead is also accepted with 100 % probability as their positions in the old chain are predetermined. The same number of different trials around the old monomeric unit however is generated, calculating the external energy for each one ($u_{i,ext}(o)$) and the external configurational partition function:

$$w_{i,ext}(o) = \sum_{i=1}^{k} \exp\left[-u_{i,ext}(\mathbf{r}_o)/k_BT\right] \tag{5.50}$$

After the old conformation is retraced, the Rosenbluth factor is calculated from

$$W_{ext}(o) = \prod_{i=1}^{l} w_{i,ext}(o) \tag{5.51}$$

The correct sampling of the transition from the old to the new chain conformation is guaranteed by the detailed balance condition, Equation 5.10. The difference with respect to the conventional MC scheme is that the transition matrix probability is biased according to the above described method of generating a new bead from the old one. It depends on the product of generating a trial orientation according to the bonded probability, Equation 5.44, and the external energy probability of the selected bead, Equation 5.47.

$$\alpha_{o \to n} = \rho_{i,bond}(n)\rho_{i,ext}(n)\alpha'_{o \to n} \tag{5.52}$$

where $\alpha'_{o \to n}$ is a symmetric transition matrix, such as the transition matrix in a conventional MC scheme.

The detailed balance condition is

$$\rho_o \alpha_{o \to n} acc_{o \to n} = \rho_n \alpha_{no} acc_{no} \tag{5.53}$$

By replacing $\alpha_{o \to n}$ with the expression in Equation 5.52, it becomes:

$$\rho_o \rho_{bond}(n)\rho_{ext}(n)\alpha'_{o \to n} acc_{o \to n} = \rho_n \rho_{bond}(o)\rho_{ext}(o)\alpha'_{no} acc_{no} \tag{5.54}$$

Since α' is symmetric and $\rho_o \propto \exp\left[-u(o)/k_B T\right]$, the left and right side of the equation can be written as follows:

1. Left side

$$\exp\left[-u(o)/k_B T\right] \frac{\exp\left[-u_{bond}(n)/k_B T\right]}{C} \frac{\exp\left[-u_{ext}(n)/k_B T\right]}{w_{ext}(n)} acc_{o \to n} \tag{5.55}$$

2. Right side

$$\exp\left[-u(n)/k_B T\right] \frac{\exp\left[-u_{bond}(o)/k_B T\right]}{C} \frac{\exp\left[-u_{ext}(o)/k_B T\right]}{w_{ext}(o)}) acc_{no} \tag{5.56}$$

Since $u(o) = u_{bond}(o) + u_{ext}(o)$, one can express the probability of being in the old configuration as

$$\exp\left[-u(o)/k_B T\right] = \exp\left[-u_{bond}(o)/k_B T\right]\ \exp\left[-u_{ext}(o)/k_B T\right] \qquad (5.57)$$

Using the above expression, the detailed balance condition can be further simplified. Having the same bonding configurational partition function for the old and new bead, the final acceptance criterion becomes

$$acc_{o\to n} = \min\left\{1, \frac{w_{ext}(n)}{w_{ext}(o)}\right\} \qquad (5.58)$$

The move is accepted based solely on the external nonbonding energy of the trials for the new and old bead. The convenience of using the Rosenbluth scheme in the off-lattice case comes from the fact that bond energy is omitted in the final acceptance rule, which decreases the computational time. If more than one bead is grown, expressions 1 and 2 would grow with additional terms, corresponding to each bead in the regrown and its counterpart old conformation. The acceptance criterion can be simplified again to give this time a product of the w_{ext} factors for each new and old bead, which are the two Rosenbluth factors, Equations 5.49 and 5.51.

$$acc_{o\longrightarrow n} = \min\left\{1, \frac{W_{ext}(n)}{W_{ext}(o)}\right\} \qquad (5.59)$$

The CBMC technique is tightly bound with the Gibbs Ensemble Monte Carlo (GEMC) method especially in the construction of phase diagrams of alkane chains. The particle exchange moves are necessary to attain equilibrium in the Gibbs Ensemble. The insertion of a chain molecule in the liquid phase must be accompanied with a change in the conformational structure of the molecule in order to avoid overlapping. This is done by inserting bead by bead, in exactly the same manner that a chain is regrown. The particle exchange move still presents a challenge for long molecules with complex architecture. The configurational bias

technique has to be implemented not only for the particle exchange, but also with the MC move inside each of the simulation boxes, for the regrowth (conformational change) of the chain. This can be avoided by replacing the MC moves with a hybrid Monte Carlo (HMC) procedure.[22,156,161]

Generation of trial positions is time consuming when a branched chain is considered. The acceptance of a trial configuration of the branched site now depends on the bond length, the torsional angle and the two angles between the bond vector and the two existing branches. The acceptance probability is decreased and the efficiency for successful generation of a branched site is about 2-10 times lower than that of a linear molecule. This method was later improved by Nath and Khare[22] by growing all the atoms from a branch point simultaneously instead of one after another. This technique, described in details by Macedonia and Maginn[162] was found to be faster and more efficient. The efficiency of generating new configurations of branched sites is an order of magnitude higher for simple molecules and increases with molecular complexity. Yet, the acceptance probability of the inserted molecule depends on the number of the preliminary established configurations of a single branched segment.

5.4.5   Wang-Landau Configurational Bias Monte Carlo (WL-CBMC)

The Wang-Landau sampling technique described earlier is this time combined with Configurational-bias Monte Carlo to study the phase behavior of four α-alkenes (propene, butene, pentene, and hexene). The use of configurational-bias facilitates molecular insertion during MC moves. WL sampling similar to the earlier description was used for an even sampling of the volume (V). The WL flat histogram technique was used for it's proven efficiency in evaluating the vapor-liquid equilibria in variety of systems.[82,139–141,151,163] Throughout the simulation four types of MC moves were performed, which included translational, rotational, regrowth, and volume changes. Following Ganzenm$\ddot{u}$ller et $al.$,[139] the joint Boltzmann distribution for a given configuration (Γ) and volume (V) was defined the same as in

Equation 5.20. Defining the isothermal-isobaric partition function Q(N, P, T) as Equation 5.60.

$$Q(N, P, T) = \int_0^\infty Q(N, V, T) \, exp(-\beta PV) dV \qquad (5.60)$$

The volume distribution is given by

$$p(V) = \int p(\Gamma, V) d\Gamma = \frac{Q(N, V, T) \, exp(-\beta PV)}{Q(N, P, T)} \qquad (5.61)$$

Combining Equations 5.20 and 5.61 leads to the bias probability ($p_{bias}(\Gamma, V)$) for a given configuration (Γ) and volume (V) given in Equation 5.22.

Like in the case of the PAHs, the pressure simplifies out of Equation (5.23) leaving the canonical partition function with variable V, and N and T as constant, as the only biasing function necessary for uniform sampling of V.

100 molecules of each alkene are used for the simulation, and the frequency of various moves was controlled by assigning fixed percentages for the rate of each move as follows: 32.8% for translation, rotation, and regrowth (configurational bias), and 1.6 % for volume changes. The low probability for the volume change ensures that after each volume change, the new volume bin is efficiently sampled before the next change. A counter variable was employed to keep track of the number of times each volume bin was visited, this ensured that a flat histogram was obtained. The terminal value of the counter was set to 500, after which it was assumed all moves had been performed equally. This implies that the coexisting density converged to the true value and the volume distribution was given by Equation 5.61. Figure 42 shows the running estimate of Q(NVT), that signifies the simulation converged for the simulation of butene at T=373 K. Once this happens then the system performs a volume change, it is not possible to predetermine the number of MC sweeps for each iteration or volume change. Instead, the system is allowed to freely check if all of the moves have been equally performed and that the criterion for a flat histogran has been satisfied.[163]
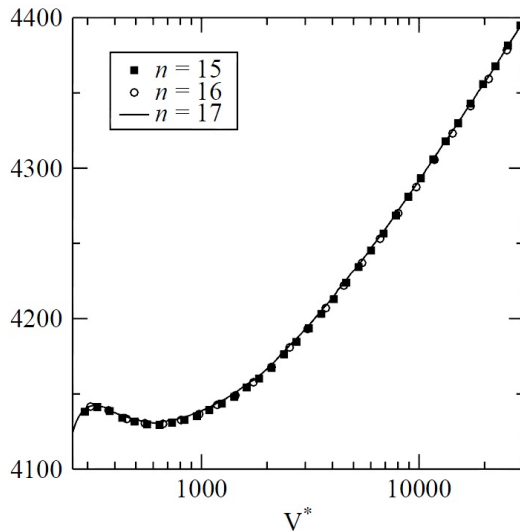
Figure 42. Convergence of the running estimate for $\ln[Q_{N,V,T}]$ after n iterations for the WLCBMC simulations of coexistence of butene at T = 373K.

The acceptance criteria for a translation or rotation move from an old configuration o with potential energy U_o, to a new configuration n with potential energy U_n, as illustrated in previous works is given by

$$acc(o{\rightarrow}n) = min\left[1, exp\left(-\frac{(U_n - U_o)}{k_b T}\right)\right] \qquad (5.62)$$

CBMC moves are employed to account for conformational changes as a result of the flexibility of the molecules. This is achieved by regrowth of the molecule that changes the internal configuration of a molecule as it is built part by part. These moves are accepted by a probability given by:

$$acc(o{\rightarrow}n) = min\left[1, \frac{W_n}{W_o}\right] \qquad (5.63)$$

where W_n and W_o are Rosenbluth factors given by Equation 5.64 for the new and old conformations respectively.[71]

$$W = \frac{\Pi_{i=2}^{i=n} \sum_{j=1}^{j=k} exp[-\beta U(i,j)]}{k^{n-1}} \qquad (5.64)$$

123

where k = number of trial positions and $U(i, j)$ = energy of the jth trial position of the ith chain segment.

It should be noted that the bond-bending potential is no longer considered for $U(i, j)$ since it is used in the generation of the trial positions.

The upper and lower limits of the volume for the different molecules are set based on chosen densities. For propene and butene these limits were 0.005 and 0.6 g/cm^3, for pentene 0.0025 and 0.68 g/cm^3 and for hexene 0.001 and 0.7 g/cm^3 respectively. The volume ranges for all the systems investigated were divided as described in the case of PAHs.

5.4.6   Results and Discussion

The data obtained for the coexistence properties of the various alkenes is presented in Figures 43. The presented results were obtained by using a combination of the Wang-Landau sampling and MC simulation method in the NPT ensemble.
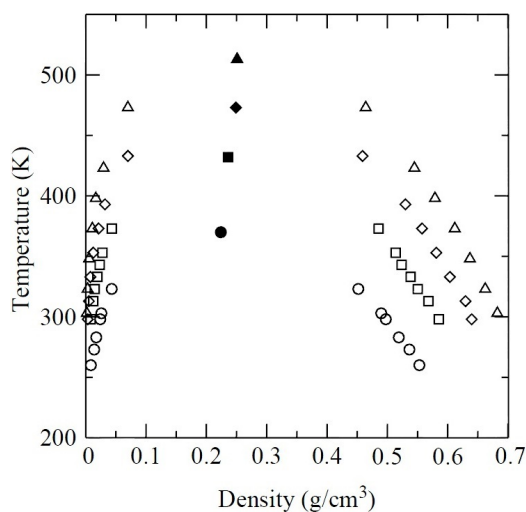
Figure 43. Vapour-liquid equilibria of the different alkenes and their corresponding critical points extrapolated from the simulation results (shown in filled symbols). Propene (circles), butene (squares), pentene (diamonds) and hexene (triangles).

The critical parameters were estimated from the simulation results by fitting WL-CBMC simulated vapor-liquid equilibria results with the density scaling law

124

(Equation 5.32), and the law of rectilinear diameters (Equation 5.33) to determine T_c and ρ_c respectively.[89,149] The results obtained for the critical temperature and density for the four alkenes studied are summarized in Table 6.

Table 6. Critical temperatures and densities obtained from the WL-CBMC simulation compared with those obtained from experiment.[164]

	WL-CBMC Simulated results		Experimental Results	
	T_c (K)	ρ_c (g/cm^3)	T_c (K)	ρ_c (g/cm^3)
Propene	370	0.224	365	0.233
Butene	432	0.236	420	0.233
Pentene	473	0.249	474	-
Hexene	513	0.251	-	-

All the results are in close agreement with experiment and previous simulation results. A relatively satisfactory agreement is observed between our simulation results and the other results like those of Nath *et. al.* as presented in Figure 44.[21] These results show a negligible discrepancy for the densities in the liquid phase, which validates our proposed method.
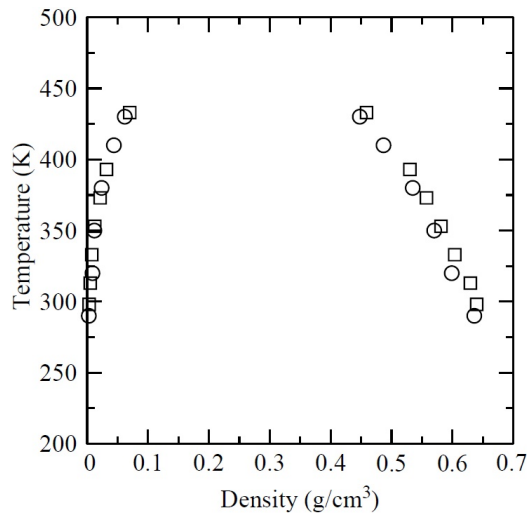
Figure 44. Comparison of results from the Gibbs ensemble Monte Carlo simulations (circles) and the WLCBMC simulations (squares) for Pentene.[21]

The results are further validated by the ability to reproduce the volume distribution for butene (Figure 45), corresponding to the convergence of the partition function shown in Figure 42. The plot in Figure 42 shows two peaks

125

analogous to the liquid and the vapor phase situated to the left and the right respectively.
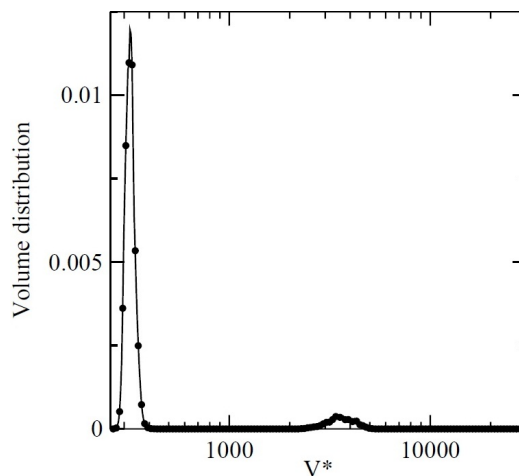
Figure 45. Volume distribution for Butene at coexistence at room temperature.

The saturation pressure P_{coex} is determined at the end of the simulation by first evaluating the area represented by each each volume in Figure 45 and applying the condition of coexistence (i.e., both areas are equal). Figure 46 give the variation of the vapor pressures as a function of temperature.
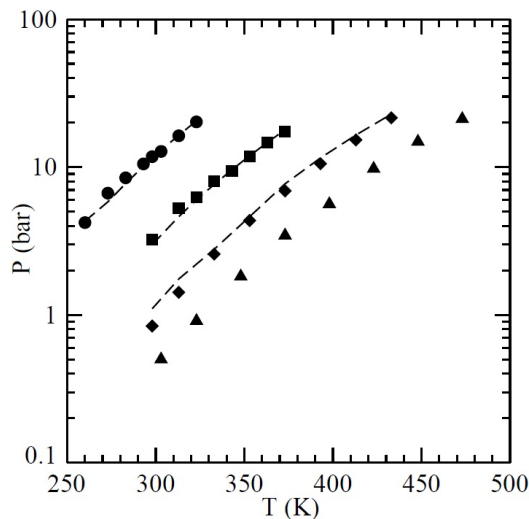
Figure 46. Variation of vapor pressure with temperature for propene (circles), butene (squares), pentene (diamonds) and hexene (triangles).[164] WL-CBMC simulation results are presented as symbols and experimental results are shown as dashed lines.

The plots in Figure 46 also show a comparison of the vapor pressures obtained

by WL-CBMC with those obtained from experiment for the first three alkenes for which experimental data is available.

CHAPTER VI

CONCLUSION

First order phase transition processes are encountered in everyday life. Knowledge of the thermodynamic properties at the point of the phase change are necessary in many applications. However, due to the difficulties of obtaining these properties by experiments, molecular simulation methods are key in assessing the properties. Here, enhanced sampling methods (Umbrella sampling and Wang-Landau sampling) are used to study both equilibrium and non-equilibrium first order transitions.

These methods are simple in that properties at coexistence can be obtained from a single simulation of equilibrium systems through efficient sampling of the phase space. This is achieved by the application of a bias potential. Umbrella sampling uses a bias potential that is a function of the order parameter to sample the solid-liquid and solid-vapor non-equilibrium transitions in Buckminster fullerene or buckyball (C_{60}). By gradually changing the order parameter, the system sampled through the free energy barrier, thus revealing properties of the critical nucleus and the crystal structure. It is observed that the nucleation and growth processes occur without passing through the BCC least stable phase as expected from previous studies on model fluids.

The mechanism of the nucleation and growth from the liquid and vapor are similar and consist only of the HCP and FCC crystal structures (Polymorph). This result is consistent with previous studies of C_{60} clusters. This observation is attributed to the steepness of the repulsive part of the potential model. This is due to the large size of the C_{60} molecule and the confinement of the liquid pocket of its phase diagram to a very tiny temperature interval. This suggests that polymorph

selection for spherical systems with dimensions in the nanometer range might require different strategies. Although there is no clear observation of polymorph selection, this study shows the successive layers of FCC and HCP in the growth phase, a process referred to as cross nucleation.

Vapor-liquid equilibrium phase transitions studies on PAHs and α-alkenes were carried out using the Wang-Landau sampling scheme. This method accurately samples the microstates of vapor and liquid phases at coexistence by estimating the partition function. The study was performed in the NPT ensemble and the convergence of the simulation was confirmed by the continuity of the canonical partition function at the simulated temperature. To account for conformational changes during the study of α-alkenes, the configurational bias Monte Carlo technique was used. This method efficiently samples the phase space by using the concept of regrowth, thus avoiding the inefficient process of particle insertion and deletion. It therefore enhances the computational demand and makes the method reliable for studying larger systems.

The Wang-Landau method has the advantage that only a single simulation at a given temperature is needed to obtain the coexistence properties of both phases. In addition prior knowledge of the chemical potential or saturation pressure is not necessary during the simulation. The simulated results using Wang-Landau techniques were in good agreements with both experimental results and results from simulations using different methods. This validates the accuracy of this method. The simplicity and accuracy of the methods proposed in this project can be explored for the study of other systems.

REFERENCES

1. Siepmann, J. I.; Karaborni, S.; Smit, B. Simulating the critical behaviour of complex fluids. *Nature* **1993**, *365*, 330–332.

2. De Pablo, J. J.; Yan, Q.; Escobedo, F. A. Simulation of phase transitions in fluids. *Annu. Rev. Phys. Chem.* **1999**, *50*, 377–411.

3. Mastny, E. A.; De Pablo, J. J. Direct calculation of solid-liquid equilibria from density-of-states Monte Carlo simulations. *J. Chem. Phys.* **2005**, *122*, 124109/1–6.

4. Roland, U.; Fomba, K. W.; Stallmach, F.; Galvosas, P.; Kärger, J.; Kopinke, F. D. Influence of phase transitions on the mobility of organic pollutants in synthetic and natural polymers. *Diffusion Fundamentals* **2005**, *2*, 129/1–2.

5. Williamsa, B.; Goldsteina, A.; Kreisberge, N.; Heringe, S. In situ measurements of gas/particle phase transitions for atmospheric semivolatile organic compounds. *PNAS* **2010**, *107*, 6676–6681.

6. Esser-Kahn, A. P.; Odom, S. A.; Sottos, N. R.; White, S. R.; Moore, J. S. Triggered release from polymer capsules. *Macromol.* **2011**, *44*, 5539–5553.

7. Choi, S. W.; Zhang, Y.; Xia, Y. A temperature-sensitive drug release system based on phase-change materials. *Angew. Chem. Int. Ed.* **2010**, *49*, 7904–7904.

8. Hornedo, N.; Murphy, D. Significance of controlling crystallization mechanisms and kinetics in pharmaceutical systems. *J. Pharm. Sci.* **1999**, *88*, 651–660.

9. Nokhodch, A. Effect of moisture on compaction and compression. *Pharm. Technol., Data Rev.* **2005**, 46–66.

10. Center for drug evaluation and research (CDER). Safety considerations for product design to minimize medication errors. 2012;
`http://www.fda.gov/downloads/Drugs/`
`GuidanceComplianceRegulatoryInformation/Guidances/UCM331810.pdf`,
Accessed March 2013.

11. Ma, X.; Taw, J.; Chiang, C. M. Control of drug crystallization in transdermal matrix system. *Int. J. Pharm.* **1996**, *142*, 115–119.

12. Mansoori, G. A. A unified perspective on the phase behaviour of petroleum fluids. *Int. J. Oil, Gas, Coal, Technol.* **2009**, *2*, 141–167.

13. Anderson, V. J.; Lekkerkerker, H. N. W. Insights into phase transition kinetics from colloid science. *Nature* **2002**, *416*, 811–815.

14. Wilding, N. B. Computer simulation of fluid phase transitions. *Am. J. Phys.* **2001**, *69*, 1147–1155.

15. Panagiotopoulos, A. Z. Molecular simulation of phase equilibria. *Appl. Sci.* **1994**, *273*, 411–437.

16. Gathers, G. R. Dynamic methods for investigating thermophysical properties of matter at very high temperatures and pressures. *Rep. Prog. Phys.* **1986**, *49*, 341–396.

17. Mooij, G. C. A. M.; Frenkel, D.; Smit, B. Direct simulation of phase equilibria of chain molecules. *J. Phys. Condens Matter* **1992**, *4*, 1255–1259.

18. Potoff, J. J.; Bernard-Brunel, D. A. Mie potentials for phase equilibria calculations: Application to alkanes and perfluoroalkanes. *J. Phys. Chem. B* **2009**, *113*, 14725–14731.

19. Krist*ó*f, T.; Liszi, J. Effective intermolecular potential for fluid hydrogen sulfide. *J. Phys. Chem. B* **1997**, *101*, 5480–5483.

20. De Koning, M.; Cai, W.; Sadigh, B.; Oppelstrup, T.; Kalos, M. H.; Bulatov, V. V. Adaptive importance sampling Monte Carlo simulation of rare transition events. *J. Chem. Phys.* **2005**, *122*, 074103/1–12.

21. Nath, S. K.; Banaszak, B. J.; De Pablo, J. J. New united atom force field for -olefins. *J. Chem. Phys.* **2001**, *114*, 3612–3616.

22. Nath, S. K.; Khare, R. New forcefield parameters for branched hydrocarbons. *J. Chem. Phys.* **2001**, *115*, 10837–10844.

23. Wick, C. D.; Martin, M. G.; Siepmann, J. I. Transferable potentials for phase equilibria. 4. United-atom description of linear and branched alkenes and alkylbenzenes. *J. Phys. Chem. B* **2000**, *104*, 8008–8016.

24. Cornell, W. D.; Cieplak, P.; Bayly, C. I.; Gould, I. R.; Merz Jr., K. M.; Ferguson, D. M.; Spellmeyer, D. C.; Fox, T.; Caldwell, J. W.; Kollman, P. A. A second generation force field for the simulation of proteins, nucleic acids, and organic molecules. *J. Am. Chem. Soc.* **1995**, *117*, 5179–5197.

25. Huang, D. M.; Faller, R.; Do, K.; Moule, A. J. Coarse-grained somputer simulations of polymer/Fullerene bulk heterojunctions for organic photovoltaic applications. *J. Chem. Theory Comput.* **2010**, *6*, 526–537.

26. Nath, S. K.; Escobedo, F. A.; De Pablo, J. J. On the simulation of vapor-liquid equilibria for alkanes. *J. Chem. Phys.* **1998**, *108*, 9905–9911.

27. MacKerell Jr., A. D. et al. All-atom empirical potential for molecular modeling and dynamics studies of proteins. *J. Phys. Chem. B* **1998**, *102*, 3586–3616.

28. Chopra, M.; Malshe, R.; Reddy, A. S.; De Pablo, J. J. Improved transition path sampling methods for simulation of rare events. *J. Chem. Phys.* **2008**, *128*, 144104/1–5.

29. Goujon, F.; Malfreyt, P.; Simon, J. M.; Boutin, A.; Rousseau, B.; Fuchs, A. H. Monte Carlo versus molecular dynamics simulations in heterogeneous systems: An application to the n-pentane liquid-vapor interface. *J. Chem. Phys.* **2004**, *121*, 12559–12571.

30. Panagiotopoulos, A. Z. Monte Carlo methods for phase equilibria of fluids. *J. Phys.: Condens. Matter* **1999**, *12*, 1–38.

31. Rudisill, E. N.; Cummings, P. T. Gibbs ensemble simulation of phase equilibrium in the hard core two-Yukawa fluid model for the Lennard-Jones fluid. *Mol. Phys.* **1989**, *68*, 629–635.

32. Kofke, D. A. Direct evaluation of phase coexistence by molecular simulation via integration along the saturation line. *J. Chem. Phys.* **1993**, *98*, 4149–4162.

33. Panagiotopoulos, A. Z. Direct determination of fluid phase equilibria by simulation in the Gibbs ensemble: A review. *Mol. Sim.* **1992**, *9*, 1–23.

34. Panagiotopoulos, A. Z. Current advances in Monte Carlo methods. *Fluid Phase Equilibria* **1996**, *116*, 257–266.

35. Mackie, A.; Panagiotopoulos, A. Z.; Kumar, S. Gibbs ensemble techniques. *J. Chem. Phys.* **1995**, *102*, 1014–1023.

36. Binder, K. Theory of first-order phase transitions. *Rep. Prog. Phys.* **1987**, *50*, 783–859.

37. Papon, P.; Leblond, J.; Meijer, P. H. E. *The physics of phase transitions: Concepts and applications*, 2nd ed.; Springer, 2006; pp 1–31.

38. Liu, R. PHYS5510 Topics in Theoretical Physics (Advanced Statistical Mechanics) Chapters 5, 6, and 7. 2012; `http://www.phy.cuhk.edu.hk/course/2012-2013/1/phys5510/download/index.html`, Accessed March 2013.

39. Swain, S. P-101 Mechanics and thermodynamics lecture notes chapter 6: Phase transitions. `http://niser.ac.in/~sanjay/teaching/P-101/Lecture/CHAP6.pdf`, Accessed March 2013.

40. Miller, W. L.; Cacciuto, A. Exploiting classical nucleation theory for reverse self-assembly. *J. Chem. Phys.* **2010**, *133*, 234108/1–6.

41. Merikanto, J.; Zapadinsky, E.; Lauri, A.; Vehkamaki, H. Origin of the failure of classical nucleation theory: Incorrect description of the smallest clusters. *Phys. Rev. Lett.* **2007**, *98*, 145702/1–4.

42. Ryu, S.; Cai, W. Validity of classical nucleation theory for Ising models. *Phys. Rev. E* **2010**, *81*, 03060/1–4.

43. Leyssale, J. M.; Delhommelle, J.; Millot, C. Hit and miss of classical nucleation theory as revealed by a molecular simulation study of crystal nucleation in supercooled sulfur hexafluoride. *J. Chem. Phys.* **2007**, *127*, 044504/1–8.

44. Sear, R. P. On the interpretation of quantitative experimental data on nucleation rates using classical nucleation theory. *J. Phys. Chem. B* **2006**, *110*, 21944–21949.

45. Shneidman, V. A.; Jackson, K. A.; Beatty, K. M. On the applicability of the classical nucleation theory in an Ising system. *J. Chem. Phys.* **1999**, *111*, 6932–6941.

46. Cacciuto, A.; Frenkel, D. Stresses inside critical nuclei. *J. Phys. Chem. B* **2005**, *109*, 6587–6594.

47. Ndumbe Ngale, K.; Desgranges, C.; Delhommelle, J. Nucleation and growth of C_{60} nanoparticles from the supersaturated vapor and from the undercooled liquid: A molecular simulation study. *J. Chem. Phys.* **2009**, *131*, 244515/1–6.

48. Erdemir, D.; Lee, A. Y.; Myerson, A. S. Nucleation of crystals from solution: classical and two-step models. *Acc. Chem. Res.* **2008**, *42*, 621–629.

49. Schmelzer, J. W. P. On the determination of the kinetic pre-factor in classical nucleation theory. *J. Non-Cryst. Solids* **2010**, *356*, 2901–2907.

50. Sear, R. P. Classical nucleation theory for the nucleation of the solid phase of spherical particles with a short-ranged attraction. **1999**, 1–10.

51. Vekilov, P. G. Nucleation. *Cryst. Growth Des.* **2010**, *10*, 5007–5019.

52. Volmer, M.; Weber, A. Nuclei formation in supersaturated states. *Z. Phys. Chem.* **1926**, *119*, 277–301.

53. Farkas, L. The velocity of nucleus formation in supersaturated vapours. *Z. Physik. Chemie* **1927**, *125*, 236–242.

54. http://www.wisegeek.com/what-is-nucleation.htm, Accessed April 2013.

55. Horsch, M.; Vrabec, J.; Hasse, H. Modification of the classical nucleation theory based on molecular simulation data for surface tension, critical nucleus size, and nucleation rate. *Phys. Rev. E* **2008**, *78*, 01160/1–9.

56. Talanquer, V.; Oxtoby, D. W. Nucleation in molecular and dipolar fluids: Interaction site model. *J. Chem. Phys.* **1995**, *103*, 3686–3695.

57. Tóth, G. I.; Gránásy, L. Crystal nucleation in the hard-sphere system revisited: A critical test of theoretical approaches. *J. Phys. Chem. B* **2009**, *113*, 5141–5148.

58. Wu, W.; Nancollas, G. H. Interfacial free energies and crystallization in aqueous media. *J. Colloid Interface Sci.* **1996**, *182*, 365–373.

59. Keasler, S. J.; Kim, H.; Chen, B. Sign preference in ion-induced nucleation: Contributions to the free energy barrier. *J. Chem. Phys.* **2012**, *137*, 174308/1–9.

60. Weinberg, M. C.; Zanotto, E. D.; Manrich, S. Classical nucleation theory with a size dependent interfacial tension: $Li_2O.2SiO_2$ crystal nucleation. *Phys. Chem. Glasses* **1992**, *33*, 98–102.

61. McQuarrie, D. A. *Statistical Mechanics*, 203rd ed.; University Science Books, 2008; pp 1–641.

62. Allen, M. P.; Tildesley, D. J. *Computer simulation of liquids*; Clarendon Press, 1987; pp 1–385.

63. Tóth, G. Z. On Lagrangian and Hamiltonian systems with homogeneous trajectories. *J. Phys. A: Math. Theor.* **2010**, *43*, 385206 /1–19.

64. Malham, S. J. An introduction to Lagrangian and Hamiltonian mechanics. 2012; `http://www.ma.hw.ac.uk/~simonm/mechanics.pdf`, Accessed March 2013.

65. Rastogi, V.; Mukherjee, A.; Dasgupta, A. A review on extension of Lagrangian-Hamiltonian mechanics. *J. Braz. Soc. Mech. Sci. Eng.* **2011**, *33*, 22–33.

66. Allen, M.; Tildesley, D. *Computer simulation of liquids*; Oxford University Press, 1987.

67. Nosé, S. A molecular dynamics method for simulations in the canonical ensemble. *Mol. Phys.* **1984**, *52*, 255–268.

68. Nosé, S. A unified formulation of the constant temperature molecular dynamics method. *J. Chem. Phys.* **1984**, *81*, 511–519.

69. Baranyai, A.; Evans, D. J. New algorithm for constrained molecular dynamics simulation of liquid benzene and naphthalene. *Mol. Phys.* **1990**, *70*, 53–63.

70. Shinoda, W.; Mikami, M. Rigid-body dynamics in the isothermal-isobaric ensemble: A test on the accuracy and computational efficiency. *J. Comput. Chem.* **2003**, *24*, 920–930.

71. Frenkel, D.; Smit, B. *Understanding molecular simulation: From algorithms to applications*, 2nd ed.; Elsevier Science, 2002; pp 1–638.

72. González, A.; White, J. A.; Román, F. L.; Velasco, S. Density functional theory of fluids in the isothermal-isobaric ensemble. *J. Chem. Phys.* **2004**, *120*, 10634–10639.

73. De Oliveira, C. R.; Werlang, T. Ergodic hypothesis in classical statistical mechanics. *Rev. Bras. Ensino Fis.* **2007**, *29*, 189–201.

74. Lichtenegger, K.; Linden, W. Annealing Strategies in the Simulation of Fullerene Formation. 2009; `http://arxiv.org/pdf/0912.4041v1.pdf`.

75. Yamaguchi, Y.; Maruyama, S. A Molecular Dynamics simulation of the Fullerene formation process. *Chem. Phys. Lett.* **1998**, *286*, 336–342.

76. Even, W.; Smith, J.; Roth, M. Molecular dynamics of noble gasses encapsulated in C_{60} fullerenes. *Mol. Simul.* **2005**, *31*, 207–213.

77. Katzgraber, H. G. Introduction to Monte Carlo Methods. 2011; `http://arxiv.org/pdf/0905.1629.pdf`, note=Accessed April 2013,.

78. Kirkpatrick, S.; Gelatt, C.; Vecchi, M. Optimization by simulated annealing. *Science, New Series* **1983**, *220*, 671–680.

79. Tomanek, D.; Schluter, M. Growth regime of carbon clusters. *Phys. Rev. Lett* **1991**, *67*, 2331–2334.

80. Chopra, M.; Müller, M.; de Pablo, J. Order-parameter-based Monte Carlo simulation of crystallization. *J. Chem. Phys.* **2006**, *124*, 134102/1–8.

81. Calvo, F. Sampling along molecular coordinates with Wang-Landau method. *Mol. Phys.* **2002**, *100*, 3421–3427.

82. Wang, F.; Landau, D. P. Efficient, multiple-range random walk algorithm to calculate the density of states. *Phys. Rev. Lett.* **2001**, *86*, 2050–2053.

83. Beskos, A.; Pillai, N. S.; Roberts, G. O.; Sanz-Serna, J. M.; Stuart, A. M. The acceptance probability of the hybrid Monte Carlo method in high-dimensional problems. *AIP Conference Proceedings* **2010**, *1281*, 23–26.

84. Forrest, B. M.; Suter, U. W. Hybrid Monte Carlo simulations of dense polymer systems. *J. chem. phys.* **1994**, *101*, 2616–2629.

85. Akhmatskaya, E.; Bou-Rabee, N.; Reich, S. A comparison of generalized hybrid Monte Carlo methods with and without momentum flip. *J. Comput. Phys.* **2009**, *228*, 2256–2265.

86. Mackay, D. J. C. Introduction to hybrid Monte Carlo methods. 1998; `http://www.inference.phy.cam.ac.uk/mackay/erice.pdf`, Accessed April 2013.

87. Duane, S.; Kennedy, A. D.; Pendleton, B. J.; Roweth, D. Hybrid Monte Carlo. *J. Phys. Lett. B* **1987**, *195*, 216–222.

88. Mehlig, B.; Heermann, D. W.; Forrest, B. M. Hybrid Monte Carlo method for condensed-matter systems. *Phys. Rev. B* **1992**, *45*, 679–685.

89. Desgranges, C.; Delhommelle, J. Phase equilibria of molecular fluids via hybrid Monte Carlo Wang-Landau simulations: Applications to benzene and n-alkanes. *J. Chem. Phys.* **2009**, *130*, 244109/1–7.

90. Hartmann, C.; Schütte, C. A constrained hybrid Monte-Carlo algorithm and the problem of calculating the free energy in several variables: Plenary lecture presented at the 75th Annual GAMM Conference, Dresden/Germany, 22-26 March 2004. *ZAMM Z. Angew. Math. Mech.* **2005**, *85*, 700–710.

91. Schaefer, S. Simulations with the hybrid Monte Carlo algorithm: Implementation and data analysis. 2009; `http://nic.desy.de/sites2009/site_nic/content/e44192/e62778/e91179/e91180/hmc_tutorial_eng.pdf`, Accessed April 2013.

92. Zhang, H. A new hybrid Monte Carlo algorithm for protein potential function test and structure refinement. *Proteins: Struct., Funct., Genet.* **1999**, *34*, 464–471.

93. Ferreira, A. L.; Toral, R. Hybrid Monte Carlo method for conserved-order-parameter systems. *Phys. Rev. E* **1993**, *47*, R3848–R3851.

94. Cundy, N. Current status of dynamical overlap project. *Nucl. Phys. B, Proc. Suppl.* **2006**, *153*, 54–61.

95. Adachi, A.; Akamatsu, N.; Iwaisako, K.; Senkoku, M.; Kobayashi, T. Removal efficiency of phenols from chemical wastewater by a treatment plant using activated carbon adsorption and coagulation precipitation processes. *Jpn. J. Toxicol. Environ. Health* **1992**, *38*, 300–303.

96. Irawan, C.; Kuo, Y. L.; Liu, J. C. Treatment of boron-containing optoelectronic wastewater by precipitation process. *Desalination* **2011**, *280*, 146–151.

97. Kim, S.; Lotz, B.; Lindrud, M.; Girard, K.; Moore, T.; Nagarajan, K.; Alvarez, M.; Lee, T.; Nikfar, F.; Davidovich, M.; Srivastava, S.; Kiang, S. Control of the particle properties of a drug substance by crystallization engineering and the effect on drug product formulation. *Organic Process Research and Development* **2005**, *9*, 894–901.

98. Lueth, V. W.; Gibbs, R. B.; North, R. M. A history of mineral collecting at the Chino Mine Grant County, New Mexico. *Rocks Minerals* **2009**, *84*, 492–500.

99. Torrie, G. M.; Valleau, J. P. Monte Carlo free energy estimate using non-Boltzmann sampling: Application to the sub-critical Lennard-Jones fluid. *J. Chem. Phys.* **1974**, *28*, 578–581.

100. Kästner, J. Umbrella sampling. *Wiley Interdiscip. Rev. Comput. Mol. Sci.* **2011**, *1*, 932–942.

101. Shen, V. K.; Debenedetti, P. G. A computational study of homogeneous liquid-vapor nucleation in the Lennard-Jones fluid. *J. Chem. Phys.* **1999**, *111*, 3581–3589.

102. Hansen, H. S.; Hünenberger, P. H. Using the local elevation method to construct optimized umbrella sampling potentials: Calculation of the relative free energies and interconversion barriers of glucopyranose ring conformers in water. *J. Comput. Chem.* **2009**, *31*, 1–23.

103. Kumar, S.; Bouzida, D.; Swendsen, R. H.; Kollman, P. A.; Rosenberg, J. M. The weighted histogram analysis method for free-energy calculations on biomolecules. I. the method. *J. Comp. Chem.* **1992**, *13*, 1011–1021.

104. Harvey, S. C.; Prabhakaran, M. Umbrella sampling: Avoiding possible artifacts and statistical biases. *J. Phys. Chem.* **1987**, *91*, 4799–4801.

105. Kästner, J.; Thiel, W. Bridging the gap between thermodynamic integration and umbrella sampling provides a novel analysis method: Umbrella integration. *J. Chem. Phys.* **2005**, *123*, 144104(1–5.

106. Roux, B. The calculation of the potential of mean force using computer simulations. *Comput. Phys. Commun.* **1995**, *91*, 275–282.

107. Beutler, T. C.; Van Gunsteren, W. F. Umbrella sampling along linear combinations of generalized coordinates. Theory and application to a glycine dipeptide. *Chem. Phys. Lett.* **1995**, *237*, 308–316.

108. Blaak, R.; Löwen, H. Umbrella sampling of non-equilibrium computer simulations. *Comput. Phys. Commun.* **2005**, *169*, 64 – 68.

109. Warmflash, A.; Bhimalapuram, P.; Dinner, A. R. Umbrella sampling for nonequilibrium processes. *J. Chem. Phys.* **2007**, *127*, 154112/1–8.

110. Schmidt, R. K.; Teo, B.; Brady, J. W. Use of umbrella sampling in the calculation of the potential of mean force for maltose in vacuum from molecular dynamics simulations. *J. Phys.Chem.* **1995**, *99*, 11339–11343.

111. Bohner, M. U.; Kästner, J. An algorithm to find minimum free energy paths using umbrella integration. *J. Chem. Phys.* **2012**, *137*, 034105/1 − 6.

112. Rosta, E.; Woodcock, H. L.; Brooks, B. R.; Hummer, G. Artificial reaction coordinate "tunneling" in free-energy calculations: The catalytic reaction of RNase H. *J. Comput. Chem.* **2009**, *30*, 1634–1641.

113. Hooft, R. W. W.; Van Eijck, B. P.; Kroon, J. An adaptive umbrella sampling procedure in conformational analysis using molecular dynamics and its application to glycol. *J. Chem. Phys.* **1992**, *97*, 6690–6694.

114. Zhang, Q.; Yang, W.; Man, N.; Zheng, F.; Shen, Y.; Sun, K.; Li, Y.; Wen, L. P. Autophagy-mediated chemosensitization in cancer cells by fullerene C60 nanocrystal. *Autophagy* **2009**, *5*, 1107–1117.

115. Harhaji, L.; Isakovic, A.; Raicevic, N.; Markovic, Z.; Markovic, B. T.; Nikolic, N.; Djuric, S. V.; Markovic, I.; Trajkovic, V. Multiple mechanisms underlying the anticancer action of nanocrystalline fullerene. *Eur. J. Pharmacol.* **2007**, *568*, 89–98.

116. Unwin, P. Fullerenes (an overview). `http://www.ch.ic.ac.uk/local/projects/unwin/Fullerenes.html`, Accessed April 2013.

117. Taylor, R. Aromatic fullerene derivatives. *J. Chem. Phys.* **2004**, *6*, 328–331.

118. Stoilova, O.; Jerome, C.; Detrembleur, C.; Mickalad, A. M.; Manolova, N.; Rashkov, I.; Jerome, R. C_{60} containing nanostructured polymeric materials with potential biomedical applications. *Poly.* **2007**, *48*, 1835–1843.

119. Beal, R. M.; Stavrinadis, A.; Warner, J. H.; Smith, J. M.; Assender, H. E.; Watt, A. A. R. The molecular structure of polymerfullerene composite solar cells and its influence on device performance. *Macromol.* **2010**, *43*, 2343–2348.

120. Ge, Z.; Duchamp, J. C.; Cai, T.; Gibson, H. W.; Dorn, H. C. Purification of endohedral trimetallic nitride fullerenes in a single, facile step. *J. Am. Chem. Soc.* **2005**, *127*, 16292–16298.

121. Canevet, D.; Gallego, M.; Isla, H.; Juan, A.; Perez, E. M.; Nazario, M. N. Macrocyclic hosts for Fullerenes: extreme changes in binding abilities with small structural variations. *J. Am. Chem. Soc.* **2011**, *133*, 3184–3190.

122. Nambo, M.; Segawa, Y.; Itami, K. Aziridinofullerene: a versatile platform for functionalized fullerenes. *J. Am. Chem. Soc.* **2011**, *133*, 2402–2405.

123. Detrembleur, C.; Stoilova, O.; Bryaskova, R.; Debuigne, A.; Mickalad, A. M.; Jerome, R. Preparation of well-defined PVOH/C_{60} nanohybrids by Cobalt-mediated radical polymerization of vinyl acetate. *Macromol. Rapid Commun.* **2006**, *27*, 498–504.

124. Marappan, S.; Kunichi, M. Size-tunable hexagonal Fullerene (C_{60}) nanosheets at the liquid-liquid interface. *J. Am. Chem. Soc.* **2007**, *129*, 13816–13817.

125. Girifalco, L. A. Molecular properties of C_{60} in the gas and solid phases. *J. Phys. Chem.* **1992**, *96*, 858–861.

126. Yu, L. Nucleation of one polymorph by another. *J. Am. Chem. Soc* **2003**, *125*, 6380–6381.

127. Desgranges, C.; Delhommelle, J. Molecular simulation of cross-nucleation between polymorphs. *J. Phys. Chem. B* **2007**, *111*, 1465–1469.

128. Steinhardt, P. J.; Nelson, D. R.; Ronchetti, M. Bond-orientational order in liquids and glasses. *Phys. Rev. B* **1983**, *28*, 784–805.

129. Desgranges, C.; Delhommelle, J. Molecular mechanism for the cross-nucleation between polymorphs. *J. Am. Chem. Soc.* **2006**, *128*, 15104–15105.

130. Boer, J. L.; Smaalen, S. V.; Petricek, V.; Dusek, M.; Verheijen, M. A.; Maijer, G. Hexagonal close-packed C_{60}. *Chem. Phys. Lett.* **1994**, *219*, 469–472.

131. Duta, A.; Geana, D. Hybrid Monte Carlo. *Turk. J. Chem.* **2002**, *26*, 481–489.

132. Nath, S. K.; Escobedo, F. A.; De Pablo, J. J.; Patramai, I. Simulation of vapor-liquid equilibria for alkane mixtures. *Ind. Eng. Chem. Res.* **1998**, *37*, 3195–3202.

133. Panagiotopoulos, A. Z. Direct determination of phase coexistence properties of fluids by Monte Carlo simulation in a new ensemble. *Mol. Phys.* **2002**, *100*, 237–246.

134. Mezei, M. A cavity-biased (T, V, mu) Monte Carlo method for computer simulation of fluids. *Mol. Phys.* **1980**, *40*, 901–906.

135. Siepmann, J. I.; Frenkel, D. Configurational bias Monte Carlo: a new sampling scheme for flexible chains. *Mol. Phys.* **1992**, *75*, 59–70.

136. Mane, M. B.; Shinde, S. N. Vapor liquid equilibria: A review. *Sci. Revs. Chem. Commun.* **2012**, *2*, 158–171.

137. Lee, H. S.; Yoo, J. W. Removal of polyaromatic hydrocarbons from scrap tires by solvent extraction. *Korean J. Chem. Eng.* **2011**, *28*, 1065–1069.

138. Stichlmair, J. R., J. G.and Fair *Distillation principles and practice*; Wiley-VCH, 1998; pp 6–69.

139. Ganzenmüller, G.; Camp, P. J. Applications of Wang-Landau sampling to determine phase equilibria in complex fluids. *J. Chem. Phys.* **2007**, *127*, 154504/1–10.

140. Aleksandrov, T.; Desgranges, C.; Delhommelle, J. Vapor-liquid equilibria of copper using hybrid Monte Carlo Wang-Landau simulations. *Fluid Phase Equilib.* **2010**, *287*, 79–83.

141. Desgranges, C.; Hicks, J. M.; Magness, A.; Delhommelle, J. Phase equilibria of polyaromatic hydrocarbons by hybrid Monte Carlo Wang-Landau simulations. *Mol. Phys.* **2010**, *108*, 151–158.

142. Wei, Y.; Zhang, X.; Zhang, J.; Dang, L.; Wei, H. Solid-liquid equilibrium of some polycyclic aromatic hydrocarbons in wash oil. *Fluid Phase Equilibria* **2012**, *319*, 23–29.

143. Hoh, E.; Hunt, R. N.; Quintana, P. J. E.; Zakarian, J. M.; Chatfield, D. A.; Wittry, B. C.; Rodriguez, E.; Matt, G. E. Environmental tobacco smoke as a source of polycyclic aromatic hydrocarbons in settled household dust. *Environ. Sci. and Technol.* **2012**, *46*, 4174–4183.

144. Berger, G. D.; Seybold, P. G. Substituent effects in chemical carcinogenesis: Chrysene and its methyl derivatives. *Int. J. Quantum Chem.* **1979**, *16*, 305–311.

145. Lee, M.; Chen, C.; Lin, H. Solid-liquid equilibria for binary mixtures composed of acenaphthene, dibenzofuran, fluorene, phenanthrene, and diphenylmethane. *J. Chem. Eng. Data* **1999**, *44*, 1058–1062.

146. Ahunbay, M.; Pérez-Pellitero, J.; Contreras-Camacho, R.; Teuler, J.; Ungerer, P.; Mackie, A.; Lachet, V. Optimized intermolecular potential for aromatic hydrocarbons based on anisotropic united atoms: III. polyaromatic and naphthenoaromatic hydrocarbons. *J. Phys. Chem. B* **2005**, *109*, 2970–2976.

147. Errington, J. R.; Panagiotopoulos, A. Z. New intermolecular potential models for benzene and cyclohexane. *J. Chem. Phys.* **1999**, *111*, 9731–9738.

148. Matubayasi, N.; Nakahara, M. Reversible molecular dynamics for rigid bodies and hybrid Monte Carlo. *J. Chem. Phys.* **1999**, *110*, 3291–3301.

149. Spyriouni, T.; Economou, I. G.; Theodorou, D. N. Molecular simulation of -olefins using a new united-atom potential model: Vapor-liquid equilibria of pure compounds and mixtures. *J. Am. Chem. Soc.* **1999**, *121*, 3407–3413.

150. Desgranges, C.; Ndumbe Ngale, K.; Delhommelle, J. Prediction of critical properties for Naphthacene, Triphenylene and Chrysene by Wang-Landau simulations. *Fluid Phase Equilib.* **2012**, *322*, 92–96.

151. Desgranges, C.; Kastl, E. A.; Aleksandrov, T.; Delhommelle, J. Optimisation of multiple time-step hybrid Monte Carlo Wang-Landau simulations in the isobaric-isothermal ensemble for the determination of phase equilibria. *Mol. Simul.* **2010**, *36*, 544–551.

152. Cui, S. T.; Cummings, P. T.; Cochran, H. D. Configurational bias Gibbs ensemble Monte Carlo simulation of vapor-liquid equilibria of linear and short-branched alkanes. *Fluid Phase Equilib.* **1997**, *141*, 45–61.

153. Ndumbe Ngale, K.; Desgranges, C.; Delhommelle, J. Wang-Landau configurational bias Monte Carlo simulations: vapour-liquid equilibria of alkenes. *Mol. Simul.* **2012**, *38*, 653–658.

154. Abreu, C. R.; Escobedo, F. A. A general framework for non-Boltzmann Monte Carlo sampling. *J. Chem. Phys.* **2006**, *124*, 054116/1–12.

155. Escobedo, F. A.; Abreu, C. R. A. On the use of transition matrix methods with extended ensembles. *J. Chem. Phys.* **2006**, *124*, 244109/1–11.

156. Nath, S. K.; De Pablo, J. J. Simulation of vapour-liquid equilibria for branched alkanes. *Mol. Phys.* **2000**, *98*, 231–238.

157. McKnight, T.; Vlugt, T.; Ramjugernath, D.; Starzak, M.; Ahlstrm, P.; Bolton, K. Simulation of 1-alkene and n-alkane binary vapour-liquid equilibrium using different united-atom transferable force fields. *Fluid Phase Equilibria* **2005**, *232*, 136–148.

158. Kremer, K.; Binder, K. Monte Carlo simulations of lattice models for macromolecules. *Comp. Phys. Rep.* **1988**, *7*, 259–310.

159. Leblanc, B.; Braunschweig, B.; Toulhoat, H.; Lutton, E. Improving the sampling efficiency of Monte Carlo molecular simulations: An evolutionary approach. *Mol. Phys.* **2003**, *101*, 3293–3308.

160. Consta, S.; Vlugt, T.; Hoeth, J.; Smit, B.; Frenkel, D. Recoil growth algorithm for chain molecules with continuous interactions. *Mol. Phys.* **1999**, *97*, 1243–1254.

161. Wescott, J. T.; Kung, P.; Nath, S. K. Vapour-liquid coexistence properties and critical points of two branched alkanes series. *Fluid Phase Equilib.* **2003**, *208*, 123–139.

162. Macedonia, M. D.; Maginn, E. J. A biased grand canonical Monte Carlo method for simulating adsorption using all-atom and branched united atom models. *Mol. Phys.* **1999**, *96*, 1375–1390.

163. Landau, D. P.; Tsai, S. H.; Exler, M. A new approach to Monte Carlo simulations in statistical physics: Wang-Landau sampling. *Am. J. Phys.* **2004**, *72*, 1294–1302.

164. Vargaftik, N. B.; Vinoradov, Y. K.; Yargin, V. S. *Handbook of physical properties of liquids and gases*; Begell House, New York, 1996.